

Cross Correlation Analysis of Ionospheric Parameters with Symmetric-H and Auroral Electrojet Indices during Geomagnetic Storms

Pitri Bhakta Adhikari¹, Samyam Pudasaini², Binod Adhikari³, Rohit Bhattarai², Iva Kumari Lamichhane², Manghang Limbu², Pramod Kamal Kharel², and Aasis Bhandari²

¹Tri-Chandra College

²Tri-Chandra M. Campus

³St.Xavier's College, ,Maitighar

December 16, 2022

Abstract

This paper investigates the effects of geomagnetic storms of 25-27 September 2011, 16- 18 March 2013, and 6-8 September 2015 over five mid latitudes stations (Dourbes, Fairford, Moscow, Rome, and Roquetes) and performs a cross correlation analysis of ionospheric and solar parameters during these storms. We observed the highest fluctuations in ionospheric variables during the main phase of storms. In addition, there is strong evidence of pre-storm phenomenon occurring at least a few hours and more than 24 hours prior to the main phase of the geomagnetic storms. We found that the TEC and foF2 parameters have strong dependence with latitudes for the events with Sudden Storm Commencement(SSC) in mid latitude region. Relatively low TEC and foF2 can be observed in Moscow which is at the highest latitude among the five stations because of a decrease in the $n(O)/n(N2)$ ratio through out the storm event. However, for the event with gradual storm commencement, there is no evidence of such dependence. The good correlation of Symmetric-H and Auroral Electrojet Indices with ionospheric parameters indicates that the coupling mechanism between magnetosphere and ionosphere produces intense electric field disturbances in the middle low latitudes.

Hosted file

951977_0_table_10527971_rmrsp.docx available at <https://authorea.com/users/566837/articles/613435-cross-correlation-analysis-of-ionospheric-parameters-with-symmetric-h-and-auroral-electrojet-indices-during-geomagnetic-storms>

1 **Cross Correlation Analysis of Ionospheric Parameters**
2 **with Symmetric-H and Auroral Electrojet Indices**
3 **during Geomagnetic Storms**

4 **Samyam Pudasaini¹, Binod Adhikari², Rohit Bhattarai¹, Iva Kumari**
5 **Lamichhane¹, Manghang Limbu¹, Pramod Kamal Kharel¹, Aasis Bhandari¹,**
6 **Pitri Bhakta Adhikari¹**

7 ¹Department of Physics, Tri-Chandra Multiple College, Tribhuvan University, Kathmandu, Nepal

8 ²Department of Physics, St. Xavier's College, Maitighar, Kathmandu, Nepal

9 **Key Points:**

- 10 • There is a strong evidence of pre-storm phenomenon occurring at least a few hours
11 and more than 24 hours prior to the main phase of the geomagnetic storms.
- 12 • The TEC and foF2 parameters have strong dependence with latitudes for the events
13 with Sudden Storm Commencement (SSC) in the middle latitudes region.
- 14 • The highest correlations of geomagnetic indices with ionospheric parameters are
15 mostly observed one day prior to main phase of geomagnetic storm.

Corresponding author: Priti Bhakta Adhikari, pbadhikari09@gmail.com

Abstract

This paper investigates the effects of geomagnetic storms of 25-27 September 2011, 16-18 March 2013, and 6-8 September 2015 over five mid latitude stations (Dourbes, Fairford, Moscow, Rome, and Roquetes) and performs a cross correlation analysis of ionospheric and solar parameters during these storms. We observed the highest fluctuations in ionospheric variables during the main phase of storms. In addition, there is strong evidence of pre-storm phenomenon occurring at least a few hours and more than 24 hours prior to the main phase of the geomagnetic storms. We found that the TEC and foF2 parameters have strong dependence with latitudes for the events with Sudden Storm Commencement (SSC) in mid latitude region. Relatively low TEC and foF2 can be observed in Moscow which is at the highest latitude among the five stations because of a decrease in the $n(O)/n(N_2)$ ratio through out the storm event. However, for the event with gradual storm commencement, there is no evidence of such dependence. The good correlation of Symmetric-H and Auroral Electrojet Indices with ionospheric parameters indicates that the coupling mechanism between magnetosphere and ionosphere produces intense electric field disturbances in the middle low latitudes.

1 Introduction

Geomagnetic storms are produced when the interplanetary magnetic field (IMF) Bz component turns southward, strengthens (IMF Bz < -10 nT), and remains southward for a substantial length of time (longer than ~ 3 hr; (W. D. Gonzalez & Tsurutani, 1987); (W. Gonzalez et al., 1994)). As this happens, a rapid increase of magnetic reconnection processes occurs at the magneto-pause. When IMF-Bz is strongly negative, open field lines are produced by magnetic reconnection between the IMF and the geomagnetic field which allow the passage of mass, energy and momentum from the solar wind to the Earth's magnetosphere. This results in more solar wind energy input into all regions of the earth-atmosphere system, resulting in a geomagnetic storm. Geomagnetic storms are an important space weather phenomenon that, apart from affecting ground and satellite-based technological and high-frequency communications systems, can severely affect the dynamics and structure of the Earth's entire thermosphere and ionosphere. The ionospheric response to a geomagnetic storm is called an ionospheric storm that describes the ionospheric variations due to geomagnetic disturbances.

Geomagnetic activity observed at the Earth is generally attributed to the occurrence of Coronal Mass Ejection (CME) on the Sun and the associated interplanetary shock waves or corotating interaction regions (CIR) produced by high-speed solar wind streams in the interplanetary medium ((Gosling, 1993a); (Gosling, 1993b); (Bothmer & Schwenn, 1994); (Luhmann, 1997); (Crooker & McAllister, 1997)). CMEs are expulsions of mass from the Sun and are generally associated with solar flares or prominences. Once launched from the Sun, CMEs travel through the interplanetary medium and, if directed toward the Earth, reach the Earth in 1–4 days depending on their speed. Therefore in order to predict geoeffectiveness of CMEs, one needs to examine the solar data from near the surface of the Sun and follow them through to the Earth. This is facilitated by an examination of ground-based and space-based multi-instrument data sets.

Ionosphere is the layer of the atmosphere that lies between 60 km and 1000 km above the Earth surface and has a great importance in high frequency (HF) and satellite communications because of its electrical and ionic structure. The ionization characteristics and electron density distribution vary according to the location on Earth, time, solar, geomagnetic and seismic effects. Ionosphere consists of three distinct layers, namely D, E, and F. The F layer is the most significant layer in the ionosphere and the central part has the greatest electron density. During day time the F layer splits into F1 and F2 layers. F2-layer, having the highest electron density, is the most stable layer for HF communications and it has major importance in satellite communications ((Kolawole, 2003)).

67 The F2 region is considered the most difficult and anomalous ionospheric region
68 to predict (Hargreaves, 1992). In order to model this region, several authors have used
69 the F2 critical frequency (foF2) and the F2 region peak height (hmF2) parameters. These
70 parameters depend on various geophysical parameters including local time, season, so-
71 lar and geomagnetic activity conditions and are believed to describe the overall behav-
72 ior of the F2 layer ((Sethi & Pandey, 2001); (Richards, 2001); (Kawamura et al., 2002);
73 (J. Liu et al., 2003); (Lei et al., 2005); (L. Liu et al., 2006); (S.-R. Zhang & Holt, 2008);
74 (Moen et al., 2008); (M.-L. Zhang et al., 2009); (Souza et al., 2010), and references therein).
75 A better understanding of the variability and modeling of foF2 and hmF2 parameters
76 is crucial for the development of ionospheric prediction capabilities, improvements in ex-
77 isting ionospheric models, and for radio propagation studies.

78 Studies have shown that, there are strong disturbances induced in the F-region of
79 the ionosphere during strong geomagnetic storms. These perturbations cause large en-
80 hancements and reduction of electron density at the F2 region described as positive and
81 negative ionospheric storm effects respectively.(see, e.g., (Fuller-Rowell et al., 1994); (Volland,
82 1995); (Buonsanto, 1999); (Mendillo, 2006).) The occurrence of positive and negative
83 storm effects depends upon the latitude, local time, and phase of the storm ((Fuller-Rowell
84 et al., 1994)).

85 The ionospheric variations can be determined from the total electron content (TEC)
86 or from the critical frequency of the F2-layer (foF2), which is a direct measure of the peak
87 electron density (NmF2) of the F2-region ionosphere. The positive ionospheric storms
88 have a high density of electrons and negative storms contain a lower density ((Fagundes
89 et al., 2016)). The total electron content (TEC) is used to measure these densities, and
90 is a key variable used in data to record and compare the intensities of ionospheric storms.

91 Ground magnetometer measures the integrated effect of all these disturbed time
92 and also quiet time ionospheric and magnetospheric currents. Geomagnetic indices like
93 Disturbance storm time index (Dst) and Symmetric H-component (SYM/H) index mainly
94 represent ring current intensity during geomagnetic storms ((Sugiura et al., 1964); (Rangarajan,
95 1989); (Wanliss & Showalter, 2006)), derived using the longitudinally distributed chain
96 of low latitude ground-based magnetometers. SYM/H is the same as Dst, but it has a
97 1-minute temporal resolution, which is very useful to study short temporal variations dur-
98 ing the geomagnetic disturbances. SYM/H is derived by first subtracting the main ge-
99 omagnetic field due to internal geodynamo and external Sq induced geomagnetic field
100 variations and then averaging residual fields. Therefore, it is a good proxy for the lon-
101 gitudinally symmetric component of the ring current. SYM/H is an indication of storm
102 ring current intensity and AE gives auroral substorm ionospheric current intensities.

103 In the present study we investigate the solar and interplanetary conditions that were
104 specific to intense geomagnetic storms of 25-27 September 2011, 16-18 March 2013, and
105 6-8 September 2015 (minimum SYM/H < -130 nT) in order to understand the rela-
106 tionships between the solar indices and ionospheric parameters associated with intense
107 geomagnetic storms.

2 Data Sources

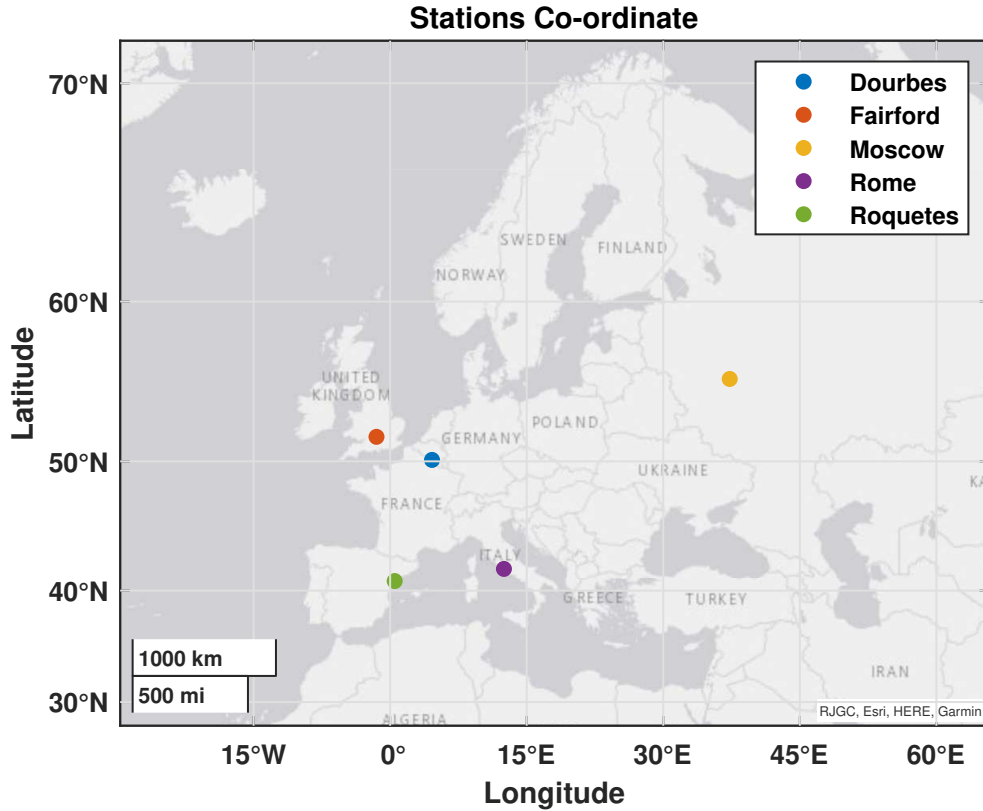


Figure 1. Map of the Stations.

Table 1. Table of stations.

S.No	Stations Name	URSI	Latitude	Longitude
1.	DOURBES	DB049	50.10	4.60
2.	FAIRFORD	FF051	51.70	358.50
3.	MOSCOW	MO155	55.47	37.30
4.	ROME	RO041	41.80	12.50
5.	ROQUETES	EB040	40.80	0.50

Figure 1 shows the map of the ionospheric stations used in this study. The observed F2-layer parameters (foF2, hmF2, and TEC) in this study are obtained from a chain of ionosondes located at Dourbes (50.1° N, 4.6° E, data temporal resolution 5 min), Fairford (51.7° N, 358.5° E, 15 min), Moscow (55.47° N, 37.3° E, 15 min), Rome (41.9° N, 12.5° E, 15 min), and Roquetes (40.8° N, 0.5° E, 5 min) during the geomagnetic storms on 25-27 September, 2011; 16-18 March, 2013; and 6-8 September, 2013. In order to investigate the F2-layer behaviors during low solar activity, the data under geomagnetic quiet-conditions on 17-19 March, 2017 are selected. The data are available at the Digital Ionogram Data Base (DIDBase) (<https://giro.uml.edu/didbase/>).

118 The modulation of solar wind (SW) and interplanetary magnetic field (IMF) com-
119 ponents (Bx, By, and Bz) high-resolution (1 min) data were obtained from OMNI Database
120 (https://omniweb.gsfc.nasa.gov/form/omni_min.html).

121 The sudden storm commencement (SSC) is often served as a reference time for the
122 onset of a magnetic storm. The reliability of SSC for the storm onset has been argued
123 for a long time. As a result, some investigators choose the main phase onset of the storm
124 instead of SSC as the start time of a storm [e.g., (Prölss, 1995)]. Here we use SSC to in-
125 dicate the onset of a magnetic storm for storms with a sudden commencement, except
126 for the event on 06-08 September, 2015 because it only had a gradual commencement.
127 The SYM/H index is used to indicate the evolution and intensity of geomagnetic storms.

128

3 Result

129

3.1 Event-1: 25-27 September, 2011

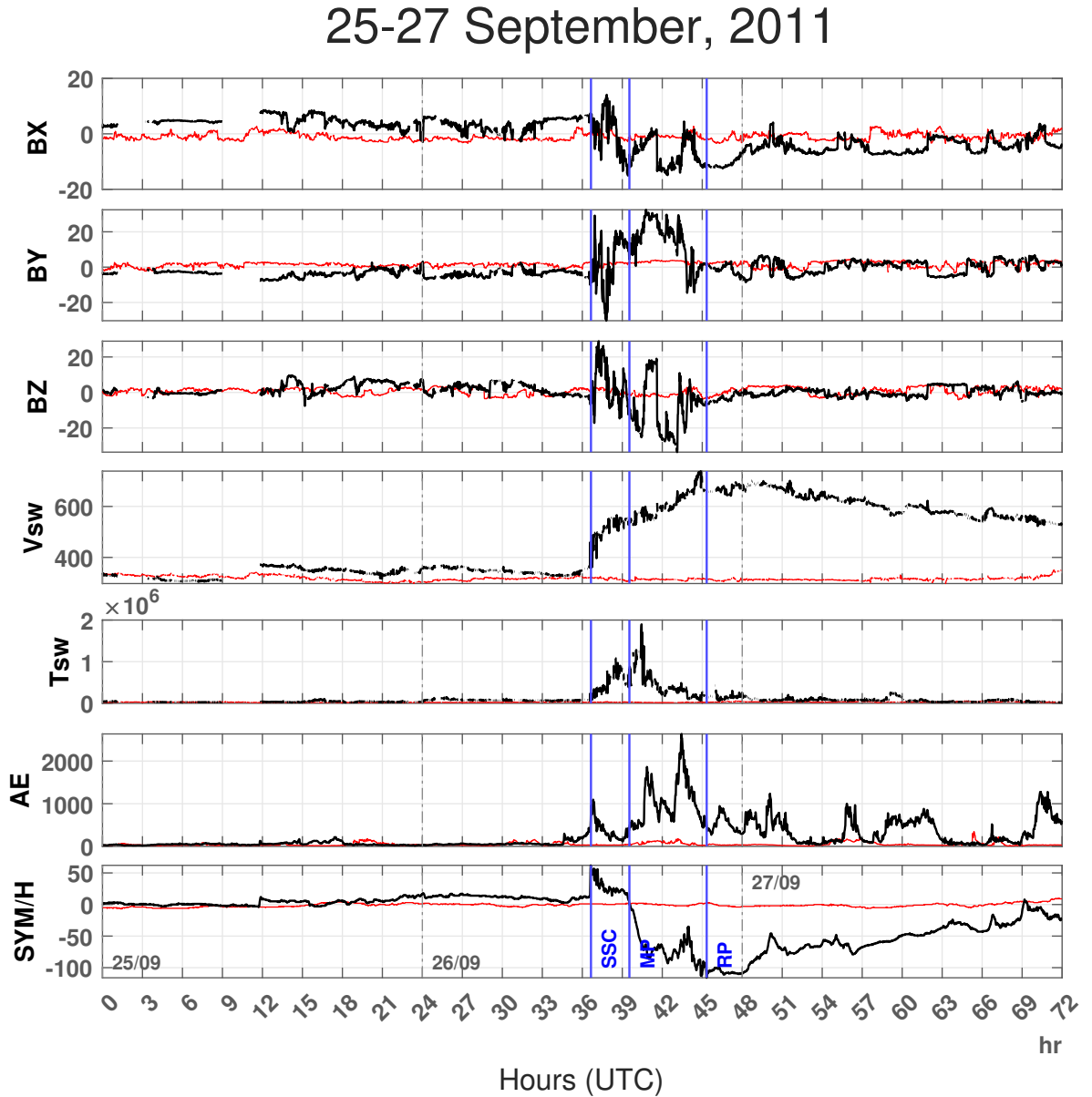


Figure 2. Variation in components of the magnetic field (in GSM co-ordinates), B_x (nT), B_y (nT) and B_z (nT), solar wind velocity V_{sw} (km/s), plasma temperature T_{sw} (K), geomagnetic indices, SYM/H (nT), and AE-index (nT) during Super Sub-Storm of 25–27 September, 2011. The red curve denotes the variation during quiet days (18–20 March, 2017).

130

131

132

133

Almost halfway through the ascending phase of the 24th solar cycle, a G2 level, moderately strong geomagnetic storm with K_p index of 6 occurred on 26 September, 2011 due to a concentrated blast of electrically-conducting solar wind plasma and tangled magnetic field lines from region 1302 (N12E47) of the Sun. The region produced a X1.9 flare,

134 a M7.1 long duration x-ray flare and a M5.8 x-ray flare on 24 September (Source: [https://](https://www.spaceweatherlive.com/)
 135 www.spaceweatherlive.com/). Figure 2 displays temporal evolution of interplanetary
 136 parameters Bx, By, Bz, solar wind velocity (Vsw), solar wind temperature (Tsw), ge-
 137 omagnetic activity indices AE (Auroral Electrojet) index, and SYM/H index for 25–27
 138 September, 2011. The differences between the various parameters during the event (in-
 139 dicated by black curves) and quiet days (indicated by red curves) are observed from the
 140 figure 2.

141 At 12:38 (UTC) of 26 September the sudden storm commencement (SSC) is seen
 142 to have occurred when the symmetric horizontal component of the geomagnetic field SYM/H
 143 rose sharply from 15 nt to the highest point of 62 nt, indicating the beginning of the
 144 initial phase. During this period, all the ionospheric parameters significantly fluctuate
 145 while the north-south interplanetary magnetic field Bz altered between positive and neg-
 146 ative values a few times with positive (negative) value indicating northward (southward)
 147 magnetic field, reaching its minimum of -33.61 nt at 19:07 (UTC) indicating a strong south-
 148 ward magnetic field. It can be observed from Figure 2, minimas in the Bz curve corre-
 149 late well with maximas in the Auroral Electrojet (AE) index. At 19:27 (UTC), 20 min-
 150 utes after Bz reached its minimum, AE-index reached its peak intensity of 2636 nT which
 151 corresponds well with the results of (Marques de Souza et al., 2018). Large amount of
 152 energy-momentum is transferred into the Earth’s magnetosphere from the solar wind which
 153 is indicated by high AE index (Pandit et al., 2021). This spike in AE index can be at-
 154 tributed to high southward interplanetary magnetic field (Bz) as the field components
 155 parallel to the ecliptic have no significant effect on sub storms (Foster et al., 1971). IMF-
 156 Bz getting negative also causes the electric field linking magnetosphere-ionosphere to in-
 157 crease (Adhikari et al., 2018). Correlation between interplanetary magnetic fields Bx and
 158 Bz can be also observed in Figure 2 as the plasma flow speed (Vsw) started increasing
 159 from the initial phase throughout the main phase as was shown by (Youssef et al., 2012).
 160 The plasma velocity (Vsw) reached its peak, 738.6 km/s at 20:53 (UTC), at the end of
 161 the main phase and decreased throughout the recovery phase. Around this time, the so-
 162 lar wind temperature (Tsw) had already cooled down reaching its peak 1.89×10^6 K
 163 earlier at 16:27 (UTC) around the beginning of the main phase. The recovery phase started
 164 when the SYM/H index was recorded to be rising after reaching its lowest at -113 nt at
 165 20:54 (UTC).

25-27 September, 2011

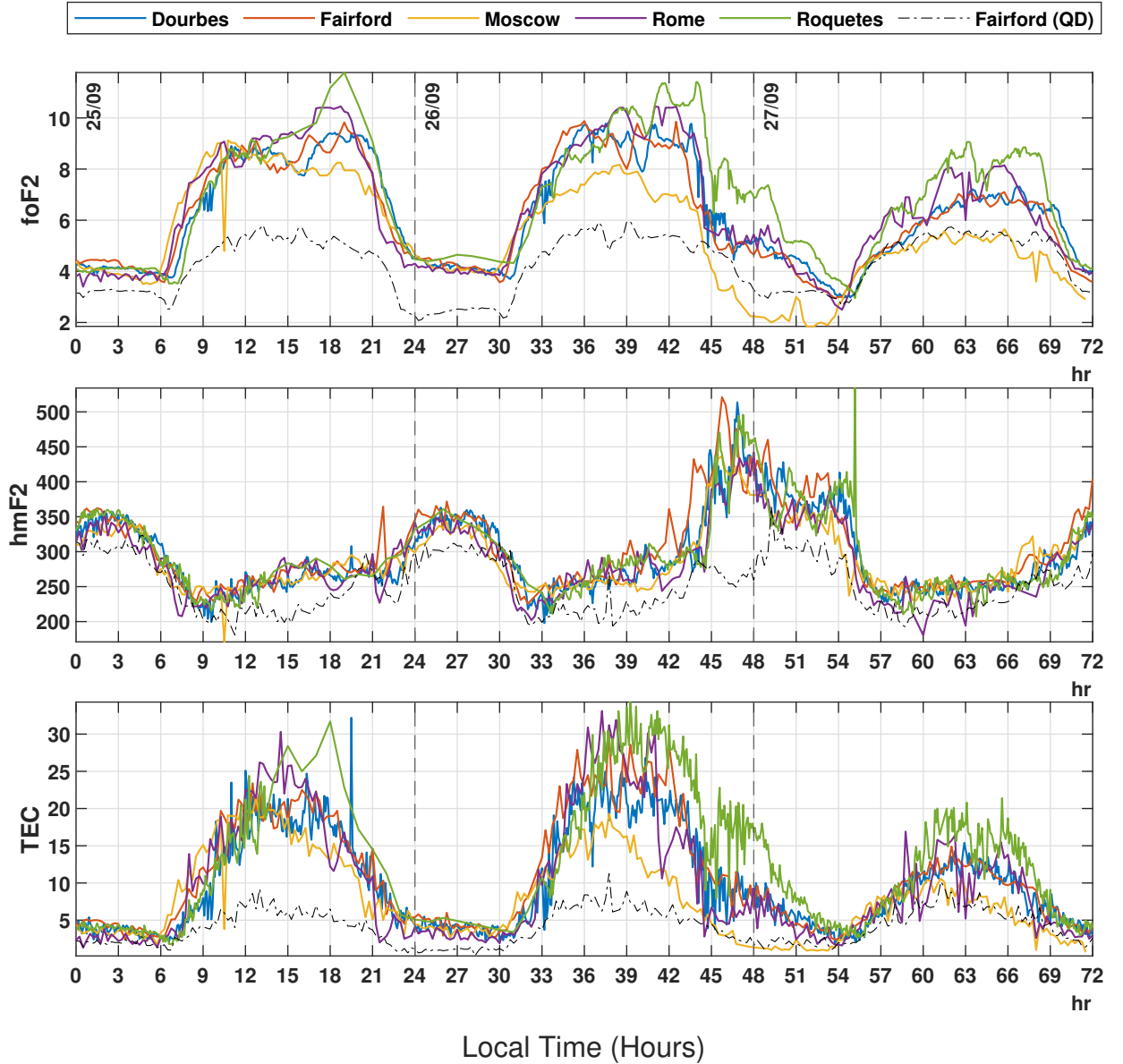


Figure 3. Changes in ionospheric parameters: F2-region critical frequency (foF2) in MHz, Total electron content (TEC) in ($\times 10^{16} m^{-2}$), Maximum Ionization Height (hmF2) in km, recorded at stations Dourbes, Fairford, Moscow, Rome and Roquetes during Super Sub-Storm on 25–27 September, 2011. The black curve denotes the variation during quiet days (18–20 March, 2017).

166 Figure 3 depicts the variations of three different ionospheric parameters: F2-region
 167 critical frequency (foF2), maximum ionization height of F2-region (hmF2), and Total Elec-
 168 tron Content (TEC) at five different stations: Dourbes, Fairford, Moscow, Rome and Roquetes.
 169 All the stations have similar variations because they all lie in the mid-latitude region.
 170 The daily variations of day and night cycle can be easily noticed in all five stations. As
 171 the sun rises at around 06:30 local time, a sudden rise in foF2 and TEC is noticed in all
 172 the stations whereas around this time hmF2 is observed to have almost reached its low-
 173 est values around 09:00 (local time) indicating a negative correlation between them.

174 Relatively low TEC and foF2 can be observed in Moscow which is at the highest
 175 latitude among the five stations because of a decrease in the $n(O)/n(N_2)$ ratio through-
 176 out the storm event (Klimenko et al., 2017). TEC and foF2 graph in Figure 3 clearly
 177 shows latitudinal dependence with high latitude stations having comparatively more neg-
 178 ative values and lower latitude stations having more positive values as shown by (W. Liu
 179 et al., 2017) and (GAO et al., 2008). Due to this reason, the ionosonde stations at Rome
 180 and Roquetes, being at the lowest latitudes, record the highest values of foF2 and TEC.

181 In panel 1, the average of highest critical frequency during daytime of the 1st day
 182 is about 10 MHz which is ~ 5 units ($\sim 100\%$) higher than that of the quiet day. The
 183 mean highest TEC on the 1st day is $\sim 25 \times 10^{16} m^{-2}$, which is ~ 17 units ($\sim 200\%$)
 184 higher than that of the quiet day (panel 3). This indicates that the positive storm had
 185 already started 1 day prior to the event day. Large amounts of energy getting deposited
 186 into the thermosphere and leading to a strong enough storm-induced circulation that fur-
 187 ther increases plasma vertical drift, increasing the electron concentration is the most fre-
 188 quent cause of positive storms but the occurrence of positive storm before SSC is one
 189 of the unsolved problems in ionospheric research (Danilov, 2001). During the nighttime
 190 of the first day, the lowest critical frequency is ~ 4 MHz which is ~ 2 units ($\sim 100\%$)
 191 higher than that of the quiet day and the lowest TEC is $\sim 3 \times 10^{16} m^{-2}$, which is much
 192 higher than that of the quiet day. The highest foF2 and TEC on the 2nd day, similar
 193 to 1st day, was ~ 5 units (100%) and ~ 20 units ($\sim 200\%$) higher than that of the quiet
 194 day respectively. Hence the storm remained positive throughout the 1st day (25 Septem-
 195 ber) and throughout the main phase on the 2nd day (26 September). This result matched
 196 with (W. Liu et al., 2017) who showed that in middle latitudes, the positive storm pre-
 197 vails during the main phase and decreases during the recovery phase. When the recov-
 198 ery phase started at 21:00 (local time) of the 2nd day (event day), the positive storm started
 199 decreasing and remained quiet throughout the 3rd day.

200 In panel 2, on the 1st day (25 September), the maximum ionization height (hmF2)
 201 above all stations remains similar to that of the quiet day. On the second day (26 Septem-
 202 ber) during the main phase, an increase in hmF2 is observed to be ~ 50 km more in all
 203 stations as compared to the quiet day. The plasma vertical drift getting increased by storm-
 204 induced circulation is the cause of uplifting of the F2 layer (Danilov, 2001). A sudden
 205 increase in hmF2 from ~ 300 km to ~ 450 km is observed at 21:00 (local time) (be-
 206 ginning of recovery phase) which is ~ 200 km more than that of the quiet day. Contin-
 207 uous substorm activity building up a high pressure zone in the polar region, reducing
 208 poleward-directed winds and enhancing equatorward-directed winds might be the cause
 209 of this sudden increase in the height of the F2 layer (Prölss & Očko, 2000). The uplift-
 210 ing decreases and almost coincides with the quiet day in the morning hours of the third
 211 day (27 September) and remains so throughout the day.

3.2 Event-2: 16-18 March, 2013

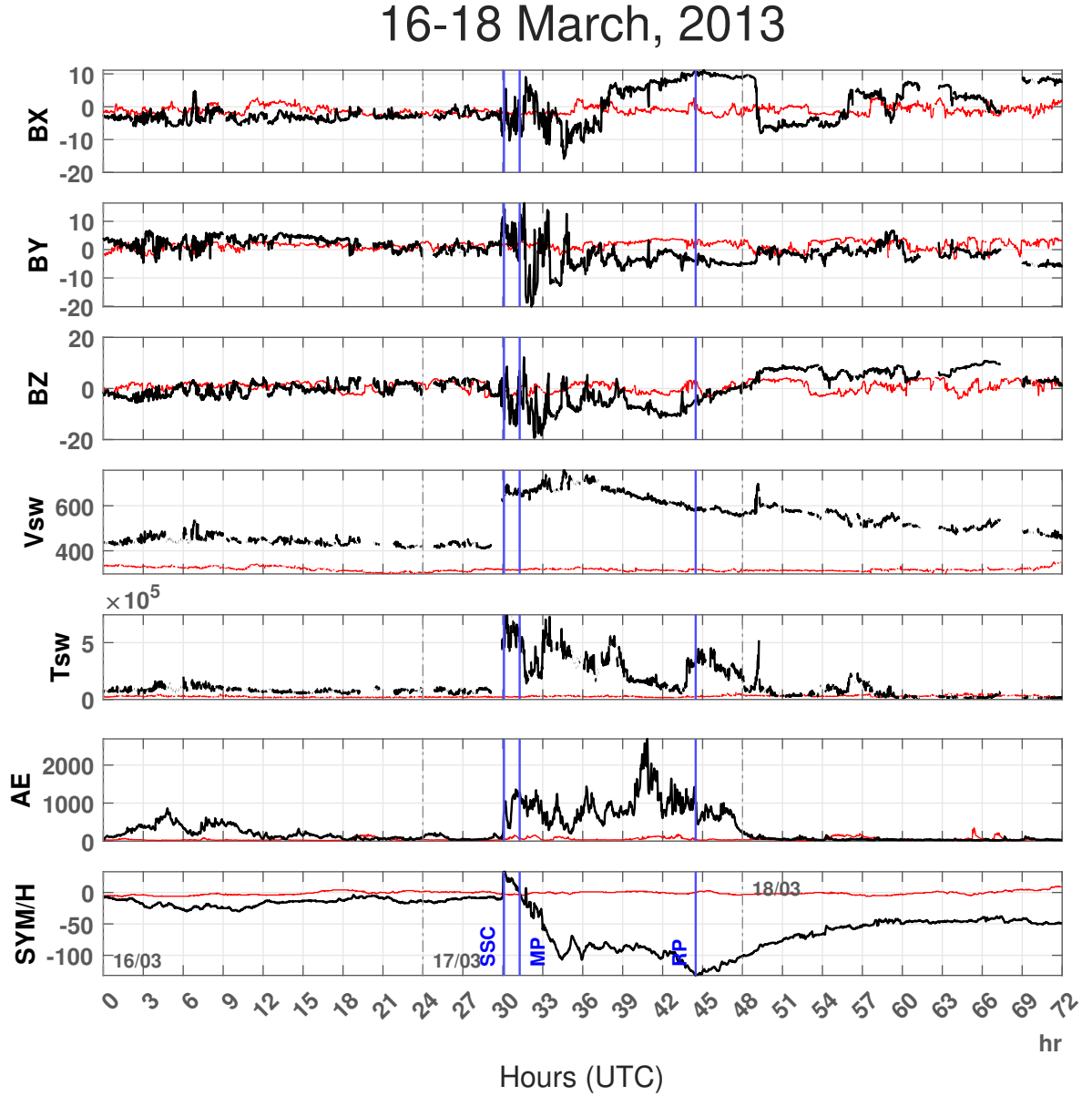


Figure 4. Variation in components of the magnetic field (in GSM coordinates), B_x (nT), B_y (nT) and B_z (nT), solar wind velocity V_{sw} (km/s), plasma temperature T_{sw} (K), geomagnetic indices, SYM/H (nT), and AE-index (nT) during Super Sub-Storm of 16–18 March, 2013. The red curve denotes the variation during quiet days (18–20 March, 2017).

A G3-Class ($K_p = 7$) Earth-directed Coronal Mass Ejection (CME) event has been observed on 17 March 2013, which is one of the strongest geomagnetic disturbances recorded during the 24th solar cycle with peak intensity of SYM/H ~ -132 nT. Figure 4 displays temporal evolution of interplanetary parameters B_x , B_y , B_z , solar wind velocity (V_{sw}), solar wind temperature (T_{sw}), geomagnetic activity indices AE (Auroral Electrojet) in-

218 dex, and the symmetric horizontal component of the geomagnetic field (SYM/H) for 17-
219 18 March 2013.

220 This storm was triggered by an Earth-directed, coronal mass ejection (Baker et al.,
221 2014) associated with M1.1 type solar flare from the sunspot 1692 (N09W03) on 15 March
222 2013 at 07:00 UT. The incoming CME enhances the Bz (north-south) to strong north-
223 ward and solar wind speed raised to 600 km/s at around 06:00 UT on 17 March 2013,
224 while magnetic field components also significantly vary. The sudden enhancement of so-
225 lar wind density and velocity because of CME hitting on magnetosphere triggers the mag-
226 netopause current, which enhances our terrestrial magnetic field, which is registered as
227 a sudden storm commencement (SSC) on SYM/H as shown in figure 4. An immediate
228 onset of intense auroral activity is seen in the AE index, reaching a magnitude as high
229 as 2000 nT, indicating the generation of energy source in the high latitude region. The
230 initial phase lasted for approximately one hour and the main phase began around 7:00
231 UT, as identified by decrease in SYM/H implying the ring current intensification, and
232 SYM/H index reached a first minimum of around -110 nT around 10:00 UT on 17 March.
233 Then it stayed nearly steady until it attained a second minimum of about -132 nT at
234 \sim 20:30 UT before recovery which means that the main phase lasted for around 13 hours.
235 The recovery phase lasted for more than 3 days as indicated by an increase in the SYM/H
236 index.

237 There is a directional discontinuity (DD) at \sim 01:12 UT on 18 March (shown by
238 a blue vertical line) clearly observed in the IMF components, solar wind temperature,
239 and solar wind velocity. The IMF Bz turns northward after the directional discontinu-
240 ity which contributes to a prompt magnetic storm recovery. This northward turning causes
241 a cessation of auroral activity due to reduced magnetic reconnection (Verkhoglyadova
242 et al., 2016). Directional discontinuities in Interplanetary Coronal Mass Ejection is an
243 important factor in determining the geoeffectiveness of the event since they are charac-
244 terized by sharp changes in coupling functions (Lugaz et al., 2015). A gradual decrease
245 in auroral activity and then a total cessation during the northward IMF interval is ob-
246 served (Du et al., 2011). The SYM/H index is observed to recover completely after about
247 3 days. This geomagnetic storm is caused by the double action of southward IMF Bz in
248 the sheath causing the storm onset and southward IMF Bz in the MC intensifying the
249 storm.

16-18 March, 2013

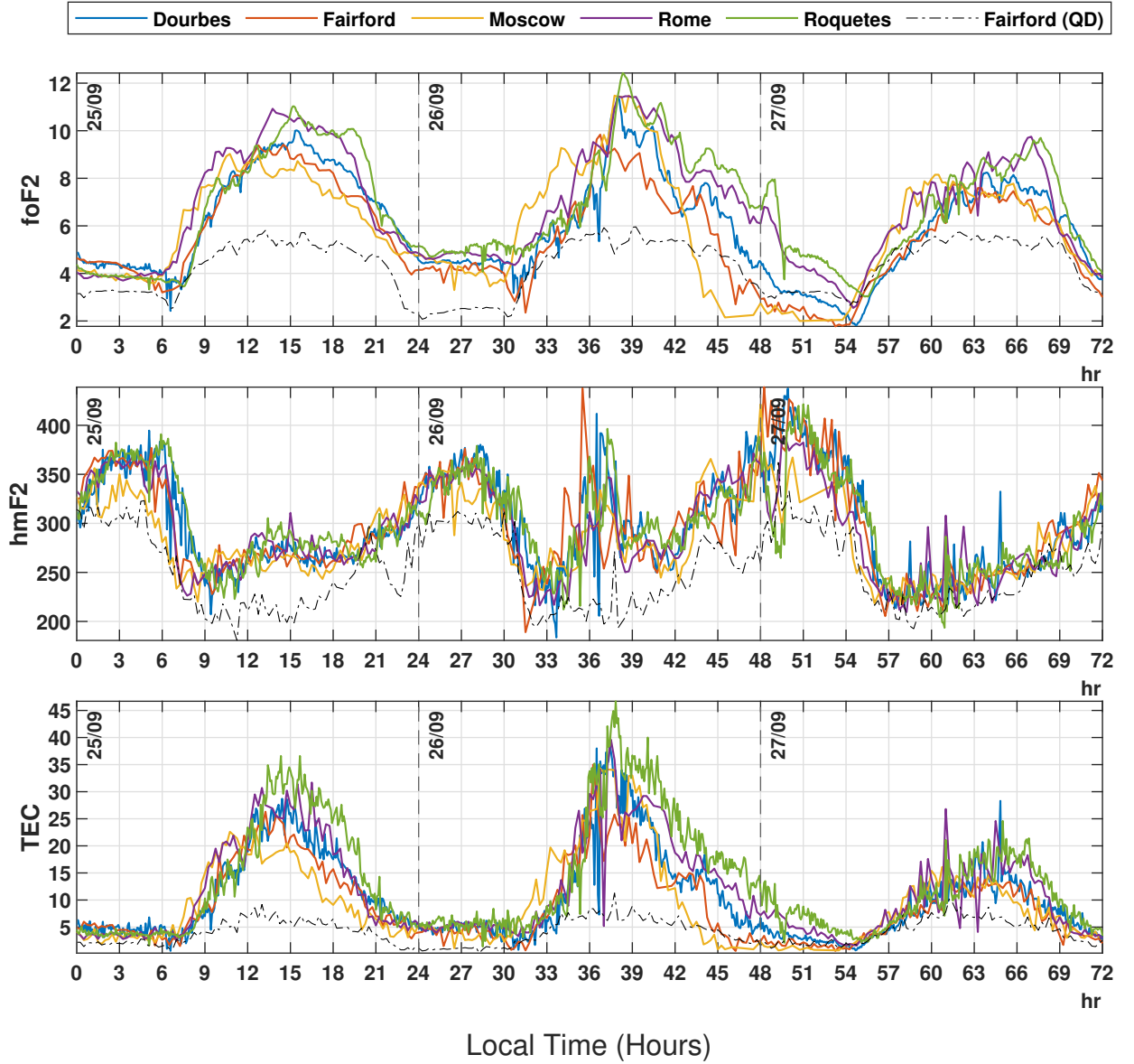


Figure 5. Change in ionospheric parameters, F2-region critical frequency (foF2) in MHz, Total electron content (TEC) in ($\times 10^{16} m^{-2}$), Maximum Ionization Height (hmF2) in km, recorded at stations Dourbes, Fairford, Moscow, Rome and Roquetes during Super Sub-Storm on 16–18 March, 2013. The black curve denotes the variation during quiet days (18–20 March, 2017).

250 Figure 5 shows F-2 layer parameters (fof2, hmF2, and TEC) between 16–18 March,
 251 2013. The top panel shows the geomagnetic index foF2, the middle panel shows the ge-
 252 omagnetic index hmF2, and the bottom panel shows the geomagnetic index TEC obtained
 253 from ionograms of Dourbes, Fairford, Moscow, Rome, and Roquetes.

254 Similar to event 1, Moscow, being at higher latitude, has the lowest TEC and foF2
 255 among the five stations for reasons similar to mentioned above in event 1 because of a
 256 decrease in the $n(O)/n(N_2)$ ratio throughout the storm event (Klimenko et al., 2017).
 257 Latitude dependence can be observed in the graph of TEC and foF2 graph as pointed

258 out in (W. Liu et al., 2017) and (GAO et al., 2008). Similarly, the ionosonde stations
 259 at Rome and Roquetes, being at the lowest latitudes, record the highest values of foF2
 260 and TEC.

261 The average of highest critical frequency during daytime of the 1st day is about
 262 10 MHz in panel 1 which is ~ 5 units ($\sim 100\%$) higher than that of the quiet day. The
 263 mean highest TEC on the 1st day is $\sim 25 \times 10^{16} m^{-2}$, which is ~ 18 units ($\sim 200\%$)
 264 higher than that of the quiet day (panel 3). Here, the positive storm had already started
 265 1 day prior to the event day. The lowest critical frequency during the nighttime of the
 266 first day is 5 MHz which is 2 units higher than that of the quiet day and the lowest TEC
 267 is $\sim 5 \times 10^{16} m^{-2}$, which is much higher than that of the quiet day. The highest foF2
 268 and TEC on the 2nd day, similar to 1st day, was ~ 5 units and ~ 25 units higher than
 269 that of the quiet day respectively. This indicates that the storm remained positive through-
 270 out the 1st day (16 March) and throughout the main phase on the 2nd day (17 March).
 271 The positive storm started decreasing when the recovery phase started at around 20:30
 272 (local time) of the 2nd day (event day) and remained less positive throughout the 3rd
 273 day.

274 On the 1st and 2nd day (16 and 17 March), in panel 2, the maximum ionization
 275 height (hmF2) above all stations showed slight increment. On the third day (18 March),
 276 hmF2 remained quiet throughout the day. During the main phase, an increase in hmF2
 277 is observed to be ~ 100 km more in all stations as compared to the quiet day. A sud-
 278 den increase in hmF2 from ~ 250 km to ~ 350 km is observed at 11:00 (local time) which
 279 is ~ 100 km more than that of the quiet day. No significant amount of variation in hmF2
 280 is observed at the event day as compared to the previous day of the event.

3.3 Event-3: 6-8 September, 2015

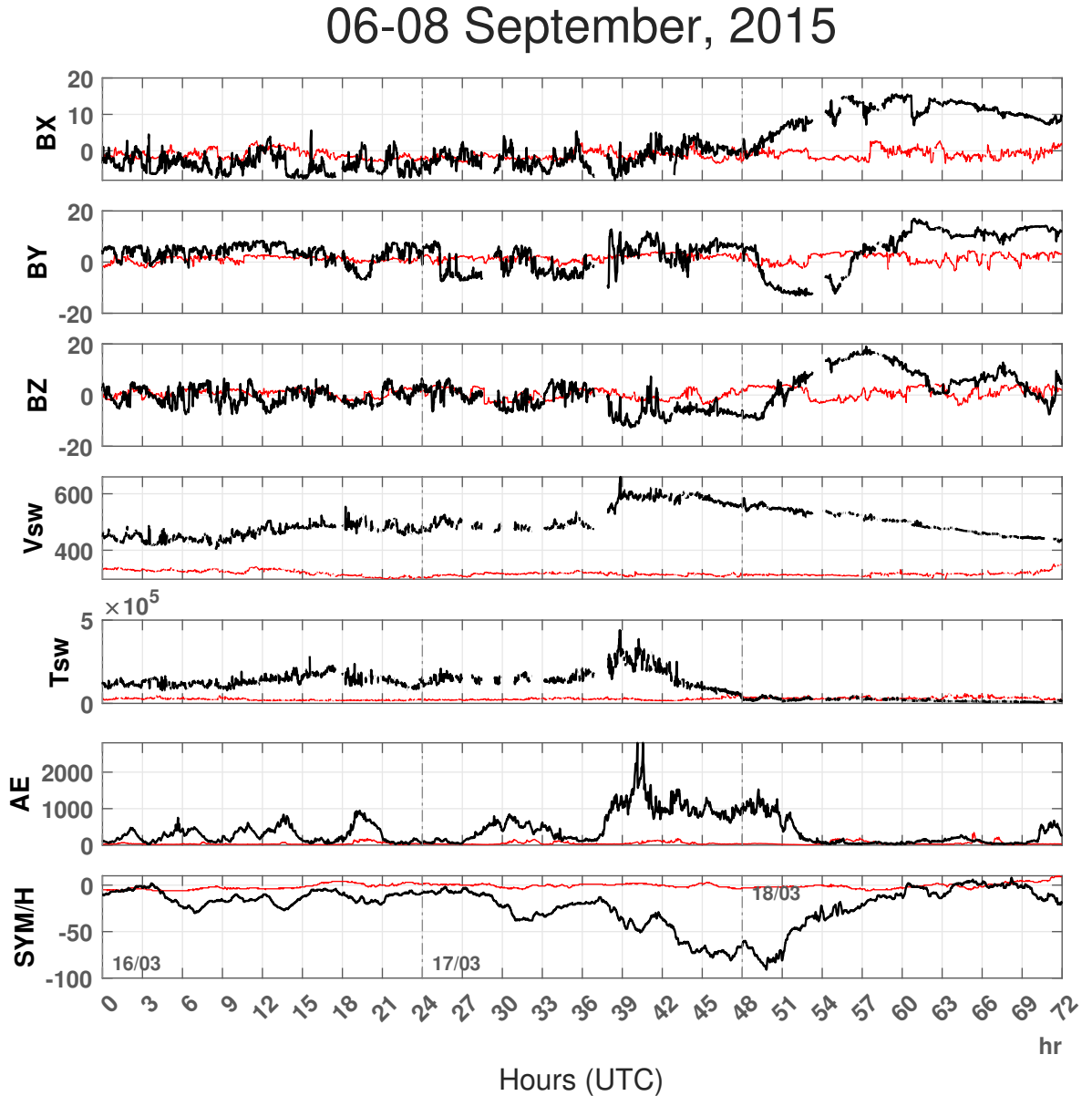


Figure 6. Variation in components of the magnetic field (in GSM coordinates), B_x (nT), B_y (nT) and B_z (nT), solar wind velocity V_{sw} (km/s), plasma temperature T_{sw} (K), geomagnetic indices, SYM/H (nT) and AE-index (nT) during Super Sub-Storm of 6–8 September, 2015. The red curve denotes the variation during quiet days (18–20 March, 2017).

282 An unforeseen powerful coronal hole solar wind stream sparked a moderate G2-Class
 283 ($K_p = 6$) geomagnetic storm on 8 September 2015, with peak intensity of SYM/H -83
 284 nT occurring at 02:00 UT on 8 September. Figure 6 shows the temporal evolution of solar
 285 wind parameters, the Interplanetary magnetic field components B_x , B_y , B_z , solar wind
 286 velocity (V_{sw}), solar wind temperature (T_{sw}), AE index and SYM/H, from 6–8 September
 287 2015. It can be inferred from the graph that there has been a pre-storm phenomenon on 06–

288 07 September with solar wind parameters fluctuating repeatedly on those days. The in-
289 coming solar wind has triggered magnetic field components to vary significantly. These
290 values oscillate to either sides of the reference value for Bz and Bz components during
291 the event. However, the Bx component's value oscillates below the reference value till
292 the recovery phase (02:00 UT, 8 September). Similarly, solar wind speed rose to 620 km/s
293 at around 17:00 UT on 07 September. The sudden enhancement of solar wind density
294 and velocity sets off the magnetopause current, represented by SYM/H as shown in fig-
295 ure 7, which amplifies our terrestrial magnetic field citesibeck1990model. An intense au-
296 roral activity is seen as the AE index reaches a magnitude as high as around 2800 nT
297 at 16:00 UT on 7 September, indicating the generation of energy sources in the high lat-
298 itude region. Likewise, Tsw has risen 2 hrs prior to the event which might be due to the
299 pre-storm effect. However, the temperature of solar wind before the storm disturbance
300 is found to be higher than the main phase (MP) of the event, indicating pre-storm phe-
301 nomena (Adekoya et al., 2012).

06-08 September, 2015

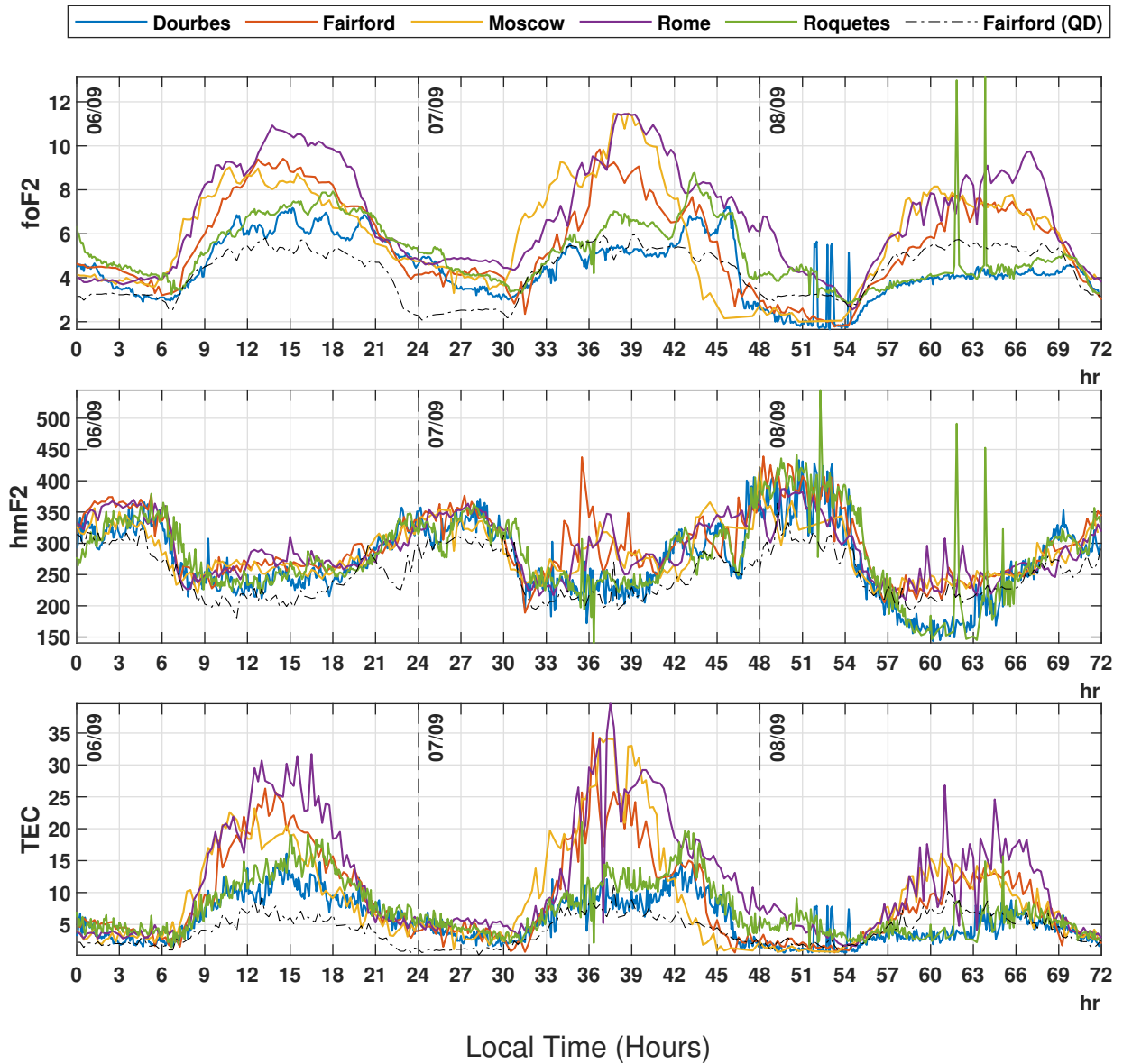


Figure 7. Change in ionospheric parameters, F2-region critical frequency (foF2) in MHz, Total electron content (TEC) in ($\times 10^{16} m^{-2}$), Maximum Ionization Height (hmF2) in Km, recorded at stations Dourbes, Fairford, Moscow, Rome and Roquetes during Super Sub-Storm on 06–08 September, 2015. The black curve denotes the variation during quiet days (18–20 March, 2017).

302 Values of ionospheric parameters, foF2, hmF2 and TEC, of five different stations
 303 due to 2015 geomagnetic storms are plotted in Figure 7. As we have chosen all the stations
 304 lying at the mid station, variation of parameters are almost the same for all stations.
 305 Value of foF2 increases slightly during the main decreasing phase of SYM/H and
 306 decreases during its increasing phase. foF2 in Roquetes has its peak value of 8.7 MHz
 307 at 19:25 LT (07 September) about 3.5 MHz more than in quiet days. Around this time,
 308 critical frequency is maximum in Rome whereas it has minimum value in Dourbes. The
 309 plot of maximum ionization height (hmF2) shows the similar pattern of changes in all

310 five stations. During the main phase (7th september), maximum increase in hmF2 is ob-
 311 served to be ~ 205 km more in Fairford station as compared to the quiet day. Also, the
 312 increase in hmf2 is observed to increase by only 135 KM in Rome and Moscow stations.
 313 However, there is only a slight increase in hmf2 in Roquetes and Dourbes stations. The
 314 plasma vertical drift getting increased by storm-induced circulation is the cause of up-
 315 lifting of the F2 layer (Danilov, 2001). The spikes on the graph decrease and almost co-
 316 incide with the quiet day in the later hours of the third day (08 September).

317 The TEC plot of five stations shows that the variation pattern is similar to each
 318 other. The maximum value of TEC during the main phase is $\sim 40 \times 10^{16} m^{-2}$ about
 319 32 times more than in quiet days, whereas during the recovery phase its value decreases
 320 to $\sim 27 \times 10^{16} m^{-2}$. This increase of TEC during the main phase is due to auroral ac-
 321 tivity, the influx of plasma, and the seasonal effect. TEC content is highest during the
 322 equinox seasons (Xiong et al., 2014). Total electron content in Rome attains its max-
 323 imum, whereas TEC in Dourbes has its lowest value. The TEC and foF2 graph in Fig-
 324 ure 7 doesn't show any latitudinal dependence which contradicts the result as shown by
 325 (W. Liu et al., 2017) and (GAO et al., 2008).

326 4 Cross-Correlation Analysis

327 For all cross-correlation analysis shown in this paper, the y-axis represents normal-
 328 ized correlation coefficients and x-axis represents time lag. Each unit in the x-axis is equiv-
 329 alent to time lag of 15 minutes. The horizontal x-axis represents time (in minutes) rang-
 330 ing (-4500 to +4500). For cross-correlation analysis here, ionospheric parameter is kept
 331 fixed and copies of solar storm indices are shifted (lagged) in all cases. Correlation co-
 332 efficient at each point of lag is calculated, normalized and plotted in the graph.

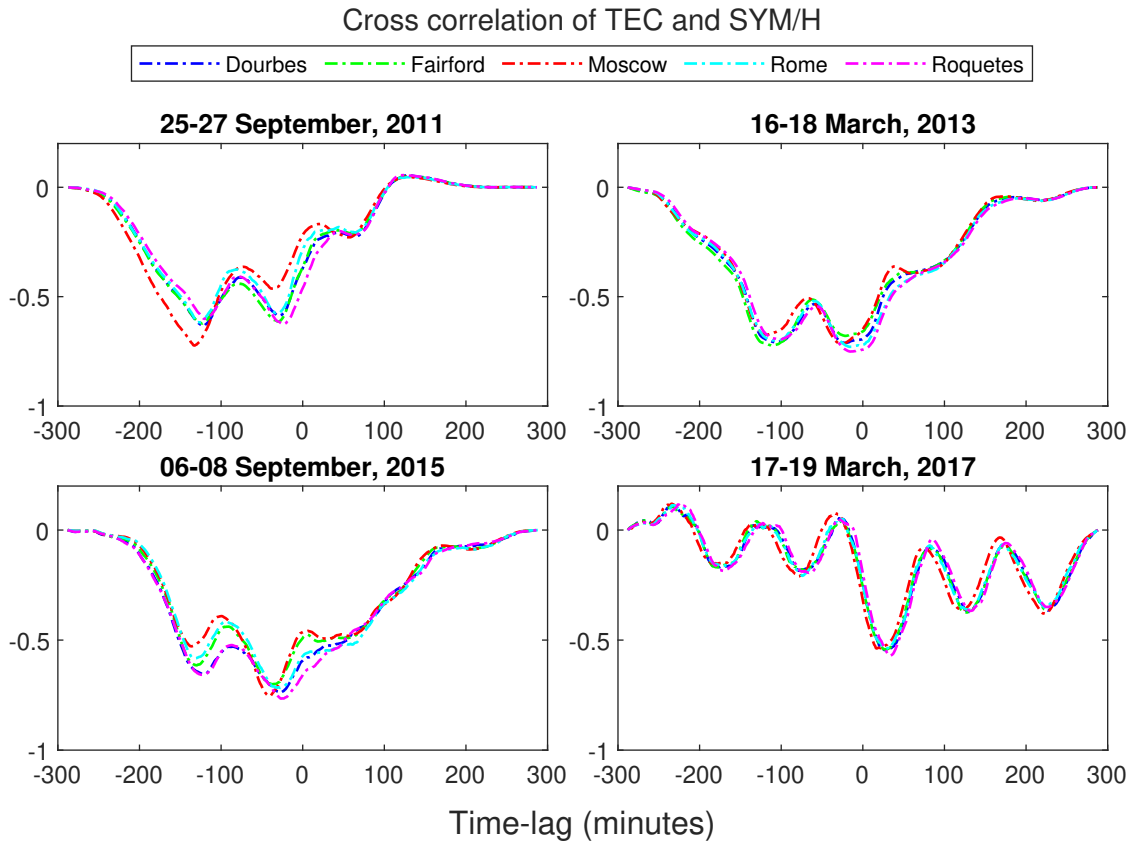


Figure 8. Cross-correlation analysis between TEC and SYM/H during geomagnetic storm of 25–27 September, 2011 (1st Panel), 6–18 March, 2013 (2nd panel), 6–8 September, 2015 (3rd panel) and quiet day on 18–20 March, 2017. X-axis represents time lag (1 unit=15 min) and Y-axis represents correlation coefficient.

333 In Figure 8, cross-correlation between TEC and SYM/H is analyzed. Here, TEC
334 is kept fixed and copies of SYM/H indices is shifted (lagged). In four of the five stations
335 in the 1st panel, TEC leads SYM/H by 1896 minutes (average) with highest negative
336 correlation of -0.6493. But in Roquetes, max negative correlation of -0.6266 leads by only
337 345 minutes. Hence, the maximum anti-correlation is not only observed at one point but
338 at two different points. Average maximum negative correlation at these two points are
339 -0.63972 and -0.5734 at time lag of -1878 minutes (1 day 7 hours and 18 minutes) and
340 -450 minutes (7 hours and 30 minutes) respectively.

341 Similarly, in 2nd panel, in every station except Fairford TEC leads SYM/H by av-
342 erage of 296 minutes with their highest negative correlation of -0.7088 whereas in Fair-
343 ford it is at 1665 minutes with correlation of -0.7580. Similar to 2011, two minimums
344 can be seen here. The average maximum negative correlation of -0.7174 and -0.7006 oc-
345 curs at time lag of -300 minutes and -1623 minutes respectively. Here the most negative
346 correlation occurs at -300 minutes (5 hours) time lag but almost equal anti-correlation
347 is observed at -1623 minutes (1 day 3 hours and 3 minutes).

348 In 3rd panel, each station had their maximum negative correlation around the same
349 time lag. Average correlation of -0.7360 was observed at time lag of -492 minutes (8 hours
350 and 12 minutes). This result matches better with the result of 2nd panel. The quiet day
351 shows moderate anti-correlation with TEC lagging behind SYM/H by about 7 hours in
352 4th panel.

353 All three cross correlation analysis of TEC and SYM/H shows high negative cor-
 354 relation between the variables. At least 5 hours of lead in variation of total electron con-
 355 tent is observed when compared to the SYM/H index. Almost equal evidence of TEC
 356 leading SYM/H by just more than one day can also be obtained from the analysis. This
 357 explains the occurrence of positive storm 1 day prior to the sudden storm commence-
 358 ment (SSC). The mechanism of pre-storm phenomenon (positive storm before main phase
 359 of the storm in mid-latitude region and negative ionospheric storm phase in the equa-
 360 torial region) is an unanswered problem in ionospheric physics (Danilov, 2001) and (Chukwuma,
 361 2010).

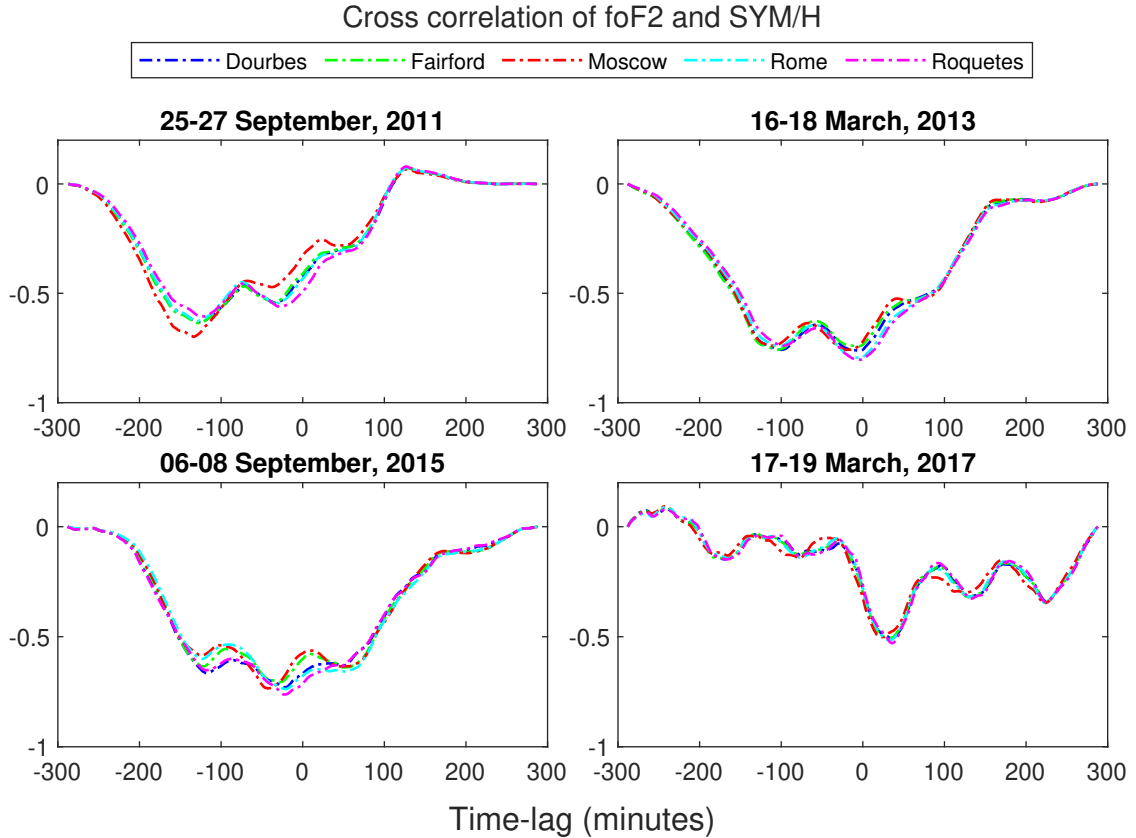


Figure 9. Cross correlation analysis between foF2 and SYM/H during geomagnetic storm of 25–27 September, 2011 (1st Panel), 6–18 March, 2013 (2nd panel), 6–8 September, 2015 (3rd panel) and quiet day on 18–20 March, 2017. X-axis represents time lag (1 unit=15 min) and Y-axis represents correlation coefficient.

362 In Figure 9, cross-correlation analysis between foF2 and SYM/H is plotted. Here,
 363 foF2 is kept fixed and copies of SYM/H indices is shifted for cross-correlation analysis.
 364 In two of the five stations in the 1st panel, Dourbes and Fairford, foF2 leads SYM/H by
 365 1905 minutes with approximately -0.63 negative correlation while Moscow shows max-
 366 imum negative correlation of -0.6992 with lag of 2010 minutes. Roquetes and Rome show
 367 negative correlation of -0.6054 and -0.6275 respectively with respective time lag of -1815
 368 and -1935 minutes. At average, foF2 leads SYM/H by 1914 minutes(1 day 7 hours 54
 369 minutes) with highest negative correlation of -0.6399.

370 Similarly, in second pannel, all stations have perfectly overlapped unlike Moscow
 371 in 2011. It was found that three of five stations, Dourbes, Rome and Roquetes, have min-
 372 imum time lag of -60 minutes from all panels with maximum negative correlation of -

373 0.7631, -0.7949 and -0.8035 respectively. Moscow also shows a maximum negative correlation of -0.7582 with a minimum time lag of -285 minutes (4 hours and 45 minutes)
 374 while Fairford shows minimum negative correlation of -0.7580 but with maximum time lag of -1575 minutes (1 day 2 hours and 15 minutes). In the second panel two minimas
 375 with high negative correlation are observed with foF2 leading SYM/H by at least 1 hour
 376 to more than a day.
 377
 378

379 In panel 3, every station has its highest negative correlation coefficient around the
 380 same time lag. The average of -0.7342 correlation coefficient at lag of -408 minutes (6 hours
 381 48 minutes) is observed. In panel 4, foF2 lags behind SYM/H by about 7 hours with moderate
 382 anti-correlation.

383 All three cross correlation analysis of FoF2 and SYM/H shows high negative correlation
 384 with at least 6 hours of lead in FoF2 signatures compared to the SYM/H index.
 385 Also, evidence of FoF2 leading SYM/H with more than one day can also be obtained from
 386 the analysis. This analysis matches well with the cross-correlation analysis between TEC
 387 and SYM/H. This shows the occurrence of pre-storm phenomena 1 day prior to the sudden
 388 storm commencement (SSC) (Chukwuma, 2010).

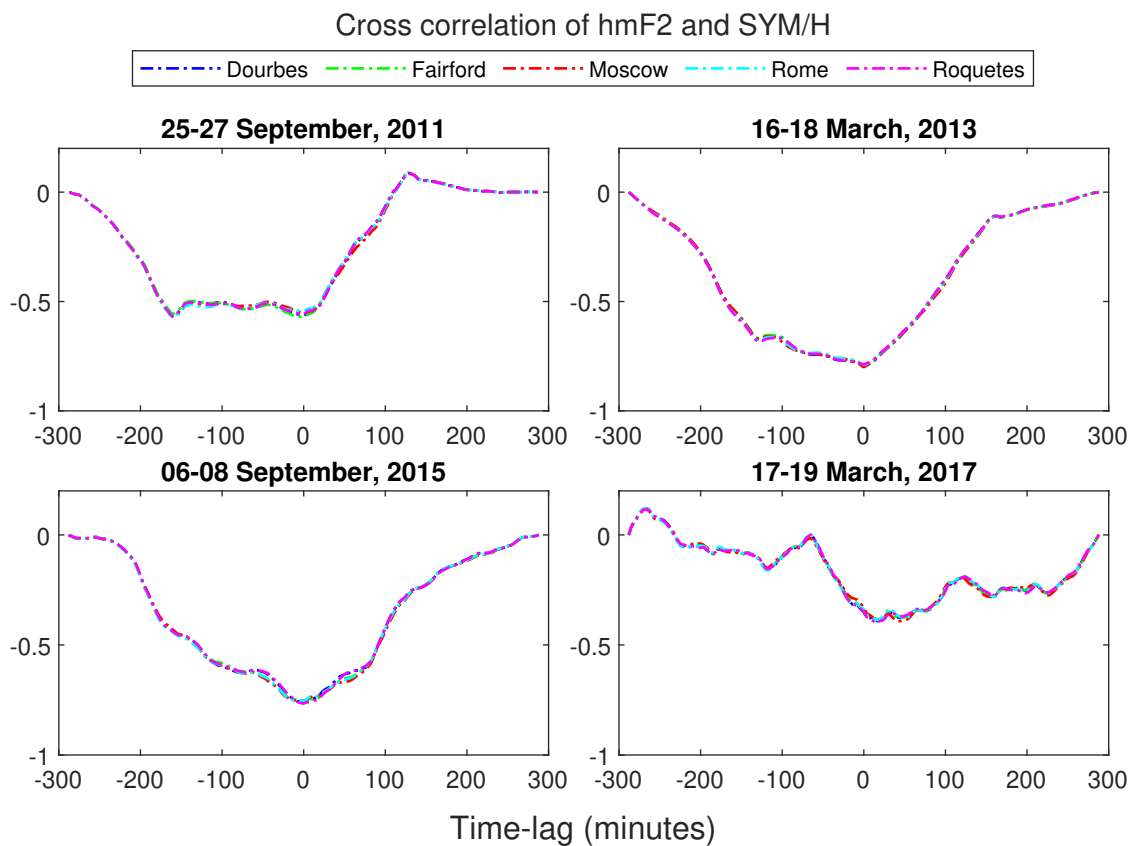


Figure 10. Cross correlation analysis between hmF2 and SYM/H during geomagnetic storm of 25–27 September, 2011 (1st Panel), 6–18 March, 2013 (2nd panel), 6–8 September, 2015 (3rd panel) and quiet day on 18–20 March, 2017. X-axis represents time lag (1 unit=15 min) and Y-axis represents correlation coefficient.

389 Figure 10 represents cross-correlation between hmF2 and SYM/H index. In this
 390 figure hmF2 is kept fixed and copies of SYM/H indices is lagged. In panel 1, there is moderate
 391 negative correlation of -0.5703 between the variables at time lag zero but almost
 392 equal anticorrelation is seen at time lag of -2400 minutes and throughout the points in

393 between. In 2nd panel, high negative correlation of -0.7945 is observed at zero lag. Sim-
 394 ilarly 3rd panel also shows high anticorrelation of -0.7945 with no lag. Compared to other
 395 panels, panel 4 has relatively low correlation at zero lag with correlation less than 0.5.
 396 So, high anti-correlation between the hmF2 and SYM/H is observed at zero lag.

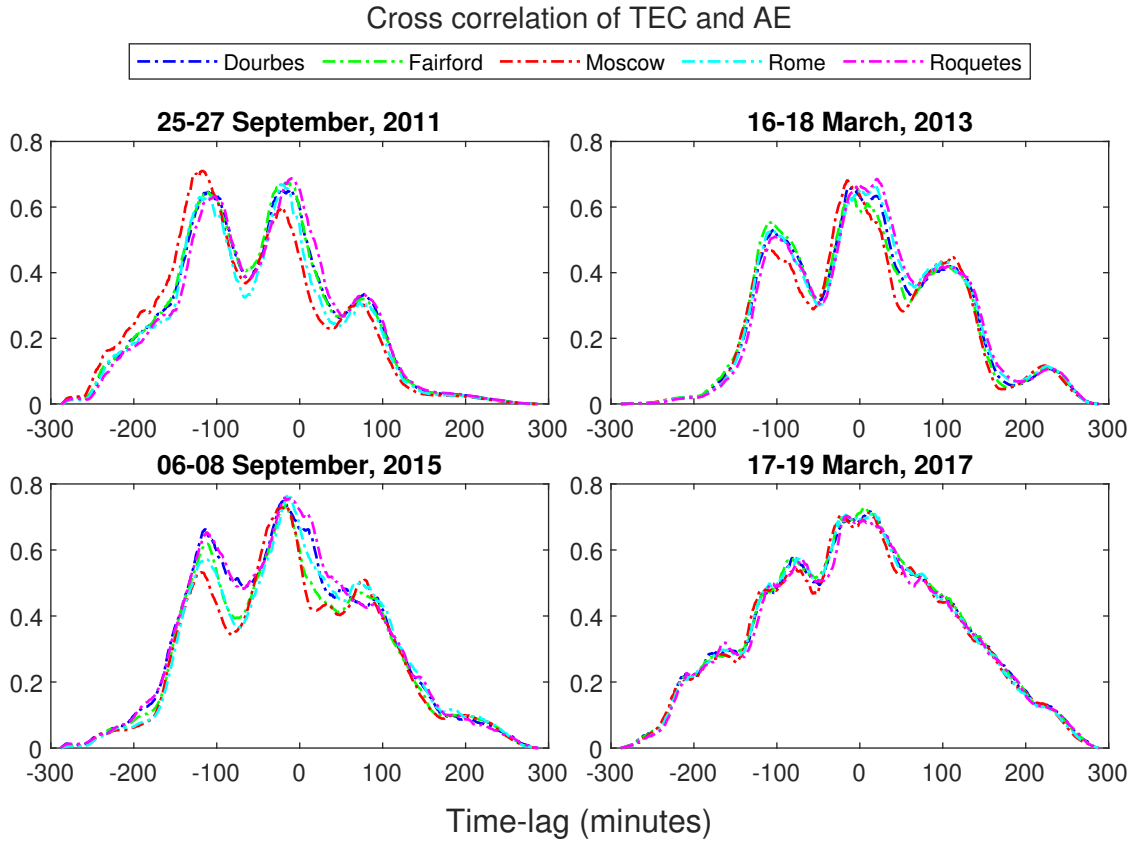


Figure 11. Cross correlation analysis between TEC and AE index during geomagnetic storm of 25–27 September, 2011 (1st Panel), 6–18 March, 2013 (2nd panel), 6–8 September, 2015 (3rd panel) and quiet day on 18–20 March, 2017. X-axis represents time lag (1 unit=15 min) and Y-axis represents correlation coefficient.

397 Cross-correlation between TEC and AE index is analyzed in Figure 11. In panel
 398 1, two maxima can be observed with TEC leading AE by about 4 hours and more than
 399 a day with correlation of 0.7. In the 2nd panel, highest correlation of 0.6649 can be ob-
 400 served at 0 minute time lag.

401 In the third panel, TEC leads AE by 4 hours with highest correlation of 0.7486.
 402 So from the above result it can be said that TEC leads AE by zero to a few hours where
 403 there is high correlation between the variables but also moderate correlation between the
 404 variables can be observed when TEC led AE index by a day. Here, in 4th panel, high
 405 correlation of 0.7 is seen at no lag. This result corresponds well with the result of cross-
 406 correlation analysis between TEC-SYM/H, foF2-SYM/H and foF2-AE as two station-
 407 ary points can be seen in all the graph around same time lag.

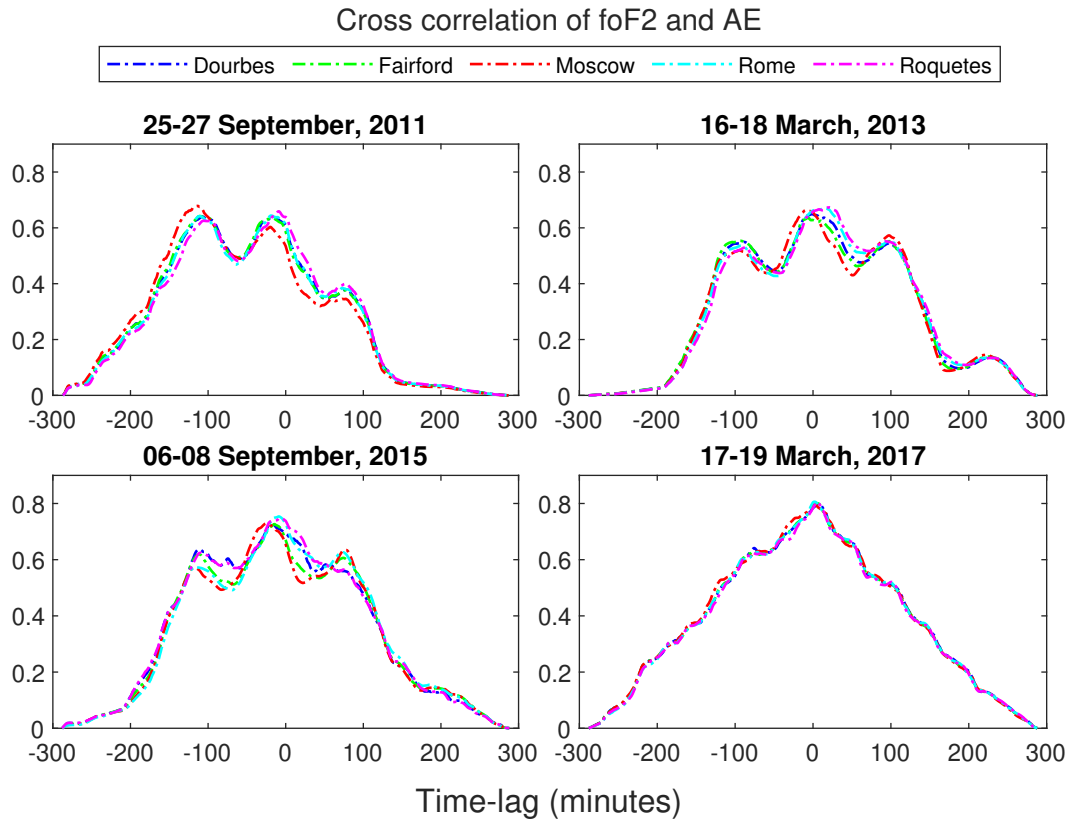


Figure 12. Cross correlation analysis between foF2 and AE index during geomagnetic storm of 25–27 September, 2011 (1st Panel), 6–18 March, 2013 (2nd panel), 6–8 September, 2015 (3rd panel) and quiet day on 18–20 March, 2017. X-axis represents time lag (1 unit=15 min) and Y-axis represents correlation coefficient.

408 In Figure 12, cross correlation between AE index and foF2 is analyzed. In 3 of the
 409 5 stations, Dourbes, Fairford, Moscow, of 1st panel, foF2 leads AE by 1 day 3 hours 40
 410 minutes (average) with highest positive correlation of 0.6536. While in other 2 stations,
 411 Rome and Roquetes, there is the highest positive correlation of 0.6442 and 0.6594 when
 412 foF2 leads AE by 4 hours 45 minutes and 2 hours 15 minutes respectively. Similar to all
 413 other cross-correlation analysis of TEC and foF2, the red curve (Moscow) in the first panel
 414 has higher correlation coefficient in the left stationary point where the ionospheric pa-
 415 rameter led solar storm indices by more than 24 hours. This indicates high pre-storm
 416 effect in Moscow in the first event as compared to the other events.

417 Similarly in 2nd panel, in all the stations, foF2 leads AE by 1 hour with highest
 418 positive correlation of 0.6582. In 3rd panel, each station had their maximum positive cor-
 419 relation around the same time lag. Average correlation of 0.65 was observed at a time
 420 lag of -14.4 (3 hours and 36 minutes). 4th panel shows high correlation at zero time lag.
 421 This result corresponds better with the result of 2013. All three cross correlation anal-
 422 ysis of foF2 and AE index shows at least 1 hours of lead in variation of foF2 when com-
 423 pared to the AE index with moderate positive correlation.

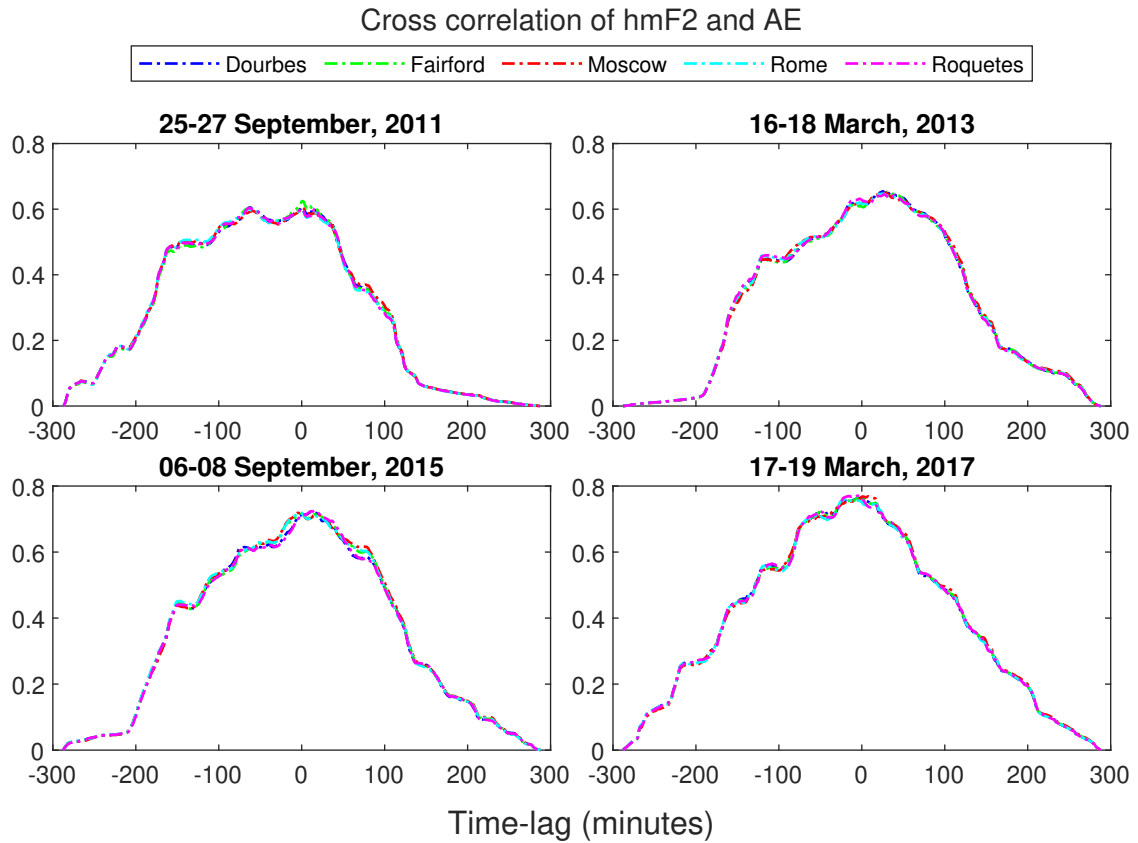


Figure 13. Cross correlation analysis between hmF2 and AE index during geomagnetic storm of 25–27 September, 2011 (1st Panel), 6–18 March, 2013 (2nd panel), 6–8 September, 2015 (3rd panel) and quiet day on 18–20 March, 2017. X-axis represents time lag (1 unit=15 min) and Y-axis represents correlation coefficient.

424 In Figure 13, cross correlation between hmF2 and AE index is analyzed. In the 1st
 425 panel, three stations show highest correlation of 0.6 at time lag of -945 minutes (15 hours
 426 and 45 minutes). Fairford shows the highest positive correlation of 0.6246 with time lag
 427 of just -15 min which is similar to that of Moscow with correlation of 0.6047 respectively.

428 But 2nd panel, in all the stations, AE leads hmF2 by average of 411 minutes (6 hours
 429 and 51 minutes) with highest positive correlation of 0.6501. In 3rd panel, in all stations,
 430 hmF2 lags behind AE by maximum positive correlation of 0.7207 by 72 minutes. There
 431 is high correlation in panel 4 at zero lag.

432 From this result it can be seen that the average lead or lag between hmF2 and AE
 433 index is about ± 2 hours depending upon the type of storm with moderate positive cor-
 434 relation.

435 5 Conclusion

436 In a nutshell, the following conclusions can be drawn out from the cross-correlation
 437 analysis of ionospheric parameters and solar storm indices.

- 438 1. It is observed that the values of Total Electron Content (TEC) and F2 region crit-
 439 ical frequency (foF2) for the events with presence of Sudden Storm Commencement
 440 (SSC) had a strong latitudinal dependence in mid-latitude regions with stations
 441 at higher latitude having relatively lower values and those at lower latitudes hav-

- 442 ing relatively higher values while the event with gradual storm commencement showed
 443 no such dependence.
- 444 2. It is found that the positive storm started a day before the events and remained
 445 so throughout the main phase, then decreased during the recovery phase.
 - 446 3. The cross-correlation analysis of TEC and foF2 with solar storm indices shows two
 447 stationary points at these two time lags with almost equal magnitude of correla-
 448 tion coefficient. This hints strongly to the occurrence of pre-storm phenomenon
 449 at least few hours prior to the main phase of the geomagnetic storm.
 - 450 4. The Maximum Ionization Height of F2 layer (hmF2), showed no pre-storm effect
 451 as highest correlation between hmF2 and solar storm indices occurred mostly at
 452 zero time lag.
 - 453 5. It is observed that there is a strong correlation of Symmetric-H and Auroral Elec-
 454 trojet Indices with other ionospheric parameters. This is attributed to the fact that
 455 the coupling mechanism between ionosphere and magnetosphere produces extreme
 456 electric field disturbances in the middle low latitude regions.
 - 457 6. The highest correlation between ionospheric parameters is mostly observed for Event
 458 1 a day prior to main phase of geomagnetic storm before. This might be due to
 459 the Event 1 being caused by the most intense solar flare (X1.9 flare) among the
 460 events selected which resulted in the strongest pre-storm effects.
 - 461 7. It is observed that despite Events 1 and 3 having the same seasonal condition, the
 462 pre-storm phenomenon is completely different. This difference stems from the na-
 463 ture of the two events i.e. Event 1 occurring with sudden storm commencement
 464 and Event 3 without SSC. Also, Moscow, which lies at the highest latitude, gets
 465 affected by pre-storm phenomenon much more significantly in Event 1 when com-
 466 pared to other events.

467 Acknowledgments

468 In this work, we have used the Omni Web (<http://omni-web.gsfc.nasa.gov/>) for in-
 469 terplanetary magnetic fields, solar wind parameters and geomagnetic indices. Global Iono-
 470 sphere Radio Observatory (GIRO) <https://giro.uml.edu/> provided the ionospheric
 471 parameters. The stations list was obtained from <https://lgdc.uml.edu/common/DIDBFastStationList>.
 472 The Authors would like to thank the support provided.

473 Authors' contributions

474 All the authors contributed equally to this work.

475 References

- 476 Adekoya, B., Chukwuma, V., Bakare, N., & David, T. (2012). On the effects of
 477 geomagnetic storms and pre storm phenomena on low and middle latitude
 478 ionospheric f2. *Astrophysics and Space Science*, *340*(2), 217–235.
- 479 Adhikari, B., Dahal, S., Sapkota, N., Baruwal, P., Bhattarai, B., Khanal, K., &
 480 Chapagain, N. P. (2018). Field-aligned current and polar cap potential and
 481 geomagnetic disturbances: A review of cross-correlation analysis. *Earth and*
 482 *Space Science*, *5*(9), 440–455.
- 483 Baker, D., Jaynes, A., Li, X., Henderson, M., Kanekal, S., Reeves, G., . . . others
 484 (2014). Gradual diffusion and punctuated phase space density enhancements
 485 of highly relativistic electrons: Van allen probes observations. *Geophysical*
 486 *Research Letters*, *41*(5), 1351–1358.
- 487 Bothmer, V., & Schwenn, R. (1994). Eruptive prominences as sources of mag-
 488 netic clouds in the solar wind. *Mass Supply and Flows in the Solar Corona*,
 489 215–220.

- 490 Buonsanto, M. J. (1999). Ionospheric storms—a review. *Space Science Reviews*,
491 88(3), 563–601.
- 492 Chukwuma, V. U. (2010). On ionospheric phenomena during pre-storm and main
493 phase of a very intense geomagnetic storm. *Acta Geophysica*, 58(6), 1164–
494 1192.
- 495 Crooker, N., & McAllister, A. (1997). Transients associated with recurrent storms.
496 *Journal of Geophysical Research: Space Physics*, 102(A7), 14041–14047.
- 497 Danilov, A. (2001). F2-region response to geomagnetic disturbances. *Journal of At-*
498 *mospheric and Solar-Terrestrial Physics*, 63(5), 441–449.
- 499 Du, A., Tsurutani, B., & Sun, W. (2011). Solar wind energy input during prolonged,
500 intense northward interplanetary magnetic fields: A new coupling function.
501 *Journal of Geophysical Research: Space Physics*, 116(A12).
- 502 Fagundes, P. R., Cardoso, F., Fejer, B., Venkatesh, K., Ribeiro, B., & Pillat, V.
503 (2016). Positive and negative gps-tec ionospheric storm effects during the ex-
504 treme space weather event of march 2015 over the brazilian sector. *Journal of*
505 *Geophysical Research: Space Physics*, 121(6), 5613–5625.
- 506 Foster, J., Fairfield, D., Ogilvie, K., & Rosenberg, T. (1971). *Relationship of in-*
507 *terplanetary parameters and occurrence of magnetospheric substorms*. (Tech.
508 Rep.). Univ. of Maryland, College Park.
- 509 Fuller-Rowell, T., Codrescu, M., Moffett, R., & Quegan, S. (1994). Response of the
510 thermosphere and ionosphere to geomagnetic storms. *Journal of Geophysical*
511 *Research: Space Physics*, 99(A3), 3893–3914.
- 512 GAO, Q., LIU, L.-B., ZHAO, B.-Q., WAN, W.-X., ZHANG, M.-L., & NING, B.-
513 Q. (2008). Statistical study of the storm effects in middle and low latitude
514 ionosphere in the east-asian sector. *Chinese Journal of geophysics*, 51(3),
515 435–443.
- 516 Gonzalez, W., Joselyn, J.-A., Kamide, Y., Kroehl, H. W., Rostoker, G., Tsurutani,
517 B., & Vasyliunas, V. (1994). What is a geomagnetic storm? *Journal of*
518 *Geophysical Research: Space Physics*, 99(A4), 5771–5792.
- 519 Gonzalez, W. D., & Tsurutani, B. T. (1987). Criteria of interplanetary parameters
520 causing intense magnetic storms (dst \geq 100 nt). *Planetary and Space Science*,
521 35(9), 1101–1109.
- 522 Gosling, J. (1993a). Coronal mass ejections: The link between solar and geomagnetic
523 activity. *Physics of Fluids B: Plasma Physics*, 5(7), 2638–2645.
- 524 Gosling, J. (1993b). *The solar flare myth in solar-terrestrial physics* (Tech. Rep.).
525 Los Alamos National Lab., NM (United States).
- 526 Hargreaves, J. K. (1992). *The solar-terrestrial environment: an introduction to*
527 *geospace—the science of the terrestrial upper atmosphere, ionosphere, and mag-*
528 *netosphere*. Cambridge university press.
- 529 Kawamura, S., Balan, N., Otsuka, Y., & Fukao, S. (2002). Annual and semian-
530 nual variations of the midlatitude ionosphere under low solar activity. *Journal*
531 *of Geophysical Research: Space Physics*, 107(A8), SIA–8.
- 532 Klimenko, M. V., Klimenko, V. V., Zakharenkova, I. E., Ratovsky, K. G., Ko-
533 renkova, N. A., Yasyukevich, Y. V., . . . Cherniak, I. V. (2017). Similarity
534 and differences in morphology and mechanisms of the fof2 and tec disturbances
535 during the geomagnetic storms on 26–30 september 2011. In *Annales geophysi-*
536 *cae* (Vol. 35, pp. 923–938).
- 537 Kolawole, M. (2003). *Radar systems, peak detection and tracking*. Elsevier.
- 538 Lei, J., Liu, L., Wan, W., & Zhang, S.-R. (2005). Variations of electron density
539 based on long-term incoherent scatter radar and ionosonde measurements over
540 millstone hill. *Radio science*, 40(2), 1–10.
- 541 Liu, J., Chen, Y., & Lin, J. (2003). Statistical investigation of the saturation ef-
542 fect in the ionospheric fof2 versus sunspot, solar radio noise, and solar euv
543 radiation. *Journal of Geophysical Research: Space Physics*, 108(A2).
- 544 Liu, L., Wan, W., Ning, B., Pirog, O., & Kurkin, V. (2006). Solar activity varia-

- 545 tions of the ionospheric peak electron density. *Journal of Geophysical Research:*
546 *Space Physics*, 111(A8).
- 547 Liu, W., Xu, L., Xiong, C., & Xu, J. (2017). The ionospheric storms in the american
548 sector and their longitudinal dependence at the northern middle latitudes. *Ad-*
549 *vances in Space Research*, 59(2), 603–613.
- 550 Lugaz, N., Farrugia, C. J., Smith, C. W., & Paulson, K. (2015). Shocks inside cmes:
551 A survey of properties from 1997 to 2006. *Journal of Geophysical Research:*
552 *Space Physics*, 120(4), 2409–2427.
- 553 Luhmann, J. (1997). What do we really know about solar wind coupling? *Advances*
554 *in Space Research*, 20(4-5), 907–911.
- 555 Marques de Souza, A., Echer, E., Bolzan, M. J. A., & Hajra, R. (2018). Cross-
556 correlation and cross-wavelet analyses of the solar wind imf b z and auroral
557 electrojet index ae coupling during hildcaas. In *Annales geophysicae* (Vol. 36,
558 pp. 205–211).
- 559 Mendillo, M. (2006). Storms in the ionosphere: Patterns and processes for total elec-
560 tron content. *Reviews of Geophysics*, 44(4).
- 561 Moen, J., Qiu, X., Carlson, H., Fujii, R., & McCrea, I. (2008). On the diurnal vari-
562 ability in f2-region plasma density above the eiscat svalbard radar. In *Annales*
563 *geophysicae* (Vol. 26, pp. 2427–2433).
- 564 Pandit, D., Chapagain, N. P., Adhikari, B., Nemirovskaya, I. A., Gordeev, V. V.,
565 Kovalenko, D., . . . others (2021). Analysis of the solar wind imf b z and auro-
566 ral electrojet index during supersubstorms. *Russian Journal of Earth Sciences*,
567 21(5), 1–10.
- 568 Prölss, G. (1995). *Ionospheric f-region storms, handbook of atmospheric electrody-*
569 *namics, vol. 2*. CRC Press/Boca Raton.
- 570 Prölss, G., & Očko, M. (2000). Propagation of upper atmospheric storm effects to-
571 wards lower latitudes. *Advances in Space Research*, 26(1), 131–135.
- 572 Rangarajan, G. (1989). Indices of geomagnetic activity. *Geomatik*, 3, 323–384.
- 573 Richards, P. (2001). Seasonal and solar cycle variations of the ionospheric peak elec-
574 tron density: Comparison of measurement and models (paper 2000ja000365).
575 *JOURNAL OF GEOPHYSICAL RESEARCH-ALL SERIES-*, 106(7; SECT
576 1), 12–803.
- 577 Sethi, N., & Pandey, V. (2001). Comparative study of electron density from in-
578 coherent scatter measurements at arecibo with the iri-95 model during solar
579 maximum. In *Annales geophysicae* (Vol. 18, pp. 1630–1634).
- 580 Souza, J., Brum, C., Abdu, M., Batista, I., Asevedo Jr, W., Bailey, G., & Bitten-
581 court, J. (2010). Parameterized regional ionospheric model and a comparison
582 of its results with experimental data and iri representations. *Advances in Space*
583 *Research*, 46(8), 1032–1038.
- 584 Sugiura, M., Kertz, W., Price, A., & Stone, D. (1964). *P. 1. hourly values of equato-*
585 *rial dst for the igy*. Pergamon Press.
- 586 Verkhoglyadova, O., Tsurutani, B., Mannucci, A., Mlynczak, M., Hunt, L., Paxton,
587 L., & Komjathy, A. (2016). Solar wind driving of ionosphere-thermosphere re-
588 sponses in three storms near st. patrick’s day in 2012, 2013, and 2015. *Journal*
589 *of Geophysical Research: Space Physics*, 121(9), 8900–8923.
- 590 Volland, H. (1995). *Handbook of atmospheric electrodynamicics* (Vol. 2). CRC Press.
- 591 Wanliss, J. A., & Showalter, K. M. (2006). High-resolution global storm index: Dst
592 versus sym-h. *Journal of Geophysical Research: Space Physics*, 111(A2).
- 593 Xiong, C., Lühr, H., Wang, H., & Johnsen, M. G. (2014). Determining the bound-
594 aries of the auroral oval from champ field-aligned current signatures–part 1. In
595 *Annales geophysicae* (Vol. 32, pp. 609–622).
- 596 Youssef, M., Mahrous, A., Mawad, R., Ghamry, E., Shaltout, M., El-Nawawy, M.,
597 & Fahim, A. (2012). The effects of the solar magnetic polarity and the solar
598 wind velocity on bz-component of the interplanetary magnetic field. *Advances*
599 *in space research*, 49(7), 1198–1202.

- 600 Zhang, M.-L., Liu, C., Wan, W., Liu, L., & Ning, B. (2009). A global model of
601 the ionospheric f2 peak height based on eof analysis. In *Annales geophysicae*
602 (Vol. 27, pp. 3203–3212).
- 603 Zhang, S.-R., & Holt, J. (2008). Ionospheric climatology and variability from
604 long-term and multiple incoherent scatter radar observations: Variability. In
605 *Annales geophysicae* (Vol. 26, pp. 1525–1537).

Table 1: Table of Stations.

S.No.	Stations Name	URSI	Latitude	Longitude
1.	DOORBES	DB049	50.10	4.60
2.	FAIRFORD	FF051	51.70	358.50
3.	MOSCOW	MO155	55.47	37.30
4.	ROME	RO041	41.80	12.50
5.	ROQUETES	EB040	40.80	0.50

Figure.

Stations Co-ordinate

Latitude

70°N

60°N

50°N

40°N

30°N



1000 km

500 mi

15°W

0°

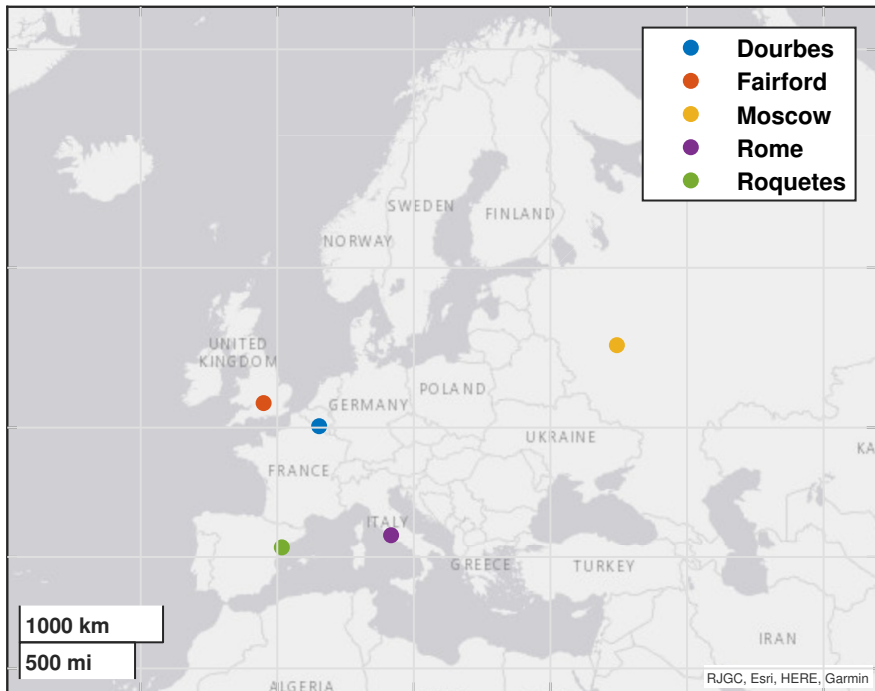
15°E

30°E

45°E

60°E

Longitude



RJGC, Esri, HERE, Garmin

Figure.

25-27 September, 2011

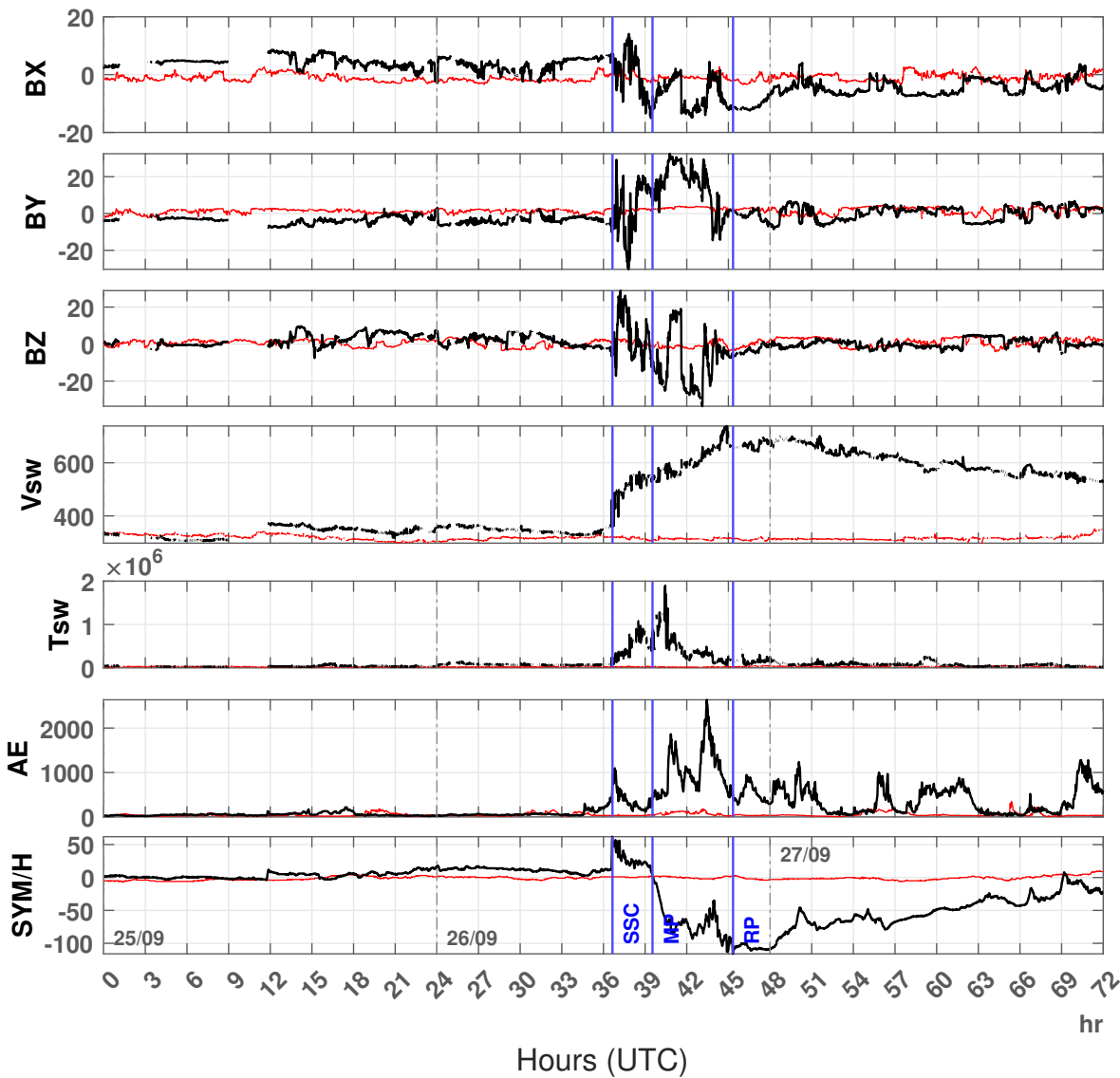
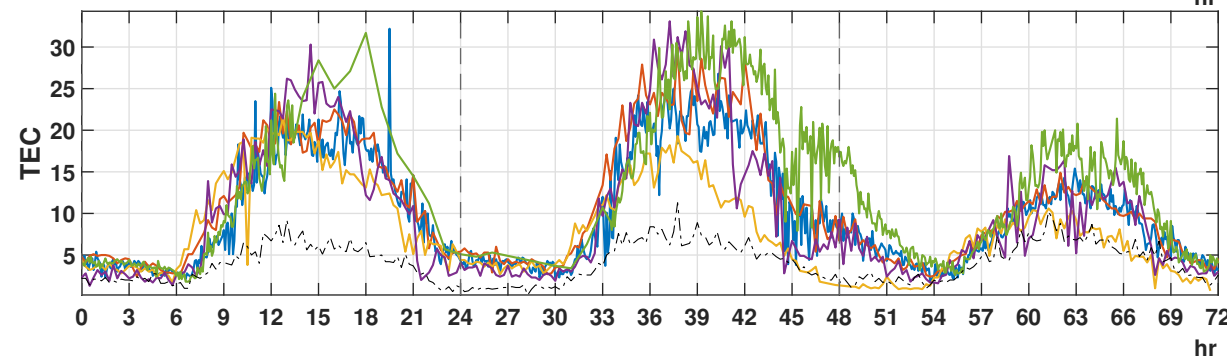
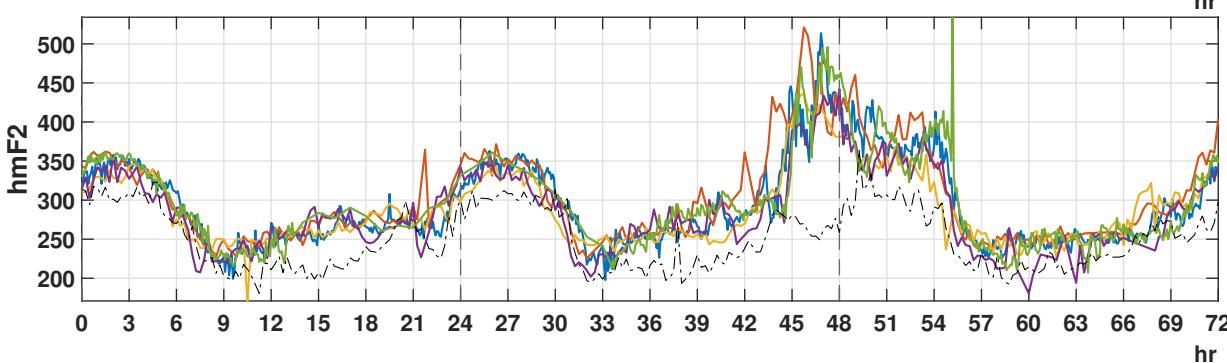
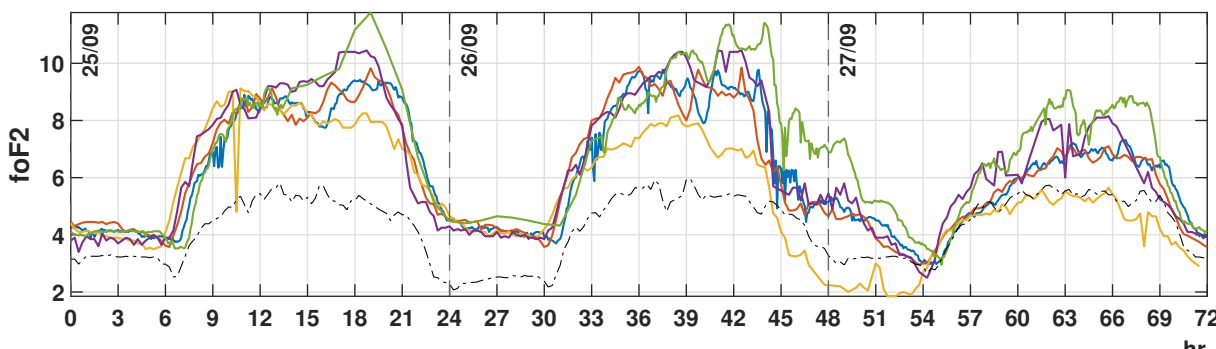


Figure.

25-27 September, 2011



Local Time (Hours)

Figure.

16-18 March, 2013

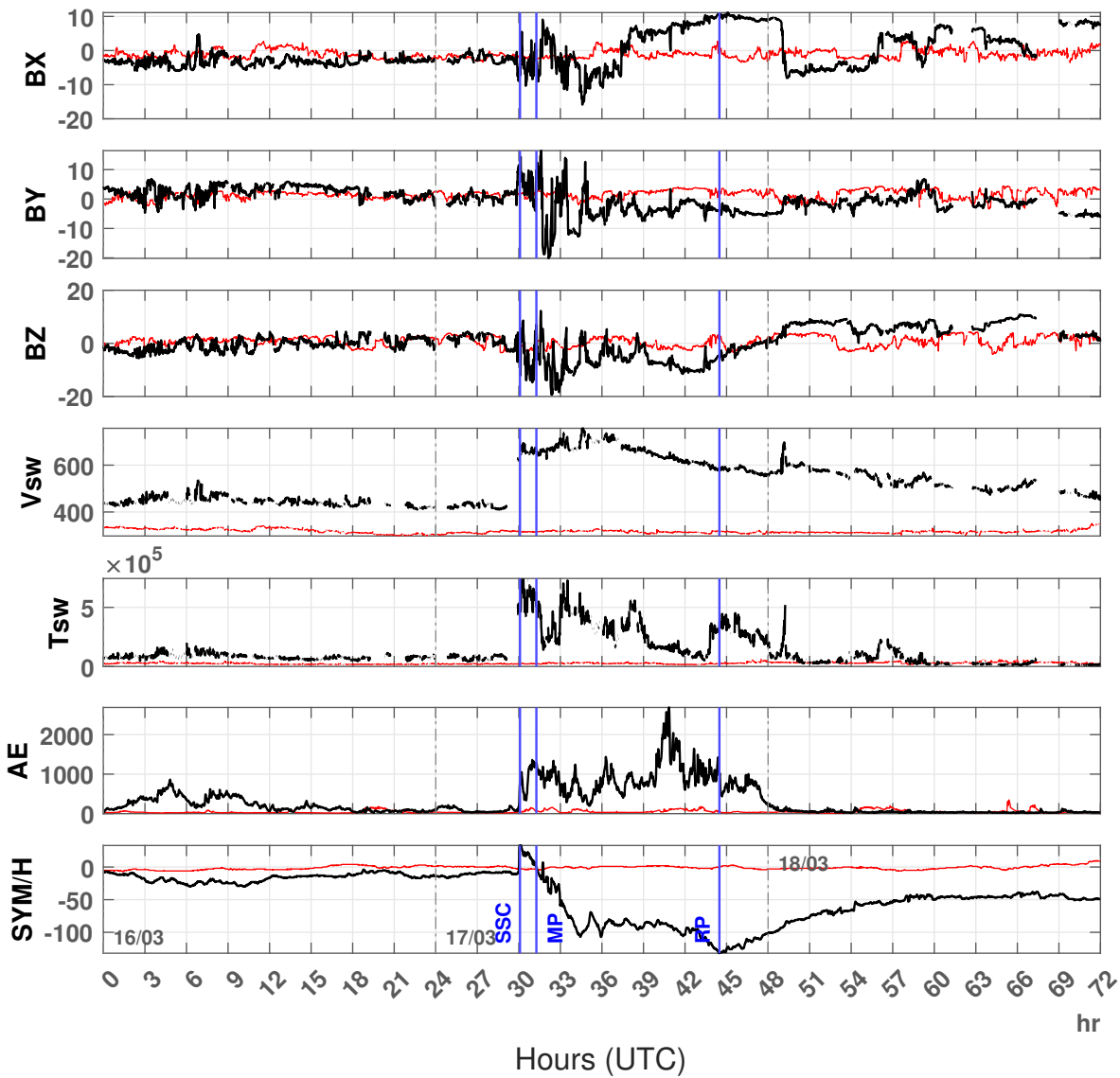
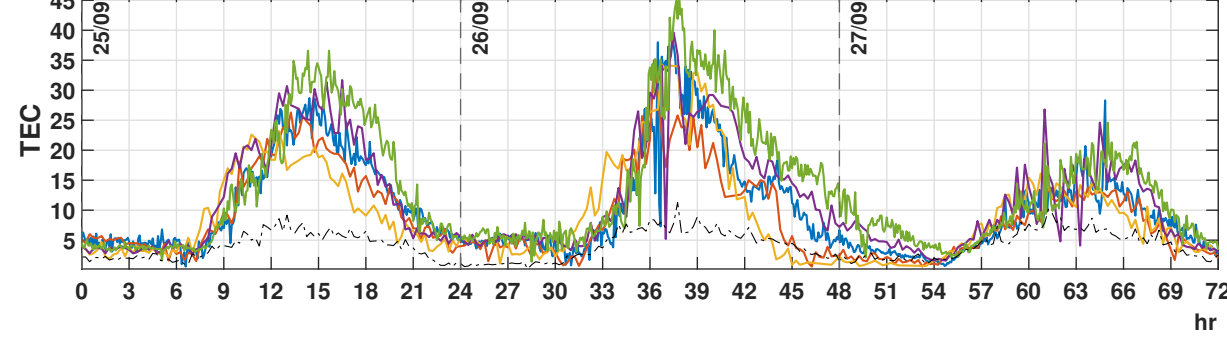
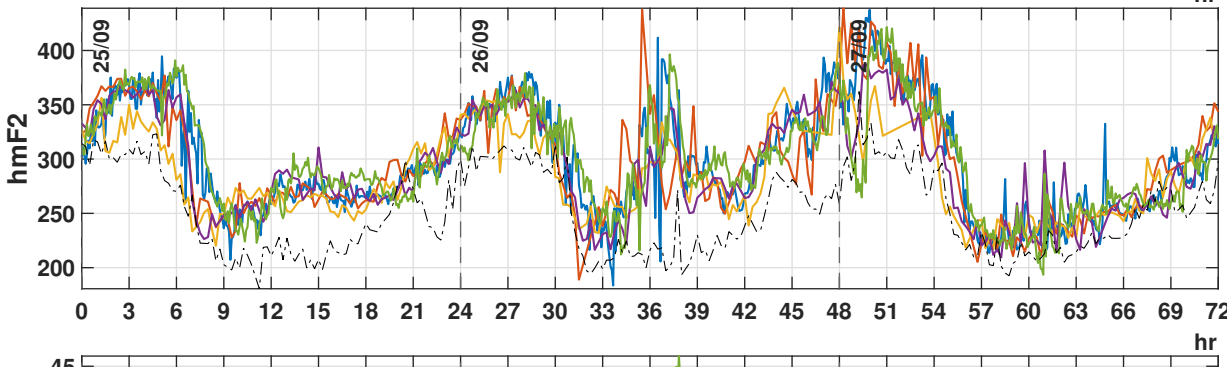
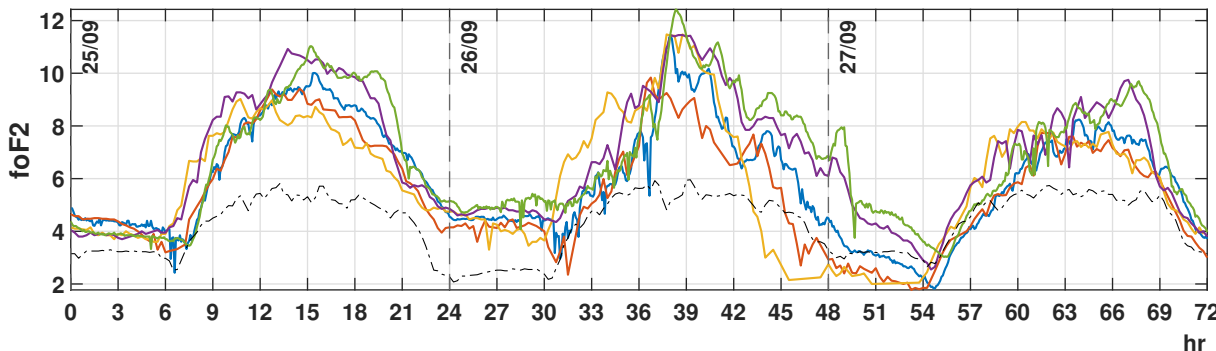


Figure.

16-18 March, 2013



Local Time (Hours)

Figure.

06-08 September, 2015

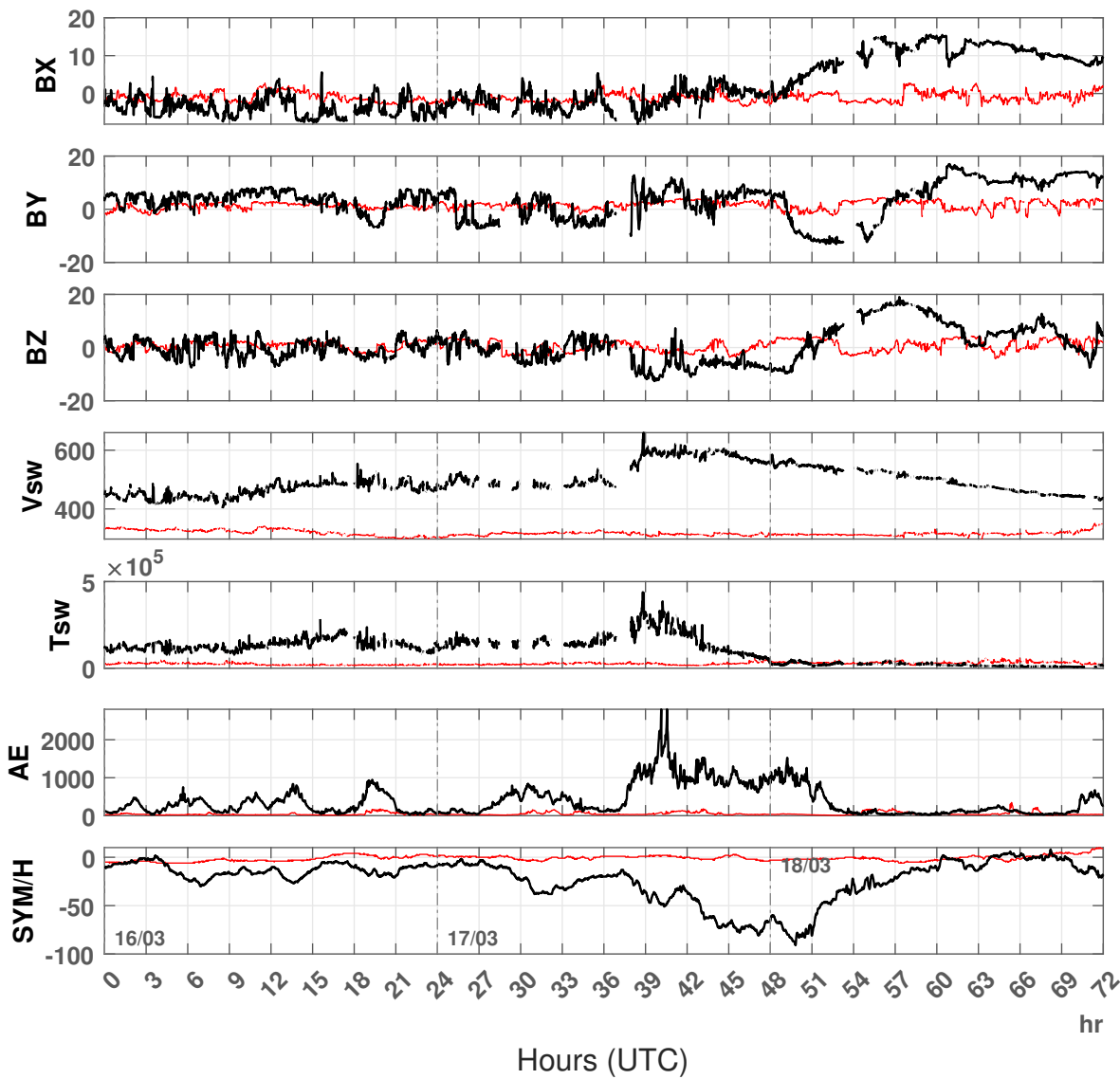
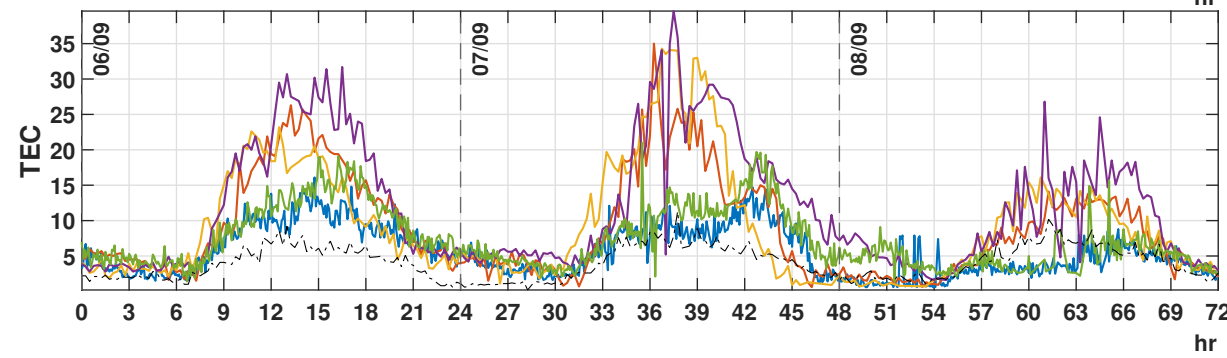
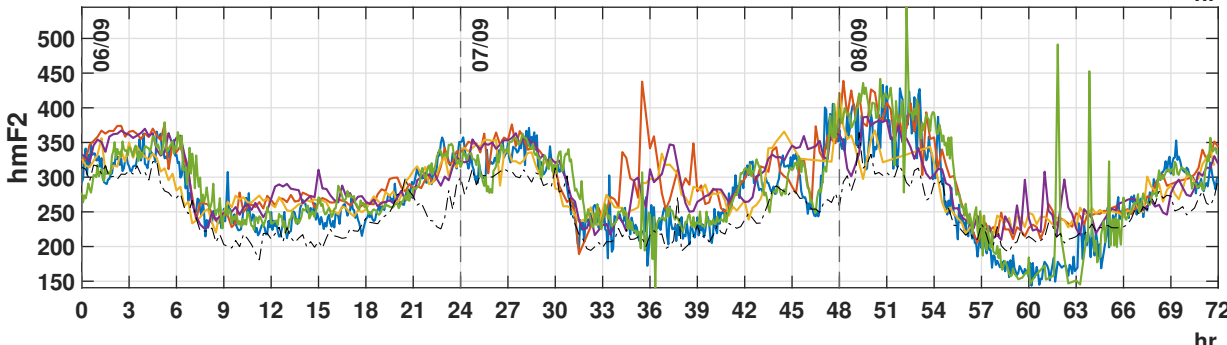
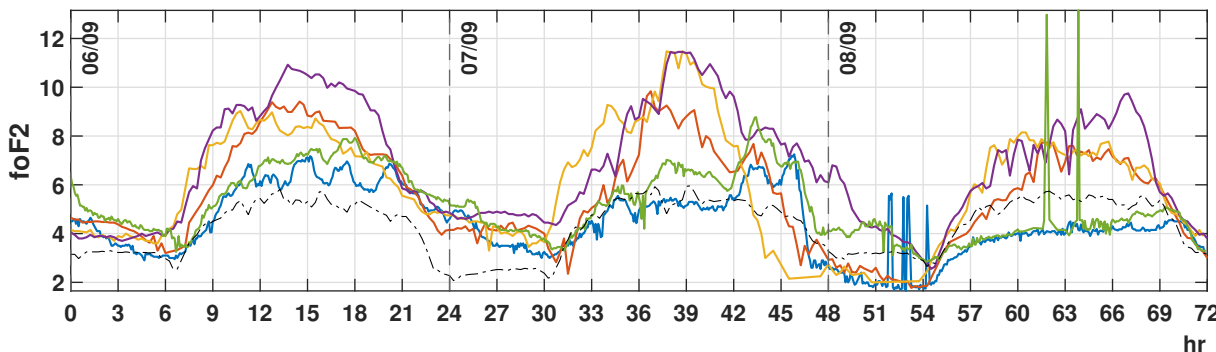


Figure.

06-08 September, 2015



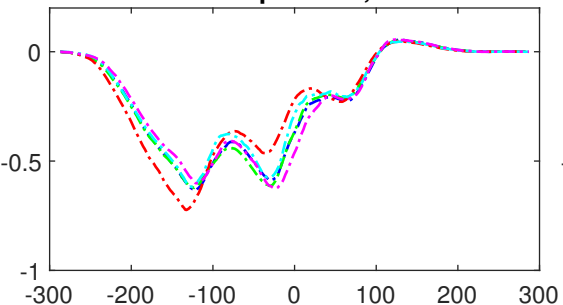
Local Time (Hours)

Figure.

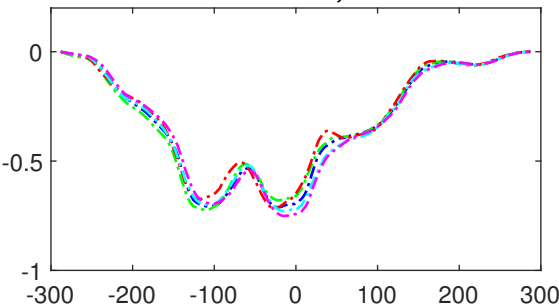
Cross correlation of TEC and SYM/H



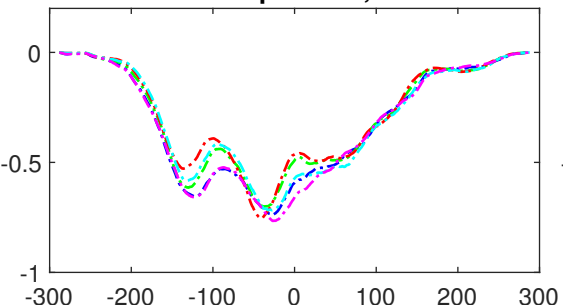
25-27 September, 2011



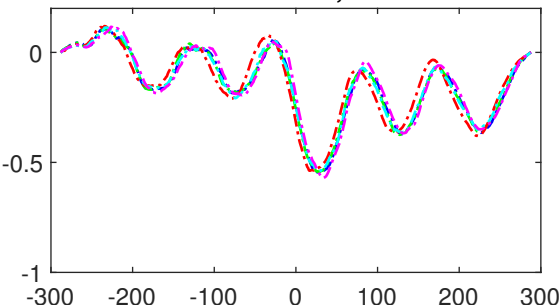
16-18 March, 2013



06-08 September, 2015



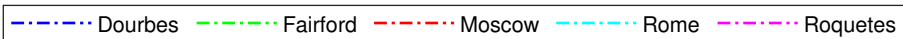
17-19 March, 2017



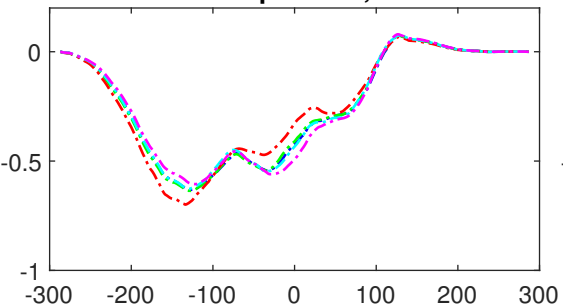
Time-lag (minutes)

Figure.

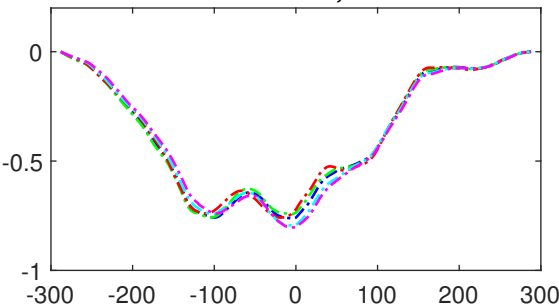
Cross correlation of foF2 and SYM/H



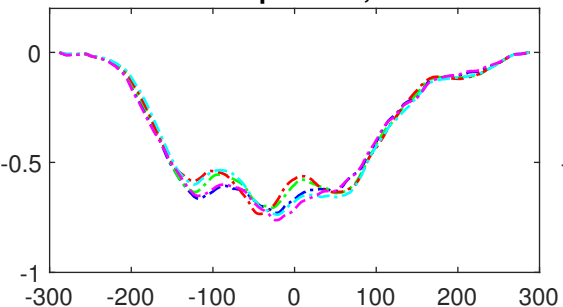
25-27 September, 2011



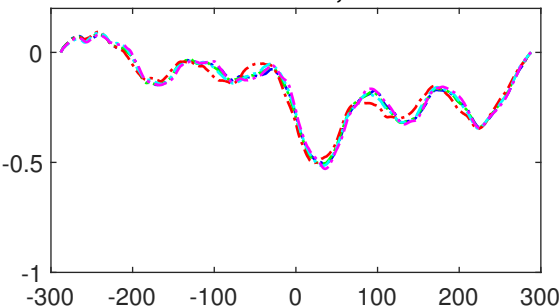
16-18 March, 2013



06-08 September, 2015



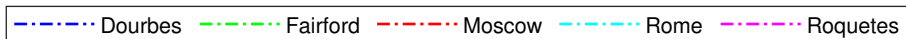
17-19 March, 2017



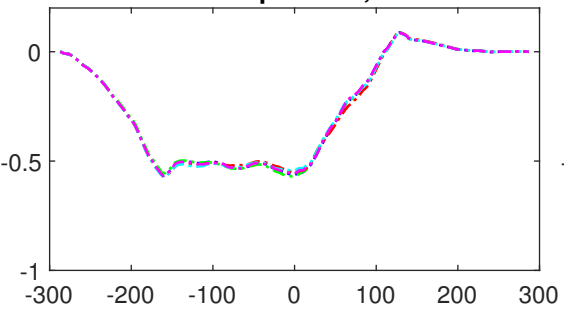
Time-lag (minutes)

Figure.

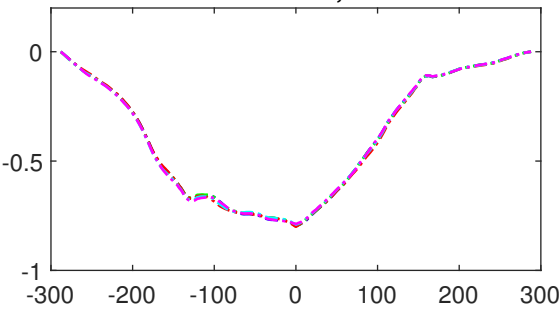
Cross correlation of hmF2 and SYM/H



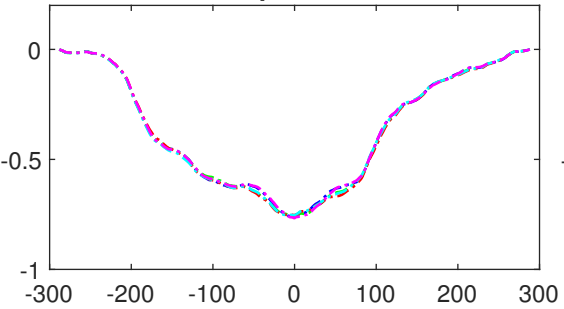
25-27 September, 2011



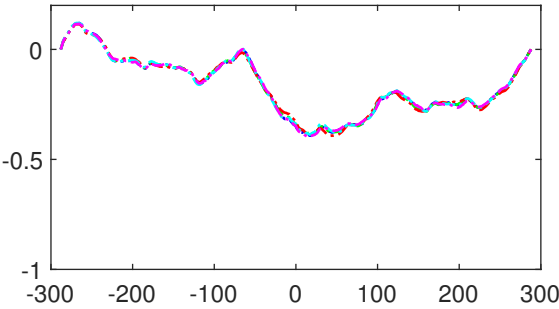
16-18 March, 2013



06-08 September, 2015



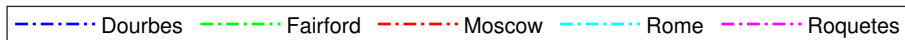
17-19 March, 2017



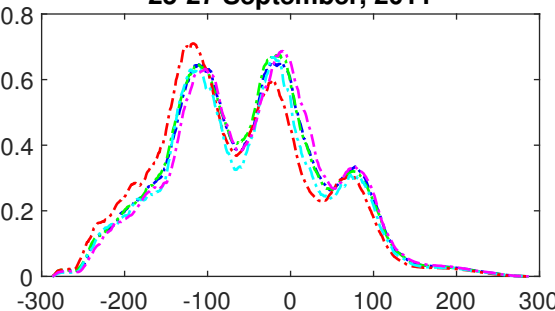
Time-lag (minutes)

Figure.

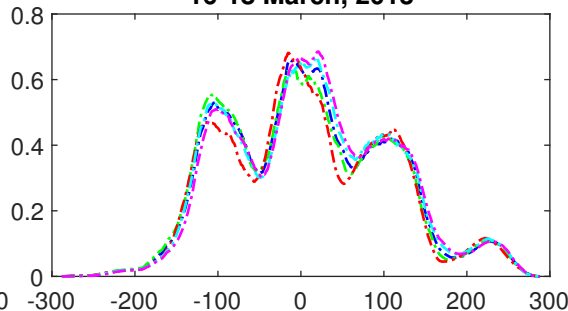
Cross correlation of TEC and AE



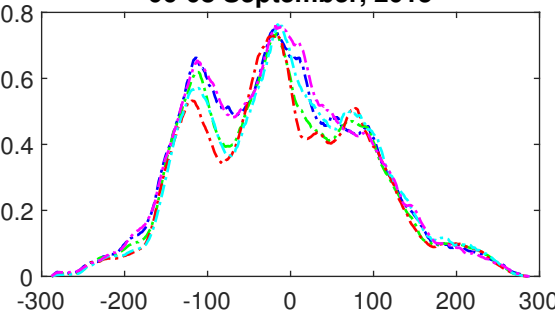
25-27 September, 2011



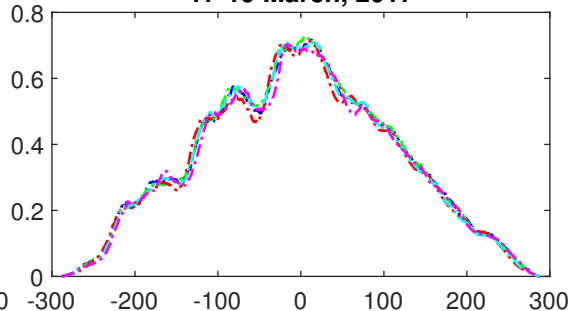
16-18 March, 2013



06-08 September, 2015



17-19 March, 2017



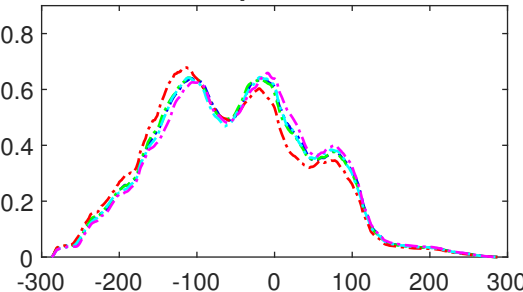
Time-lag (minutes)

Figure.

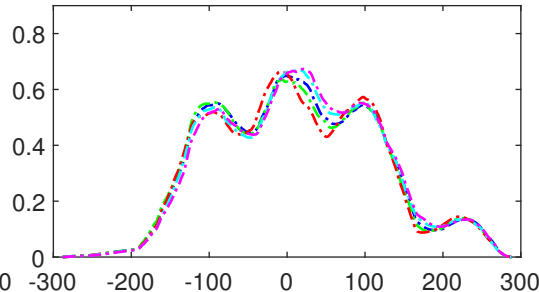
Cross correlation of foF2 and AE



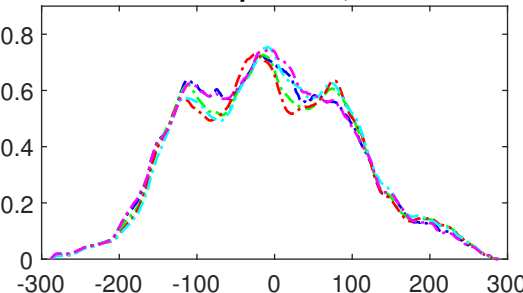
25-27 September, 2011



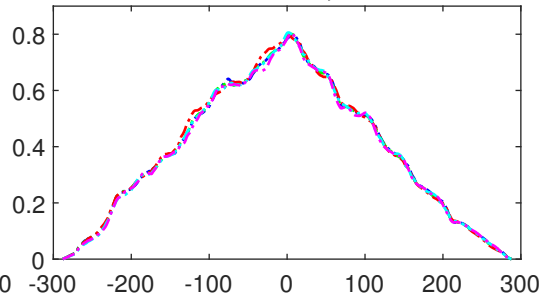
16-18 March, 2013



06-08 September, 2015



17-19 March, 2017



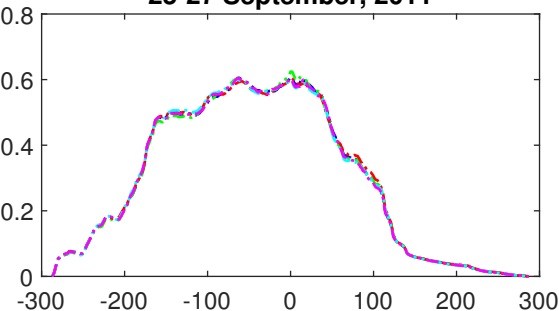
Time-lag (minutes)

Figure.

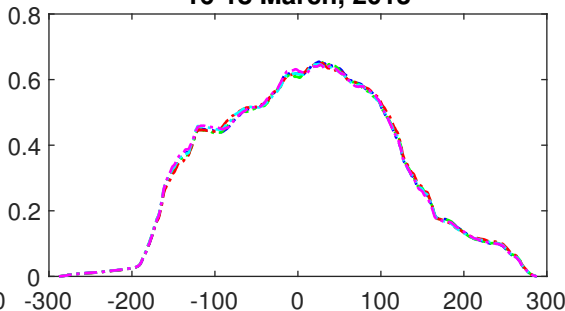
Cross correlation of hmF2 and AE



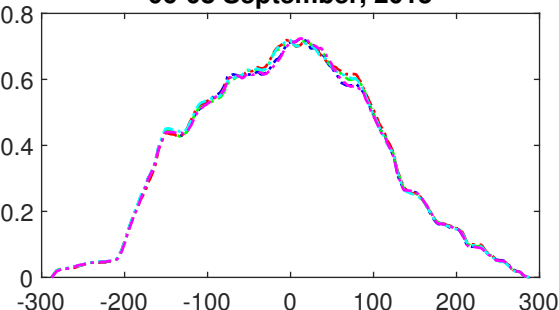
25-27 September, 2011



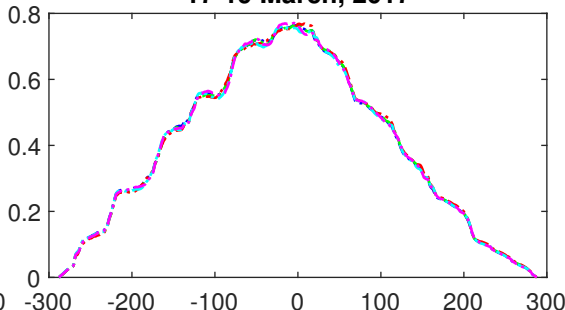
16-18 March, 2013



06-08 September, 2015



17-19 March, 2017



Time-lag (minutes)

1 **Cross Correlation Analysis of Ionospheric Parameters**
2 **with Symmetric-H and Auroral Electrojet Indices**
3 **during Geomagnetic Storms**

4 **Samyam Pudasaini¹, Binod Adhikari², Rohit Bhattarai¹, Iva Kumari**
5 **Lamichhane¹, Manghang Limbu¹, Pramod Kamal Kharel¹, Aasis Bhandari¹,**
6 **Pitri Bhakta Adhikari¹**

7 ¹Department of Physics, Tri-Chandra Multiple College, Tribhuvan University, Kathmandu, Nepal

8 ²Department of Physics, St. Xavier's College, Maitighar, Kathmandu, Nepal

9 **Key Points:**

- 10 • There is a strong evidence of pre-storm phenomenon occurring at least a few hours
11 and more than 24 hours prior to the main phase of the geomagnetic storms.
- 12 • The TEC and foF2 parameters have strong dependence with latitudes for the events
13 with Sudden Storm Commencement (SSC) in the middle latitudes region.
- 14 • The highest correlations of geomagnetic indices with ionospheric parameters are
15 mostly observed one day prior to main phase of geomagnetic storm.

Corresponding author: Priti Bhakta Adhikari, pbadhikari09@gmail.com

Abstract

This paper investigates the effects of geomagnetic storms of 25-27 September 2011, 16-18 March 2013, and 6-8 September 2015 over five mid latitude stations (Dourbes, Fairford, Moscow, Rome, and Roquetes) and performs a cross correlation analysis of ionospheric and solar parameters during these storms. We observed the highest fluctuations in ionospheric variables during the main phase of storms. In addition, there is strong evidence of pre-storm phenomenon occurring at least a few hours and more than 24 hours prior to the main phase of the geomagnetic storms. We found that the TEC and foF2 parameters have strong dependence with latitudes for the events with Sudden Storm Commencement (SSC) in mid latitude region. Relatively low TEC and foF2 can be observed in Moscow which is at the highest latitude among the five stations because of a decrease in the $n(O)/n(N_2)$ ratio through out the storm event. However, for the event with gradual storm commencement, there is no evidence of such dependence. The good correlation of Symmetric-H and Auroral Electrojet Indices with ionospheric parameters indicates that the coupling mechanism between magnetosphere and ionosphere produces intense electric field disturbances in the middle low latitudes.

1 Introduction

Geomagnetic storms are produced when the interplanetary magnetic field (IMF) Bz component turns southward, strengthens (IMF Bz < -10 nT), and remains southward for a substantial length of time (longer than ~ 3 hr; (W. D. Gonzalez & Tsurutani, 1987); (W. Gonzalez et al., 1994)). As this happens, a rapid increase of magnetic reconnection processes occurs at the magneto-pause. When IMF-Bz is strongly negative, open field lines are produced by magnetic reconnection between the IMF and the geomagnetic field which allow the passage of mass, energy and momentum from the solar wind to the Earth's magnetosphere. This results in more solar wind energy input into all regions of the earth-atmosphere system, resulting in a geomagnetic storm. Geomagnetic storms are an important space weather phenomenon that, apart from affecting ground and satellite-based technological and high-frequency communications systems, can severely affect the dynamics and structure of the Earth's entire thermosphere and ionosphere. The ionospheric response to a geomagnetic storm is called an ionospheric storm that describes the ionospheric variations due to geomagnetic disturbances.

Geomagnetic activity observed at the Earth is generally attributed to the occurrence of Coronal Mass Ejection (CME) on the Sun and the associated interplanetary shock waves or corotating interaction regions (CIR) produced by high-speed solar wind streams in the interplanetary medium ((Gosling, 1993a); (Gosling, 1993b); (Bothmer & Schwenn, 1994); (Luhmann, 1997); (Crooker & McAllister, 1997)). CMEs are expulsions of mass from the Sun and are generally associated with solar flares or prominences. Once launched from the Sun, CMEs travel through the interplanetary medium and, if directed toward the Earth, reach the Earth in 1-4 days depending on their speed. Therefore in order to predict geoeffectiveness of CMEs, one needs to examine the solar data from near the surface of the Sun and follow them through to the Earth. This is facilitated by an examination of ground-based and space-based multi-instrument data sets.

Ionosphere is the layer of the atmosphere that lies between 60 km and 1000 km above the Earth surface and has a great importance in high frequency (HF) and satellite communications because of its electrical and ionic structure. The ionization characteristics and electron density distribution vary according to the location on Earth, time, solar, geomagnetic and seismic effects. Ionosphere consists of three distinct layers, namely D, E, and F. The F layer is the most significant layer in the ionosphere and the central part has the greatest electron density. During day time the F layer splits into F1 and F2 layers. F2-layer, having the highest electron density, is the most stable layer for HF communications and it has major importance in satellite communications ((Kolawole, 2003)).

67 The F2 region is considered the most difficult and anomalous ionospheric region
68 to predict (Hargreaves, 1992). In order to model this region, several authors have used
69 the F2 critical frequency (foF2) and the F2 region peak height (hmF2) parameters. These
70 parameters depend on various geophysical parameters including local time, season, so-
71 lar and geomagnetic activity conditions and are believed to describe the overall behav-
72 ior of the F2 layer ((Sethi & Pandey, 2001); (Richards, 2001); (Kawamura et al., 2002);
73 (J. Liu et al., 2003); (Lei et al., 2005); (L. Liu et al., 2006); (S.-R. Zhang & Holt, 2008);
74 (Moen et al., 2008); (M.-L. Zhang et al., 2009); (Souza et al., 2010), and references therein).
75 A better understanding of the variability and modeling of foF2 and hmF2 parameters
76 is crucial for the development of ionospheric prediction capabilities, improvements in ex-
77 isting ionospheric models, and for radio propagation studies.

78 Studies have shown that, there are strong disturbances induced in the F-region of
79 the ionosphere during strong geomagnetic storms. These perturbations cause large en-
80 hancements and reduction of electron density at the F2 region described as positive and
81 negative ionospheric storm effects respectively.(see, e.g., (Fuller-Rowell et al., 1994); (Volland,
82 1995); (Buonsanto, 1999); (Mendillo, 2006).) The occurrence of positive and negative
83 storm effects depends upon the latitude, local time, and phase of the storm ((Fuller-Rowell
84 et al., 1994)).

85 The ionospheric variations can be determined from the total electron content (TEC)
86 or from the critical frequency of the F2-layer (foF2), which is a direct measure of the peak
87 electron density (NmF2) of the F2-region ionosphere. The positive ionospheric storms
88 have a high density of electrons and negative storms contain a lower density ((Fagundes
89 et al., 2016)). The total electron content (TEC) is used to measure these densities, and
90 is a key variable used in data to record and compare the intensities of ionospheric storms.

91 Ground magnetometer measures the integrated effect of all these disturbed time
92 and also quiet time ionospheric and magnetospheric currents. Geomagnetic indices like
93 Disturbance storm time index (Dst) and Symmetric H-component (SYM/H) index mainly
94 represent ring current intensity during geomagnetic storms ((Sugiura et al., 1964); (Rangarajan,
95 1989); (Wanliss & Showalter, 2006)), derived using the longitudinally distributed chain
96 of low latitude ground-based magnetometers. SYM/H is the same as Dst, but it has a
97 1-minute temporal resolution, which is very useful to study short temporal variations dur-
98 ing the geomagnetic disturbances. SYM/H is derived by first subtracting the main ge-
99 omagnetic field due to internal geodynamo and external Sq induced geomagnetic field
100 variations and then averaging residual fields. Therefore, it is a good proxy for the lon-
101 gitudinally symmetric component of the ring current. SYM/H is an indication of storm
102 ring current intensity and AE gives auroral substorm ionospheric current intensities.

103 In the present study we investigate the solar and interplanetary conditions that were
104 specific to intense geomagnetic storms of 25-27 September 2011, 16-18 March 2013, and
105 6-8 September 2015 (minimum SYM/H < -130 nT) in order to understand the rela-
106 tionships between the solar indices and ionospheric parameters associated with intense
107 geomagnetic storms.

2 Data Sources

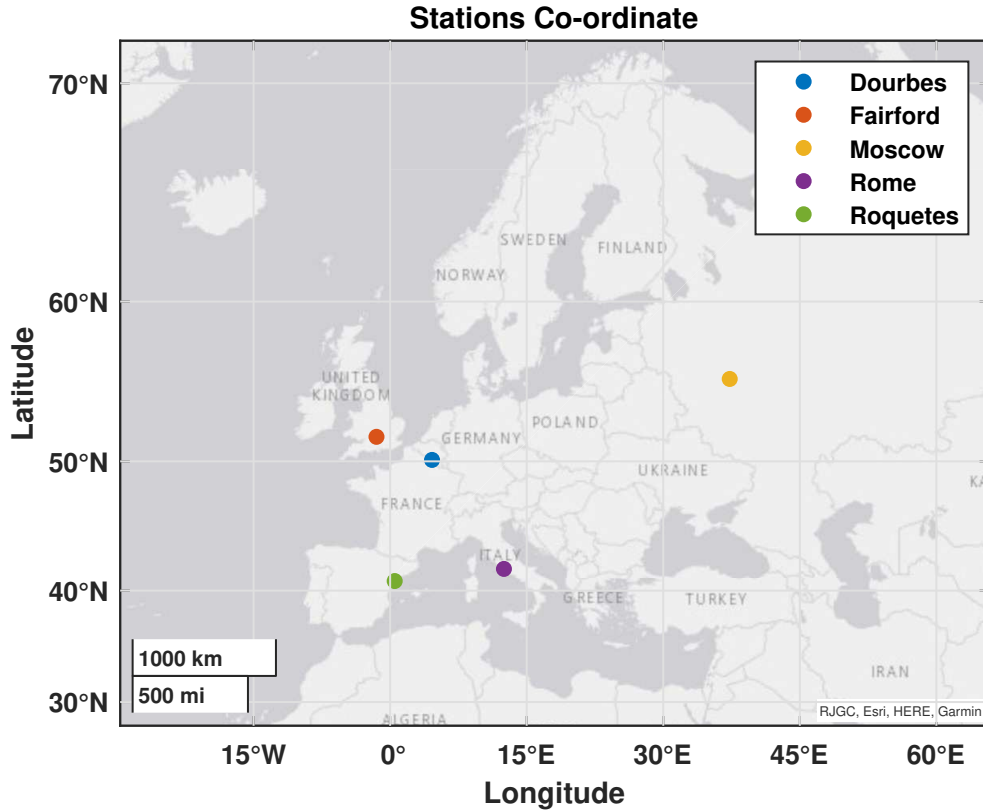


Figure 1. Map of the Stations.

Table 1. Table of stations.

S.No	Stations Name	URSI	Latitude	Longitude
1.	DOURBES	DB049	50.10	4.60
2.	FAIRFORD	FF051	51.70	358.50
3.	MOSCOW	MO155	55.47	37.30
4.	ROME	RO041	41.80	12.50
5.	ROQUETES	EB040	40.80	0.50

Figure 1 shows the map of the ionospheric stations used in this study. The observed F2-layer parameters (f_oF_2 , h_mF_2 , and TEC) in this study are obtained from a chain of ionosondes located at Dourbes (50.1° N, 4.6° E, data temporal resolution 5 min), Fairford (51.7° N, 358.5° E, 15 min), Moscow (55.47° N, 37.3° E, 15 min), Rome (41.9° N, 12.5° E, 15 min), and Roquetes (40.8° N, 0.5° E, 5 min) during the geomagnetic storms on 25-27 September, 2011; 16-18 March, 2013; and 6-8 September, 2013. In order to investigate the F2-layer behaviors during low solar activity, the data under geomagnetic quiet-conditions on 17-19 March, 2017 are selected. The data are available at the Digital Ionogram Data Base (DIDBase) (<https://giro.uml.edu/didbase/>).

118 The modulation of solar wind (SW) and interplanetary magnetic field (IMF) com-
119 ponents (Bx, By, and Bz) high-resolution (1 min) data were obtained from OMNI Database
120 (https://omniweb.gsfc.nasa.gov/form/omni_min.html).

121 The sudden storm commencement (SSC) is often served as a reference time for the
122 onset of a magnetic storm. The reliability of SSC for the storm onset has been argued
123 for a long time. As a result, some investigators choose the main phase onset of the storm
124 instead of SSC as the start time of a storm [e.g., (Prölss, 1995)]. Here we use SSC to in-
125 dicate the onset of a magnetic storm for storms with a sudden commencement, except
126 for the event on 06-08 September, 2015 because it only had a gradual commencement.
127 The SYM/H index is used to indicate the evolution and intensity of geomagnetic storms.

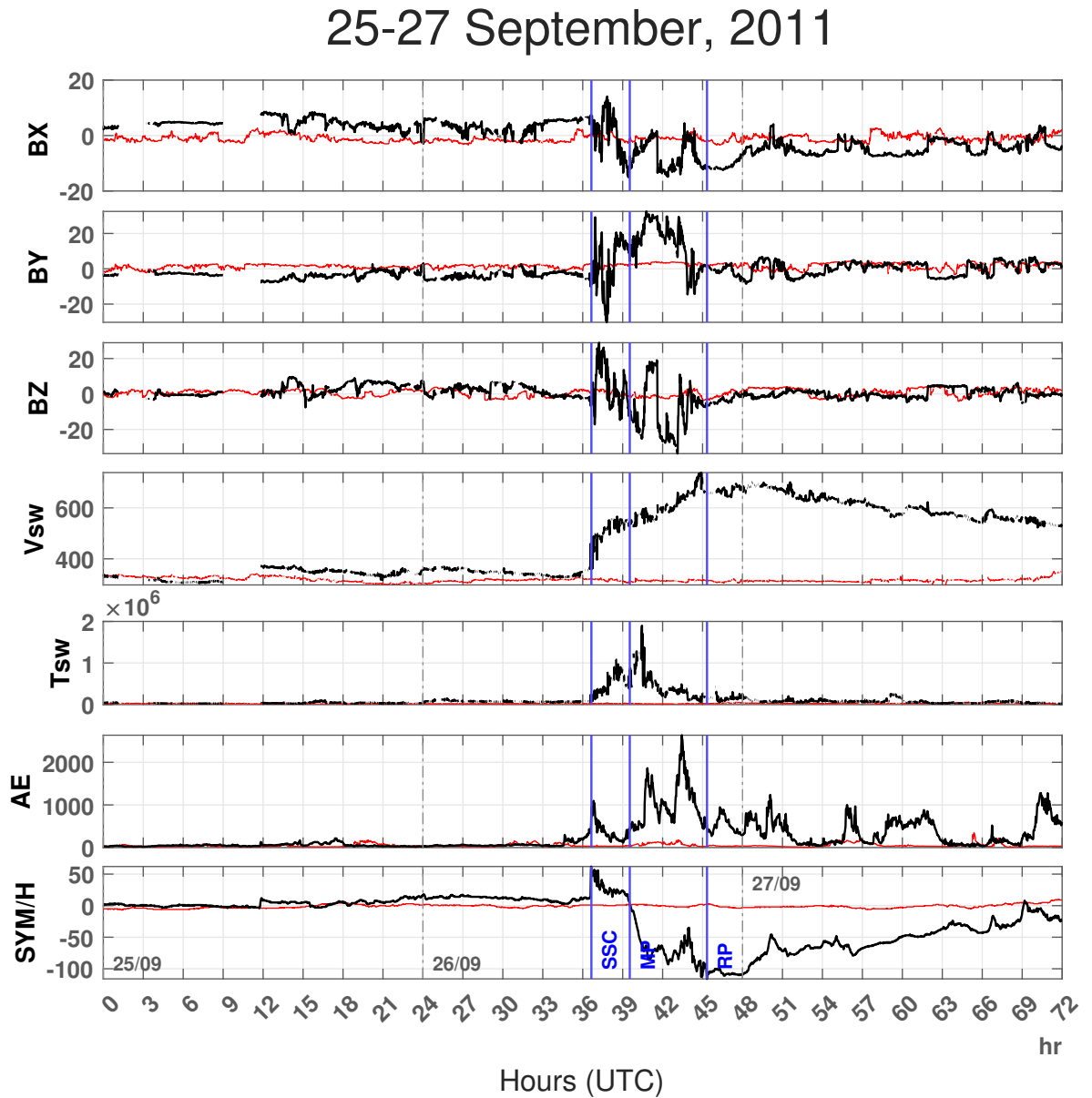
128 **3 Result**129 **3.1 Event-1: 25-27 September, 2011**

Figure 2. Variation in components of the magnetic field (in GSM co-ordinates), B_x (nT), B_y (nT) and B_z (nT), solar wind velocity V_{sw} (km/s), plasma temperature T_{sw} (K), geomagnetic indices, SYM/H (nT), and AE-index (nT) during Super Sub-Storm of 25–27 September, 2011. The red curve denotes the variation during quiet days (18–20 March, 2017).

130 Almost halfway through the ascending phase of the 24th solar cycle, a G2 level, moder-
 131 ately strong geomagnetic storm with Kp index of 6 occurred on 26 September, 2011
 132 due to a concentrated blast of electrically-conducting solar wind plasma and tangled mag-
 133 netic field lines from region 1302 (N12E47) of the Sun. The region produced a X1.9 flare,

134 a M7.1 long duration x-ray flare and a M5.8 x-ray flare on 24 September (Source: [https://](https://www.spaceweatherlive.com/)
 135 www.spaceweatherlive.com/). Figure 2 displays temporal evolution of interplanetary
 136 parameters Bx, By, Bz, solar wind velocity (Vsw), solar wind temperature (Tsw), ge-
 137 omagnetic activity indices AE (Auroral Electrojet) index, and SYM/H index for 25–27
 138 September, 2011. The differences between the various parameters during the event (in-
 139 dicated by black curves) and quiet days (indicated by red curves) are observed from the
 140 figure 2.

141 At 12:38 (UTC) of 26 September the sudden storm commencement (SSC) is seen
 142 to have occurred when the symmetric horizontal component of the geomagnetic field SYM/H
 143 rose sharply from 15 nt to the highest point of 62 nt, indicating the beginning of the
 144 initial phase. During this period, all the ionospheric parameters significantly fluctuate
 145 while the north-south interplanetary magnetic field Bz altered between positive and neg-
 146 ative values a few times with positive (negative) value indicating northward (southward)
 147 magnetic field, reaching its minimum of -33.61 nt at 19:07 (UTC) indicating a strong south-
 148 ward magnetic field. It can be observed from Figure 2, minimas in the Bz curve corre-
 149 late well with maximas in the Auroral Electrojet (AE) index. At 19:27 (UTC), 20 min-
 150 utes after Bz reached its minimum, AE-index reached its peak intensity of 2636 nT which
 151 corresponds well with the results of (Marques de Souza et al., 2018). Large amount of
 152 energy-momentum is transferred into the Earth’s magnetosphere from the solar wind which
 153 is indicated by high AE index (Pandit et al., 2021). This spike in AE index can be at-
 154 tributed to high southward interplanetary magnetic field (Bz) as the field components
 155 parallel to the ecliptic have no significant effect on sub storms (Foster et al., 1971). IMF-
 156 Bz getting negative also causes the electric field linking magnetosphere-ionosphere to in-
 157 crease (Adhikari et al., 2018). Correlation between interplanetary magnetic fields Bx and
 158 Bz can be also observed in Figure 2 as the plasma flow speed (Vsw) started increasing
 159 from the initial phase throughout the main phase as was shown by (Youssef et al., 2012).
 160 The plasma velocity (Vsw) reached its peak, 738.6 km/s at 20:53 (UTC), at the end of
 161 the main phase and decreased throughout the recovery phase. Around this time, the so-
 162 lar wind temperature (Tsw) had already cooled down reaching its peak 1.89×10^6 K
 163 earlier at 16:27 (UTC) around the beginning of the main phase. The recovery phase started
 164 when the SYM/H index was recorded to be rising after reaching its lowest at -113 nt at
 165 20:54 (UTC).

25-27 September, 2011

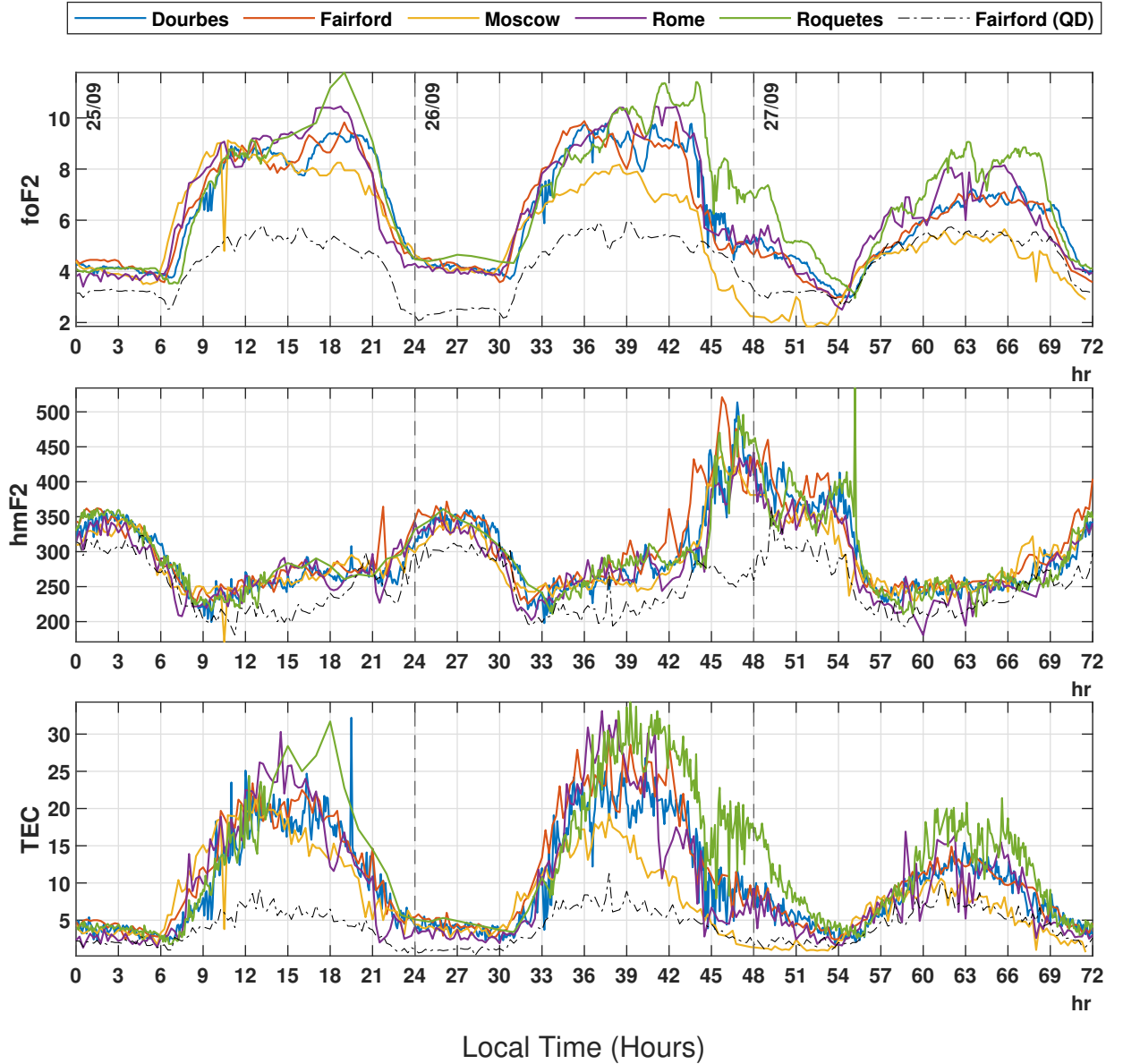


Figure 3. Changes in ionospheric parameters: F2-region critical frequency (foF2) in MHz, Total electron content (TEC) in ($\times 10^{16} m^{-2}$), Maximum Ionization Height (hmF2) in km, recorded at stations Dourbes, Fairford, Moscow, Rome and Roquetes during Super Sub-Storm on 25–27 September, 2011. The black curve denotes the variation during quiet days (18–20 March, 2017).

166 Figure 3 depicts the variations of three different ionospheric parameters: F2-region
 167 critical frequency (foF2), maximum ionization height of F2-region (hmF2), and Total Elec-
 168 tron Content (TEC) at five different stations: Dourbes, Fairford, Moscow, Rome and Roquetes.
 169 All the stations have similar variations because they all lie in the mid-latitude region.
 170 The daily variations of day and night cycle can be easily noticed in all five stations. As
 171 the sun rises at around 06:30 local time, a sudden rise in foF2 and TEC is noticed in all
 172 the stations whereas around this time hmF2 is observed to have almost reached its low-
 173 est values around 09:00 (local time) indicating a negative correlation between them.

174 Relatively low TEC and foF2 can be observed in Moscow which is at the highest
 175 latitude among the five stations because of a decrease in the $n(O)/n(N_2)$ ratio through-
 176 out the storm event (Klimenko et al., 2017). TEC and foF2 graph in Figure 3 clearly
 177 shows latitudinal dependence with high latitude stations having comparatively more neg-
 178 ative values and lower latitude stations having more positive values as shown by (W. Liu
 179 et al., 2017) and (GAO et al., 2008). Due to this reason, the ionosonde stations at Rome
 180 and Roquetes, being at the lowest latitudes, record the highest values of foF2 and TEC.

181 In panel 1, the average of highest critical frequency during daytime of the 1st day
 182 is about 10 MHz which is ~ 5 units ($\sim 100\%$) higher than that of the quiet day. The
 183 mean highest TEC on the 1st day is $\sim 25 \times 10^{16} m^{-2}$, which is ~ 17 units ($\sim 200\%$)
 184 higher than that of the quiet day (panel 3). This indicates that the positive storm had
 185 already started 1 day prior to the event day. Large amounts of energy getting deposited
 186 into the thermosphere and leading to a strong enough storm-induced circulation that fur-
 187 ther increases plasma vertical drift, increasing the electron concentration is the most fre-
 188 quent cause of positive storms but the occurrence of positive storm before SSC is one
 189 of the unsolved problems in ionospheric research (Danilov, 2001). During the nighttime
 190 of the first day, the lowest critical frequency is ~ 4 MHz which is ~ 2 units ($\sim 100\%$)
 191 higher than that of the quiet day and the lowest TEC is $\sim 3 \times 10^{16} m^{-2}$, which is much
 192 higher than that of the quiet day. The highest foF2 and TEC on the 2nd day, similar
 193 to 1st day, was ~ 5 units (100%) and ~ 20 units ($\sim 200\%$) higher than that of the quiet
 194 day respectively. Hence the storm remained positive throughout the 1st day (25 Septem-
 195 ber) and throughout the main phase on the 2nd day (26 September). This result matched
 196 with (W. Liu et al., 2017) who showed that in middle latitudes, the positive storm pre-
 197 vails during the main phase and decreases during the recovery phase. When the recov-
 198 ery phase started at 21:00 (local time) of the 2nd day (event day), the positive storm started
 199 decreasing and remained quiet throughout the 3rd day.

200 In panel 2, on the 1st day (25 September), the maximum ionization height (hmF2)
 201 above all stations remains similar to that of the quiet day. On the second day (26 Septem-
 202 ber) during the main phase, an increase in hmF2 is observed to be ~ 50 km more in all
 203 stations as compared to the quiet day. The plasma vertical drift getting increased by storm-
 204 induced circulation is the cause of uplifting of the F2 layer (Danilov, 2001). A sudden
 205 increase in hmF2 from ~ 300 km to ~ 450 km is observed at 21:00 (local time) (be-
 206 ginning of recovery phase) which is ~ 200 km more than that of the quiet day. Contin-
 207 uous substorm activity building up a high pressure zone in the polar region, reducing
 208 poleward-directed winds and enhancing equatorward-directed winds might be the cause
 209 of this sudden increase in the height of the F2 layer (Prölss & Očko, 2000). The uplift-
 210 ing decreases and almost coincides with the quiet day in the morning hours of the third
 211 day (27 September) and remains so throughout the day.

3.2 Event-2: 16-18 March, 2013

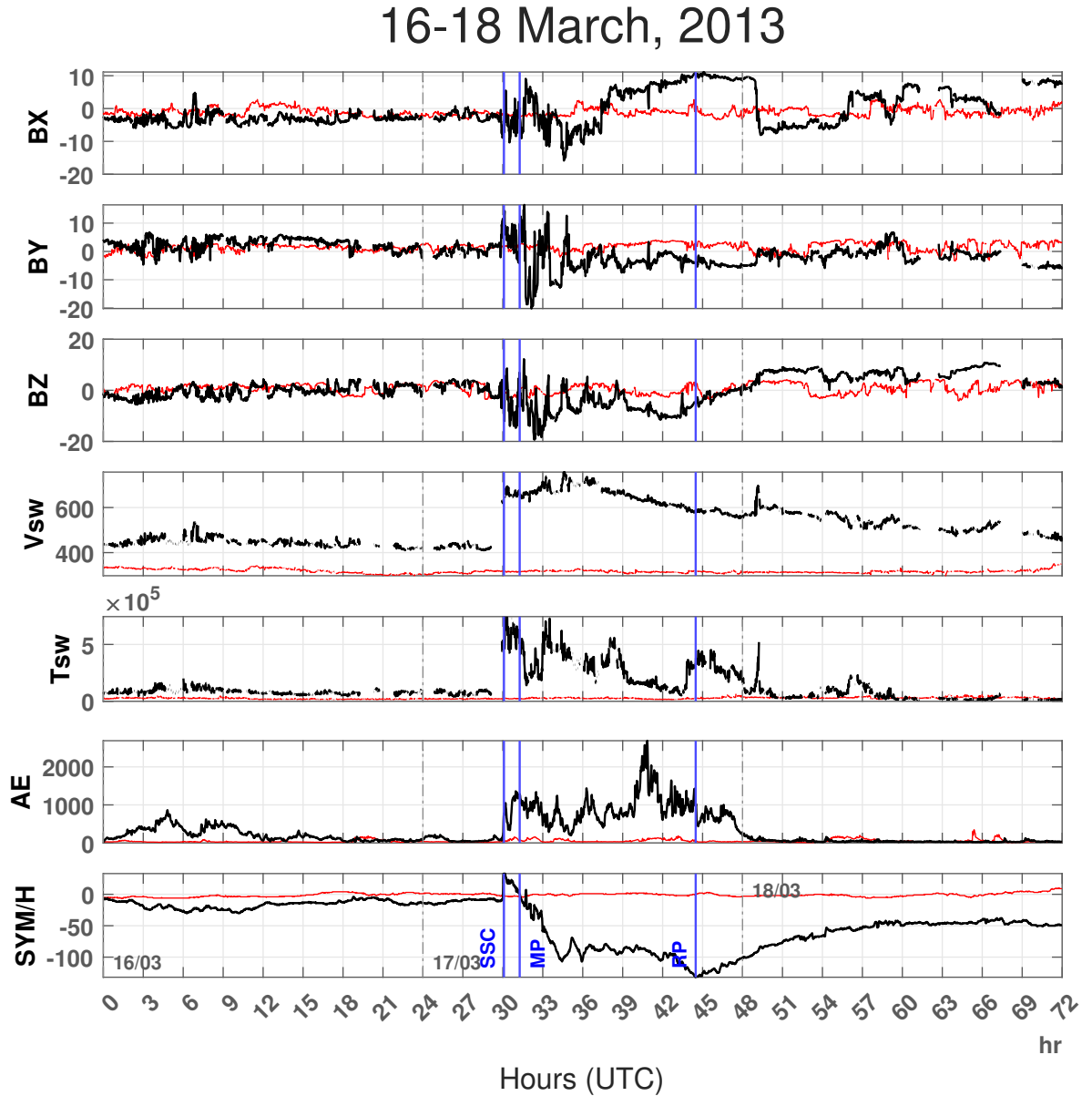


Figure 4. Variation in components of the magnetic field (in GSM coordinates), B_x (nT), B_y (nT) and B_z (nT), solar wind velocity V_{sw} (km/s), plasma temperature T_{sw} (K), geomagnetic indices, SYM/H (nT), and AE-index (nT) during Super Sub-Storm of 16–18 March, 2013. The red curve denotes the variation during quiet days (18–20 March, 2017).

A G3-Class ($K_p = 7$) Earth-directed Coronal Mass Ejection (CME) event has been observed on 17 March 2013, which is one of the strongest geomagnetic disturbances recorded during the 24th solar cycle with peak intensity of SYM/H ~ -132 nT. Figure 4 displays temporal evolution of interplanetary parameters B_x , B_y , B_z , solar wind velocity (V_{sw}), solar wind temperature (T_{sw}), geomagnetic activity indices AE (Auroral Electrojet) in-

218 dex, and the symmetric horizontal component of the geomagnetic field (SYM/H) for 17-
219 18 March 2013.

220 This storm was triggered by an Earth-directed, coronal mass ejection (Baker et al.,
221 2014) associated with M1.1 type solar flare from the sunspot 1692 (N09W03) on 15 March
222 2013 at 07:00 UT. The incoming CME enhances the Bz (north-south) to strong north-
223 ward and solar wind speed raised to 600 km/s at around 06:00 UT on 17 March 2013,
224 while magnetic field components also significantly vary. The sudden enhancement of so-
225 lar wind density and velocity because of CME hitting on magnetosphere triggers the mag-
226 netopause current, which enhances our terrestrial magnetic field, which is registered as
227 a sudden storm commencement (SSC) on SYM/H as shown in figure 4. An immediate
228 onset of intense auroral activity is seen in the AE index, reaching a magnitude as high
229 as 2000 nT, indicating the generation of energy source in the high latitude region. The
230 initial phase lasted for approximately one hour and the main phase began around 7:00
231 UT, as identified by decrease in SYM/H implying the ring current intensification, and
232 SYM/H index reached a first minimum of around -110 nT around 10:00 UT on 17 March.
233 Then it stayed nearly steady until it attained a second minimum of about -132 nT at
234 \sim 20:30 UT before recovery which means that the main phase lasted for around 13 hours.
235 The recovery phase lasted for more than 3 days as indicated by an increase in the SYM/H
236 index.

237 There is a directional discontinuity (DD) at \sim 01:12 UT on 18 March (shown by
238 a blue vertical line) clearly observed in the IMF components, solar wind temperature,
239 and solar wind velocity. The IMF Bz turns northward after the directional discontinu-
240 ity which contributes to a prompt magnetic storm recovery. This northward turning causes
241 a cessation of auroral activity due to reduced magnetic reconnection (Verkhoglyadova
242 et al., 2016). Directional discontinuities in Interplanetary Coronal Mass Ejection is an
243 important factor in determining the geoeffectiveness of the event since they are charac-
244 terized by sharp changes in coupling functions (Lugaz et al., 2015). A gradual decrease
245 in auroral activity and then a total cessation during the northward IMF interval is ob-
246 served (Du et al., 2011). The SYM/H index is observed to recover completely after about
247 3 days. This geomagnetic storm is caused by the double action of southward IMF Bz in
248 the sheath causing the storm onset and southward IMF Bz in the MC intensifying the
249 storm.

16-18 March, 2013

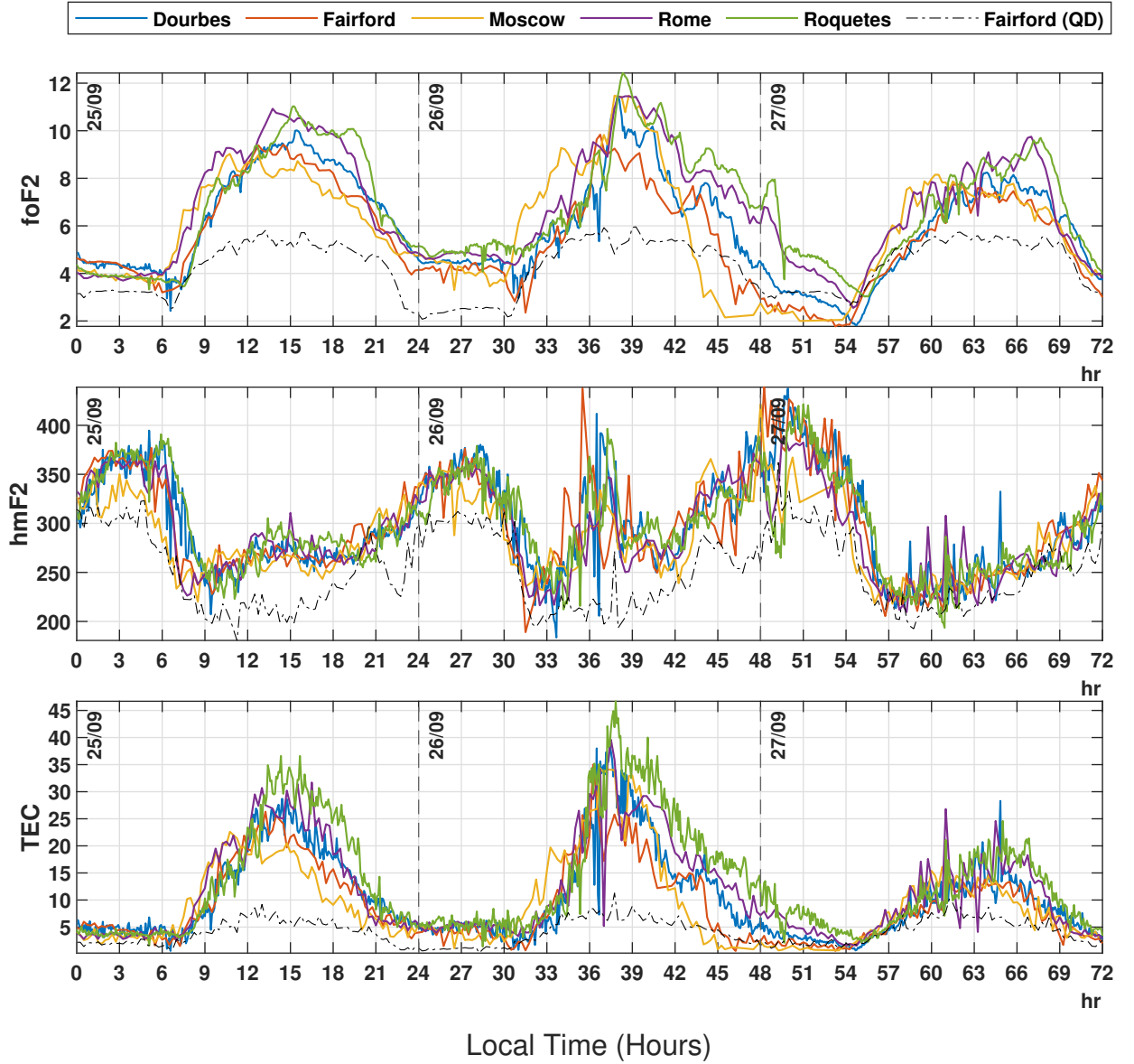


Figure 5. Change in ionospheric parameters, F2-region critical frequency (foF2) in MHz, Total electron content (TEC) in ($\times 10^{16} m^{-2}$), Maximum Ionization Height (hmF2) in km, recorded at stations Dourbes, Fairford, Moscow, Rome and Roquetes during Super Sub-Storm on 16–18 March, 2013. The black curve denotes the variation during quiet days (18–20 March, 2017).

250 Figure 5 shows F-2 layer parameters (fof2, hmF2, and TEC) between 16–18 March,
 251 2013. The top panel shows the geomagnetic index foF2, the middle panel shows the ge-
 252 omagnetic index hmF2, and the bottom panel shows the geomagnetic index TEC obtained
 253 from ionograms of Dourbes, Fairford, Moscow, Rome, and Roquetes.

254 Similar to event 1, Moscow, being at higher latitude, has the lowest TEC and foF2
 255 among the five stations for reasons similar to mentioned above in event 1 because of a
 256 decrease in the $n(O)/n(N_2)$ ratio throughout the storm event (Klimenko et al., 2017).
 257 Latitude dependence can be observed in the graph of TEC and foF2 graph as pointed

258 out in (W. Liu et al., 2017) and (GAO et al., 2008). Similarly, the ionosonde stations
 259 at Rome and Roquetes, being at the lowest latitudes, record the highest values of foF2
 260 and TEC.

261 The average of highest critical frequency during daytime of the 1st day is about
 262 10 MHz in panel 1 which is ~ 5 units ($\sim 100\%$) higher than that of the quiet day. The
 263 mean highest TEC on the 1st day is $\sim 25 \times 10^{16} m^{-2}$, which is ~ 18 units ($\sim 200\%$)
 264 higher than that of the quiet day (panel 3). Here, the positive storm had already started
 265 1 day prior to the event day. The lowest critical frequency during the nighttime of the
 266 first day is 5 MHz which is 2 units higher than that of the quiet day and the lowest TEC
 267 is $\sim 5 \times 10^{16} m^{-2}$, which is much higher than that of the quiet day. The highest foF2
 268 and TEC on the 2nd day, similar to 1st day, was ~ 5 units and ~ 25 units higher than
 269 that of the quiet day respectively. This indicates that the storm remained positive through-
 270 out the 1st day (16 March) and throughout the main phase on the 2nd day (17 March).
 271 The positive storm started decreasing when the recovery phase started at around 20:30
 272 (local time) of the 2nd day (event day) and remained less positive throughout the 3rd
 273 day.

274 On the 1st and 2nd day (16 and 17 March), in panel 2, the maximum ionization
 275 height (hmF2) above all stations showed slight increment. On the third day (18 March),
 276 hmF2 remained quiet throughout the day. During the main phase, an increase in hmF2
 277 is observed to be ~ 100 km more in all stations as compared to the quiet day. A sud-
 278 den increase in hmF2 from ~ 250 km to ~ 350 km is observed at 11:00 (local time) which
 279 is ~ 100 km more than that of the quiet day. No significant amount of variation in hmF2
 280 is observed at the event day as compared to the previous day of the event.

3.3 Event-3: 6-8 September, 2015

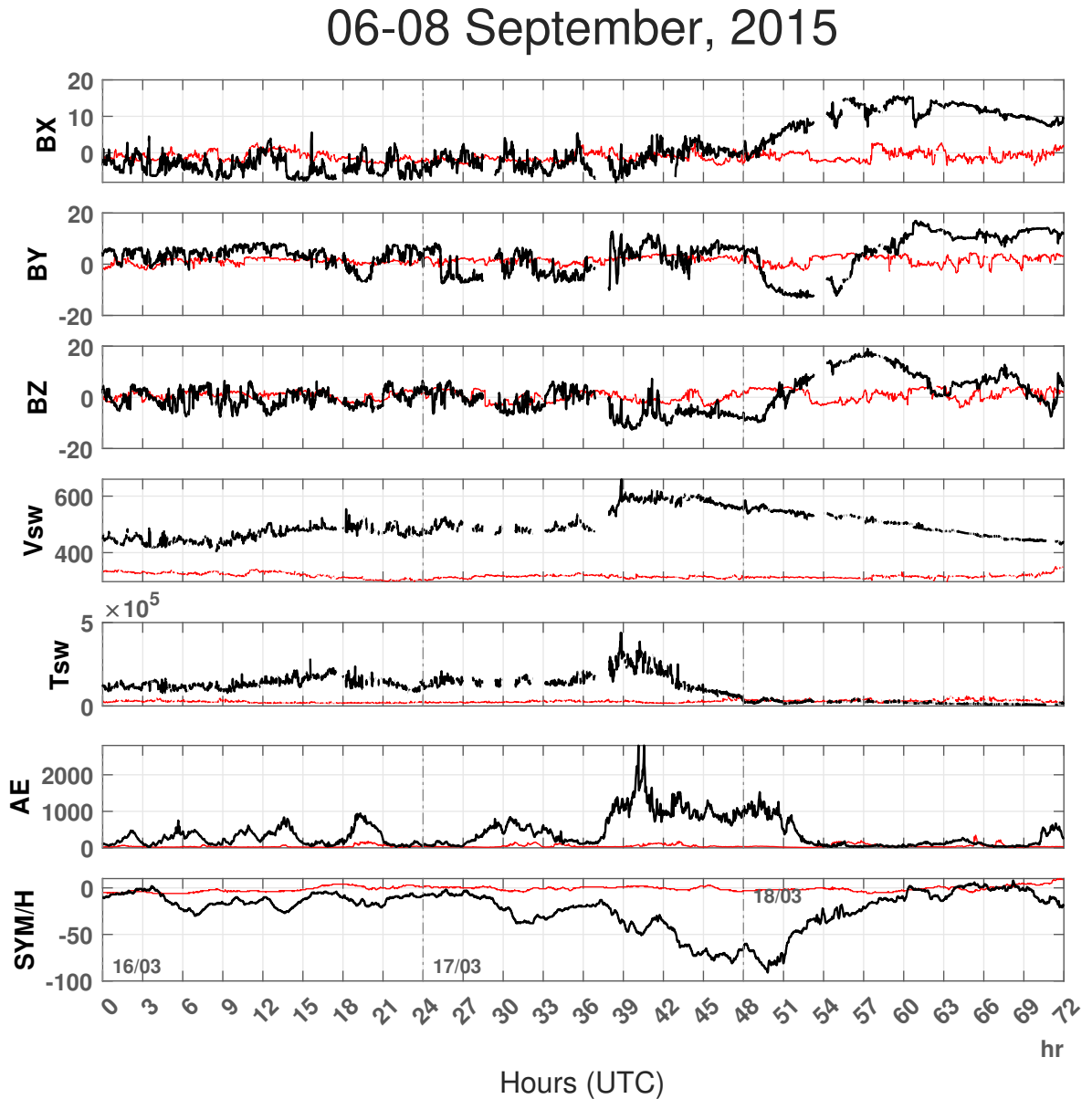


Figure 6. Variation in components of the magnetic field (in GSM coordinates), B_x (nT), B_y (nT) and B_z (nT), solar wind velocity V_{sw} (km/s), plasma temperature T_{sw} (K), geomagnetic indices, SYM/H (nT) and AE-index (nT) during Super Sub-Storm of 6–8 September, 2015. The red curve denotes the variation during quiet days (18–20 March, 2017).

282 An unforeseen powerful coronal hole solar wind stream sparked a moderate G2-Class
 283 ($K_p = 6$) geomagnetic storm on 8 September 2015, with peak intensity of SYM/H -83
 284 nT occurring at 02:00 UT on 8 September. Figure 6 shows the temporal evolution of solar
 285 wind parameters, the Interplanetary magnetic field components B_x , B_y , B_z , solar wind
 286 velocity (V_{sw}), solar wind temperature (T_{sw}), AE index and SYM/H, from 6–8 September
 287 2015. It can be inferred from the graph that there has been a pre-storm phenomenon on 06–

288 07 September with solar wind parameters fluctuating repeatedly on those days. The in-
289 coming solar wind has triggered magnetic field components to vary significantly. These
290 values oscillate to either sides of the reference value for Bz and Bz components during
291 the event. However, the Bx component's value oscillates below the reference value till
292 the recovery phase (02:00 UT, 8 September). Similarly, solar wind speed rose to 620 km/s
293 at around 17:00 UT on 07 September. The sudden enhancement of solar wind density
294 and velocity sets off the magnetopause current, represented by SYM/H as shown in fig-
295 ure 7, which amplifies our terrestrial magnetic field citesibeck1990model. An intense au-
296 roral activity is seen as the AE index reaches a magnitude as high as around 2800 nT
297 at 16:00 UT on 7 September, indicating the generation of energy sources in the high lat-
298 itude region. Likewise, Tsw has risen 2 hrs prior to the event which might be due to the
299 pre-storm effect. However, the temperature of solar wind before the storm disturbance
300 is found to be higher than the main phase (MP) of the event, indicating pre-storm phe-
301 nomena (Adekoya et al., 2012).

06-08 September, 2015

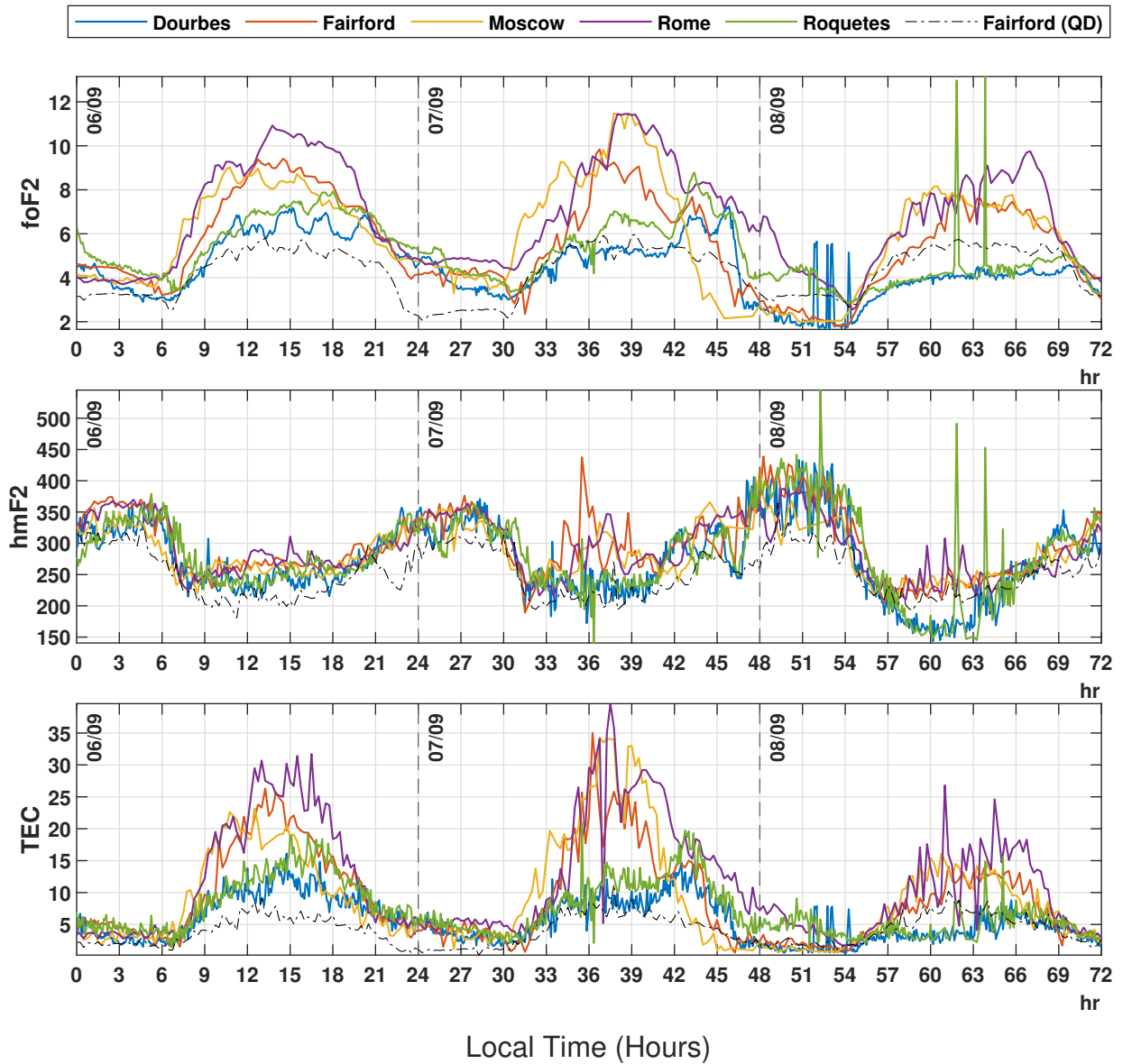


Figure 7. Change in ionospheric parameters, F2-region critical frequency (foF2) in MHz, Total electron content (TEC) in ($\times 10^{16} m^{-2}$), Maximum Ionization Height (hmF2) in Km, recorded at stations Dourbes, Fairford, Moscow, Rome and Roquetes during Super Sub-Storm on 06–08 September, 2015. The black curve denotes the variation during quiet days (18–20 March, 2017).

302 Values of ionospheric parameters, foF2, hmF2 and TEC, of five different stations
 303 due to 2015 geomagnetic storms are plotted in Figure 7. As we have chosen all the stations
 304 lying at the mid station, variation of parameters are almost the same for all stations.
 305 Value of foF2 increases slightly during the main decreasing phase of SYM/H and
 306 decreases during its increasing phase. foF2 in Roquetes has its peak value of 8.7 MHz
 307 at 19:25 LT (07 September) about 3.5 MHz more than in quiet days. Around this time,
 308 critical frequency is maximum in Rome whereas it has minimum value in Dourbes. The
 309 plot of maximum ionization height (hmF2) shows the similar pattern of changes in all

310 five stations. During the main phase (7th september), maximum increase in hmF2 is ob-
 311 served to be ~ 205 km more in Fairford station as compared to the quiet day. Also, the
 312 increase in hmf2 is observed to increase by only 135 KM in Rome and Moscow stations.
 313 However, there is only a slight increase in hmf2 in Roquetes and Dourbes stations. The
 314 plasma vertical drift getting increased by storm-induced circulation is the cause of up-
 315 lifting of the F2 layer (Danilov, 2001). The spikes on the graph decrease and almost co-
 316 incide with the quiet day in the later hours of the third day (08 September).

317 The TEC plot of five stations shows that the variation pattern is similar to each
 318 other. The maximum value of TEC during the main phase is $\sim 40 \times 10^{16} m^{-2}$ about
 319 32 times more than in quiet days, whereas during the recovery phase its value decreases
 320 to $\sim 27 \times 10^{16} m^{-2}$. This increase of TEC during the main phase is due to auroral ac-
 321 tivity, the influx of plasma, and the seasonal effect. TEC content is highest during the
 322 equinox seasons (Xiong et al., 2014). Total electron content in Rome attains its max-
 323 imum, whereas TEC in Dourbes has its lowest value. The TEC and foF2 graph in Fig-
 324 ure 7 doesn't show any latitudinal dependence which contradicts the result as shown by
 325 (W. Liu et al., 2017) and (GAO et al., 2008).

326 4 Cross-Correlation Analysis

327 For all cross-correlation analysis shown in this paper, the y-axis represents normal-
 328 ized correlation coefficients and x-axis represents time lag. Each unit in the x-axis is equiv-
 329 alent to time lag of 15 minutes. The horizontal x-axis represents time (in minutes) rang-
 330 ing (-4500 to +4500). For cross-correlation analysis here, ionospheric parameter is kept
 331 fixed and copies of solar storm indices are shifted (lagged) in all cases. Correlation co-
 332 efficient at each point of lag is calculated, normalized and plotted in the graph.

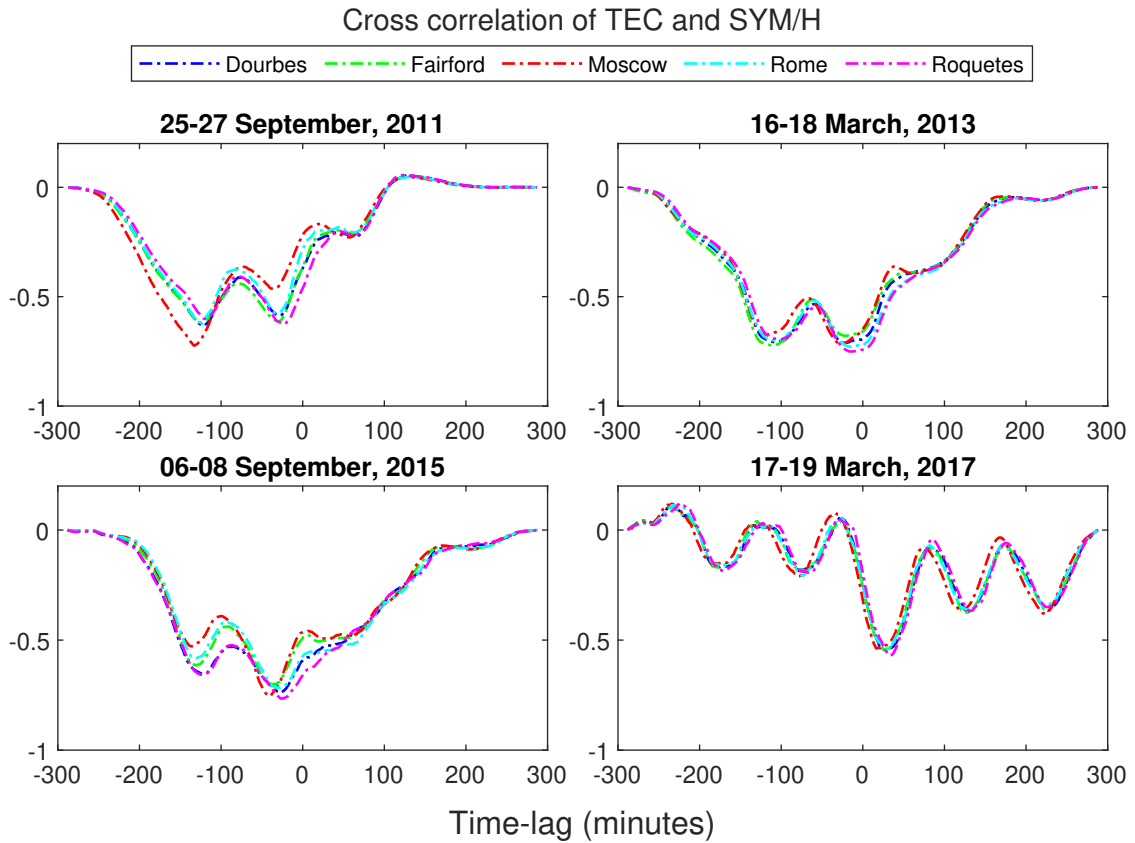


Figure 8. Cross-correlation analysis between TEC and SYM/H during geomagnetic storm of 25–27 September, 2011 (1st Panel), 6–18 March, 2013 (2nd panel), 6–8 September, 2015 (3rd panel) and quiet day on 18–20 March, 2017. X-axis represents time lag (1 unit=15 min) and Y-axis represents correlation coefficient.

333 In Figure 8, cross-correlation between TEC and SYM/H is analyzed. Here, TEC
334 is kept fixed and copies of SYM/H indices is shifted (lagged). In four of the five stations
335 in the 1st panel, TEC leads SYM/H by 1896 minutes (average) with highest negative
336 correlation of -0.6493. But in Roquetes, max negative correlation of -0.6266 leads by only
337 345 minutes. Hence, the maximum anti-correlation is not only observed at one point but
338 at two different points. Average maximum negative correlation at these two points are
339 -0.63972 and -0.5734 at time lag of -1878 minutes (1 day 7 hours and 18 minutes) and
340 -450 minutes (7 hours and 30 minutes) respectively.

341 Similarly, in 2nd panel, in every station except Fairford TEC leads SYM/H by av-
342 erage of 296 minutes with their highest negative correlation of -0.7088 whereas in Fair-
343 ford it is at 1665 minutes with correlation of -0.7580. Similar to 2011, two minimums
344 can be seen here. The average maximum negative correlation of -0.7174 and -0.7006 oc-
345 curs at time lag of -300 minutes and -1623 minutes respectively. Here the most negative
346 correlation occurs at -300 minutes (5 hours) time lag but almost equal anti-correlation
347 is observed at -1623 minutes (1 day 3 hours and 3 minutes).

348 In 3rd panel, each station had their maximum negative correlation around the same
349 time lag. Average correlation of -0.7360 was observed at time lag of -492 minutes (8 hours
350 and 12 minutes). This result matches better with the result of 2nd panel. The quiet day
351 shows moderate anti-correlation with TEC lagging behind SYM/H by about 7 hours in
352 4th panel.

353 All three cross correlation analysis of TEC and SYM/H shows high negative cor-
 354 relation between the variables. At least 5 hours of lead in variation of total electron con-
 355 tent is observed when compared to the SYM/H index. Almost equal evidence of TEC
 356 leading SYM/H by just more than one day can also be obtained from the analysis. This
 357 explains the occurrence of positive storm 1 day prior to the sudden storm commence-
 358 ment (SSC). The mechanism of pre-storm phenomenon (positive storm before main phase
 359 of the storm in mid-latitude region and negative ionospheric storm phase in the equa-
 360 torial region) is an unanswered problem in ionospheric physics (Danilov, 2001) and (Chukwuma,
 361 2010).

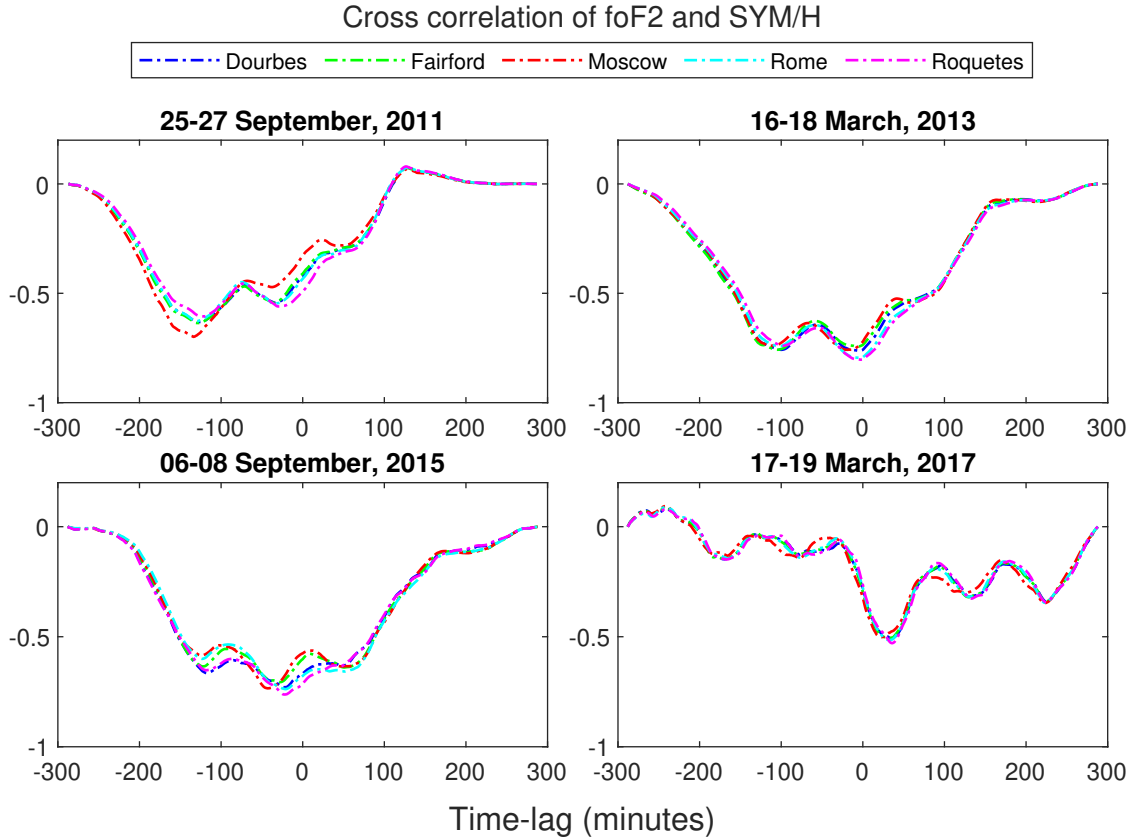


Figure 9. Cross correlation analysis between foF2 and SYM/H during geomagnetic storm of 25–27 September, 2011 (1st Panel), 6–18 March, 2013 (2nd panel), 6–8 September, 2015 (3rd panel) and quiet day on 18–20 March, 2017. X-axis represents time lag (1 unit=15 min) and Y-axis represents correlation coefficient.

362 In Figure 9, cross-correlation analysis between foF2 and SYM/H is plotted. Here,
 363 foF2 is kept fixed and copies of SYM/H indices is shifted for cross-correlation analysis.
 364 In two of the five stations in the 1st panel, Dourbes and Fairford, foF2 leads SYM/H by
 365 1905 minutes with approximately -0.63 negative correlation while Moscow shows max-
 366 imum negative correlation of -0.6992 with lag of 2010 minutes. Roquetes and Rome show
 367 negative correlation of -0.6054 and -0.6275 respectively with respective time lag of -1815
 368 and -1935 minutes. At average, foF2 leads SYM/H by 1914 minutes(1 day 7 hours 54
 369 minutes) with highest negative correlation of -0.6399.

370 Similarly, in second pannel, all stations have perfectly overlapped unlike Moscow
 371 in 2011. It was found that three of five stations, Dourbes, Rome and Roquetes, have min-
 372 imum time lag of -60 minutes from all panels with maximum negative correlation of -

373 0.7631, -0.7949 and -0.8035 respectively. Moscow also shows a maximum negative correlation of -0.7582 with a minimum time lag of -285 minutes (4 hours and 45 minutes)
 374 while Fairford shows minimum negative correlation of -0.7580 but with maximum time lag of -1575 minutes (1 day 2 hours and 15 minutes). In the second panel two minimas
 375 with high negative correlation are observed with foF2 leading SYM/H by at least 1 hour
 376 to more than a day.
 377
 378

379 In panel 3, every station has its highest negative correlation coefficient around the
 380 same time lag. The average of -0.7342 correlation coefficient at lag of -408 minutes (6 hours
 381 48 minutes) is observed. In panel 4, foF2 lags behind SYM/H by about 7 hours with moderate
 382 anti-correlation.

383 All three cross correlation analysis of FoF2 and SYM/H shows high negative correlation
 384 with at least 6 hours of lead in FoF2 signatures compared to the SYM/H index.
 385 Also, evidence of FoF2 leading SYM/H with more than one day can also be obtained from
 386 the analysis. This analysis matches well with the cross-correlation analysis between TEC
 387 and SYM/H. This shows the occurrence of pre-storm phenomena 1 day prior to the sudden
 388 storm commencement (SSC) (Chukwuma, 2010).

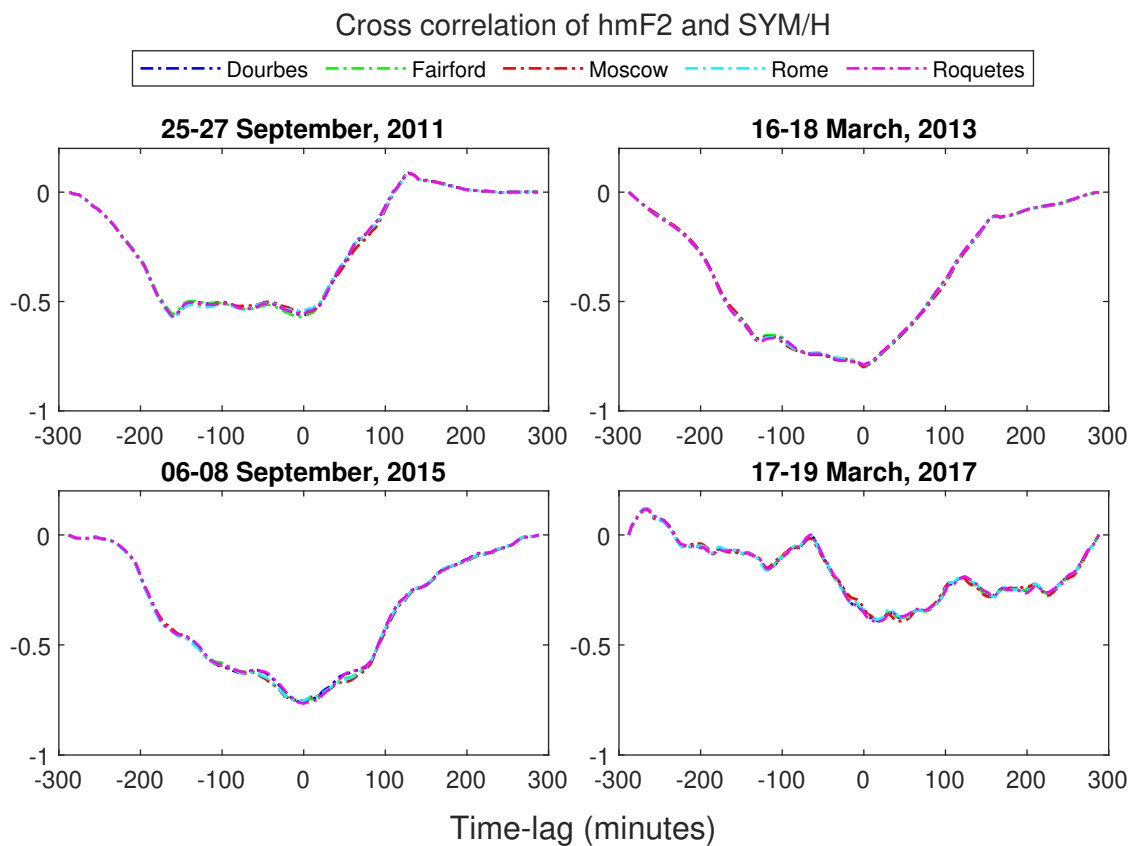


Figure 10. Cross correlation analysis between hmF2 and SYM/H during geomagnetic storm of 25–27 September, 2011 (1st Panel), 6–18 March, 2013 (2nd panel), 6–8 September, 2015 (3rd panel) and quiet day on 18–20 March, 2017. X-axis represents time lag (1 unit=15 min) and Y-axis represents correlation coefficient.

389 Figure 10 represents cross-correlation between hmF2 and SYM/H index. In this
 390 figure hmF2 is kept fixed and copies of SYM/H indices is lagged. In panel 1, there is moderate
 391 negative correlation of -0.5703 between the variables at time lag zero but almost
 392 equal anticorrelation is seen at time lag of -2400 minutes and throughout the points in

393 between. In 2nd panel, high negative correlation of -0.7945 is observed at zero lag. Sim-
 394 ilarly 3rd panel also shows high anticorrelation of -0.7945 with no lag. Compared to other
 395 panels, panel 4 has relatively low correlation at zero lag with correlation less than 0.5.
 396 So, high anti-correlation between the hmF2 and SYM/H is observed at zero lag.

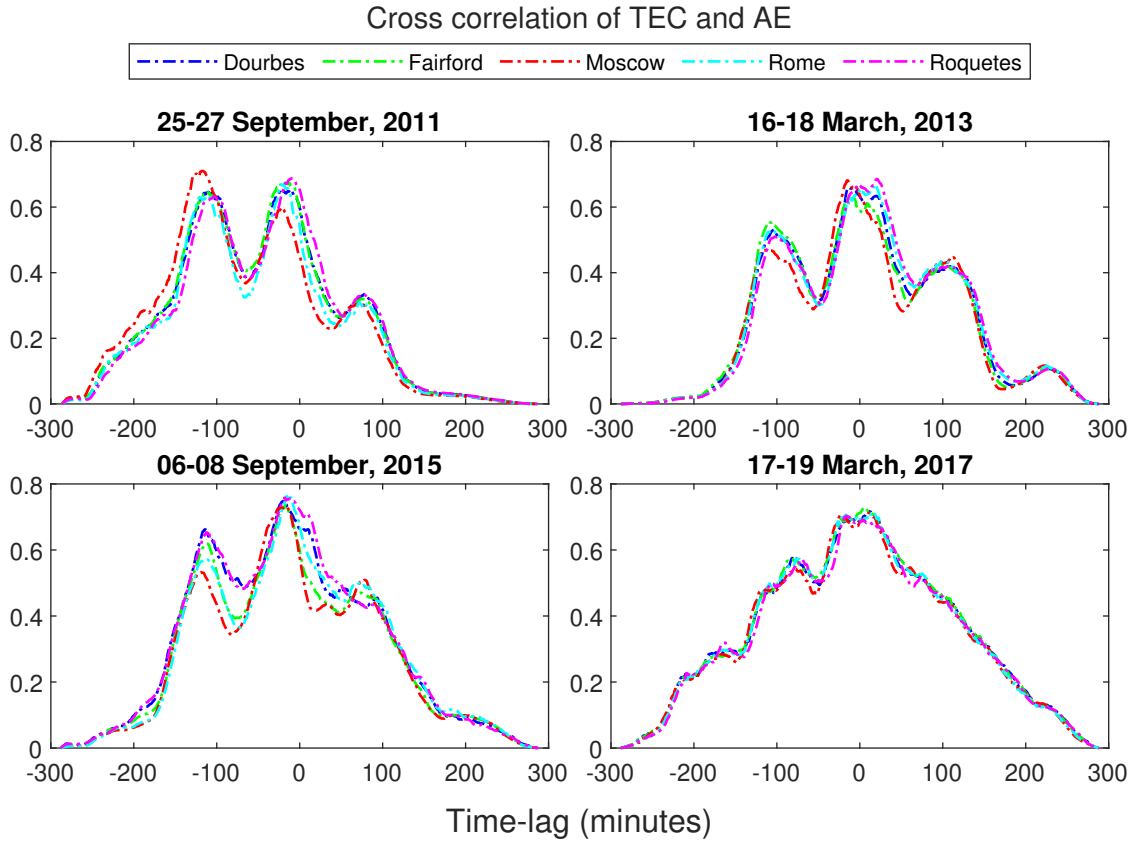


Figure 11. Cross correlation analysis between TEC and AE index during geomagnetic storm of 25–27 September, 2011 (1st Panel), 6–18 March, 2013 (2nd panel), 6–8 September, 2015 (3rd panel) and quiet day on 18–20 March, 2017. X-axis represents time lag (1 unit=15 min) and Y-axis represents correlation coefficient.

397 Cross-correlation between TEC and AE index is analyzed in Figure 11. In panel
 398 1, two maxima can be observed with TEC leading AE by about 4 hours and more than
 399 a day with correlation of 0.7. In the 2nd panel, highest correlation of 0.6649 can be ob-
 400 served at 0 minute time lag.

401 In the third panel, TEC leads AE by 4 hours with highest correlation of 0.7486.
 402 So from the above result it can be said that TEC leads AE by zero to a few hours where
 403 there is high correlation between the variables but also moderate correlation between the
 404 variables can be observed when TEC led AE index by a day. Here, in 4th panel, high
 405 correlation of 0.7 is seen at no lag. This result corresponds well with the result of cross-
 406 correlation analysis between TEC-SYM/H, foF2-SYM/H and foF2-AE as two station-
 407 ary points can be seen in all the graph around same time lag.

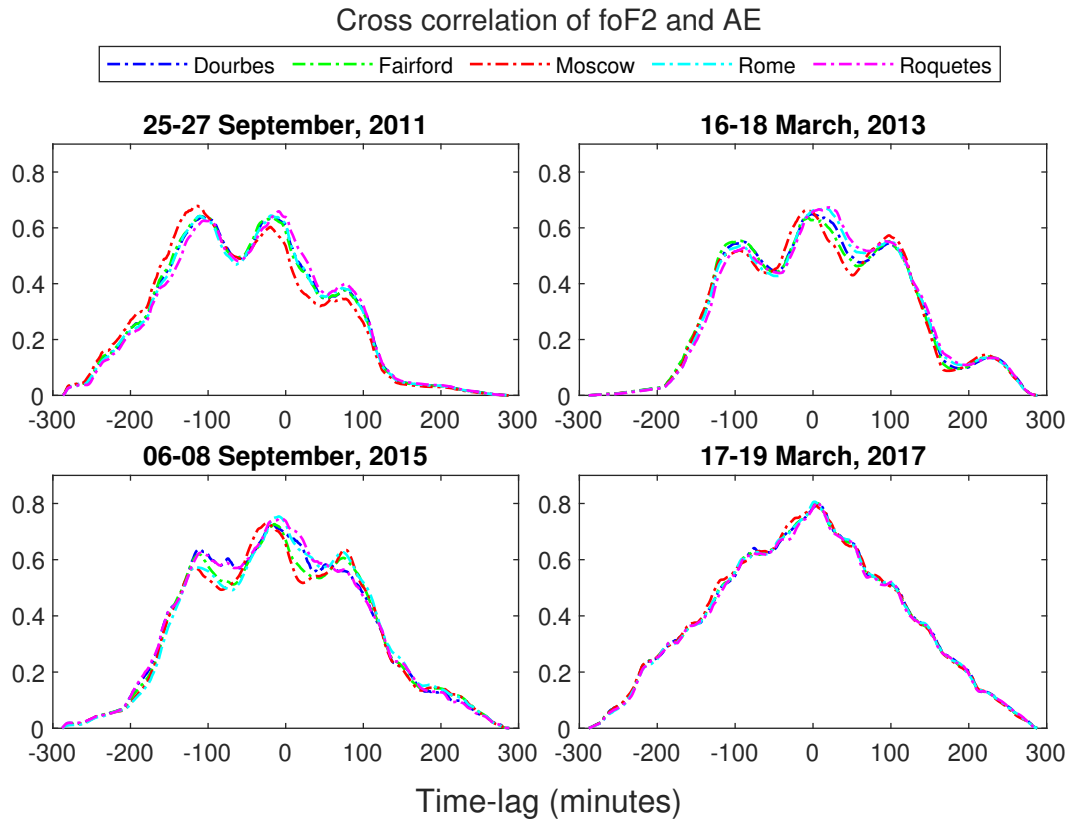


Figure 12. Cross correlation analysis between foF2 and AE index during geomagnetic storm of 25–27 September, 2011 (1st Panel), 6–18 March, 2013 (2nd panel), 6–8 September, 2015 (3rd panel) and quiet day on 18–20 March, 2017. X-axis represents time lag (1 unit=15 min) and Y-axis represents correlation coefficient.

408 In Figure 12, cross correlation between AE index and foF2 is analyzed. In 3 of the
 409 5 stations, Dourbes, Fairford, Moscow, of 1st panel, foF2 leads AE by 1 day 3 hours 40
 410 minutes (average) with highest positive correlation of 0.6536. While in other 2 stations,
 411 Rome and Roquetes, there is the highest positive correlation of 0.6442 and 0.6594 when
 412 foF2 leads AE by 4 hours 45 minutes and 2 hours 15 minutes respectively. Similar to all
 413 other cross-correlation analysis of TEC and foF2, the red curve (Moscow) in the first panel
 414 has higher correlation coefficient in the left stationary point where the ionospheric pa-
 415 rameter led solar storm indices by more than 24 hours. This indicates high pre-storm
 416 effect in Moscow in the first event as compared to the other events.

417 Similarly in 2nd panel, in all the stations, foF2 leads AE by 1 hour with highest
 418 positive correlation of 0.6582. In 3rd panel, each station had their maximum positive cor-
 419 relation around the same time lag. Average correlation of 0.65 was observed at a time
 420 lag of -14.4 (3 hours and 36 minutes). 4th panel shows high correlation at zero time lag.
 421 This result corresponds better with the result of 2013. All three cross correlation anal-
 422 ysis of foF2 and AE index shows at least 1 hours of lead in variation of foF2 when com-
 423 pared to the AE index with moderate positive correlation.

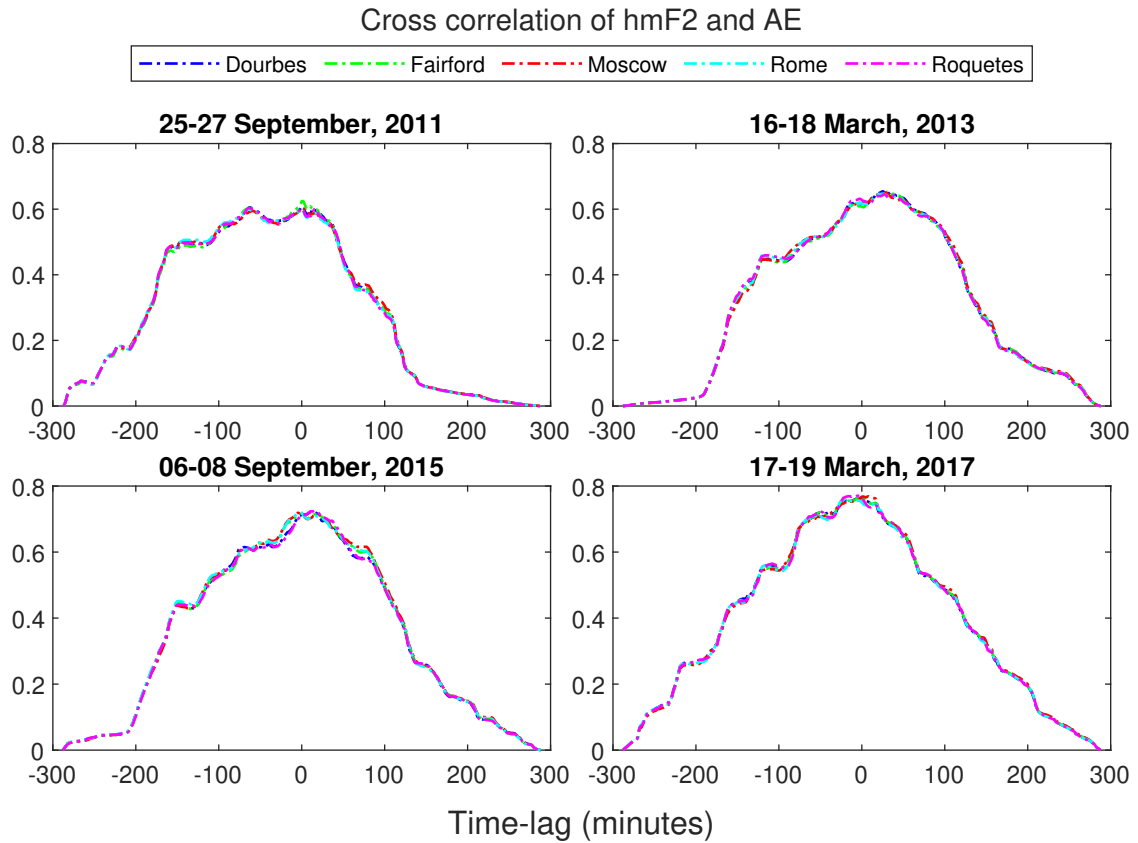


Figure 13. Cross correlation analysis between hmF2 and AE index during geomagnetic storm of 25–27 September, 2011 (1st Panel), 6–18 March, 2013 (2nd panel), 6–8 September, 2015 (3rd panel) and quiet day on 18–20 March, 2017. X-axis represents time lag (1 unit=15 min) and Y-axis represents correlation coefficient.

424 In Figure 13, cross correlation between hmF2 and AE index is analyzed. In the 1st
 425 panel, three stations show highest correlation of 0.6 at time lag of -945 minutes (15 hours
 426 and 45 minutes). Fairford shows the highest positive correlation of 0.6246 with time lag
 427 of just -15 min which is similar to that of Moscow with correlation of 0.6047 respectively.

428 But 2nd panel, in all the stations, AE leads hmF2 by average of 411 minutes (6 hours
 429 and 51 minutes) with highest positive correlation of 0.6501. In 3rd panel, in all stations,
 430 hmF2 lags behind AE by maximum positive correlation of 0.7207 by 72 minutes. There
 431 is high correlation in panel 4 at zero lag.

432 From this result it can be seen that the average lead or lag between hmF2 and AE
 433 index is about ± 2 hours depending upon the type of storm with moderate positive cor-
 434 relation.

435 5 Conclusion

436 In a nutshell, the following conclusions can be drawn out from the cross-correlation
 437 analysis of ionospheric parameters and solar storm indices.

- 438 1. It is observed that the values of Total Electron Content (TEC) and F2 region crit-
 439 ical frequency (foF2) for the events with presence of Sudden Storm Commencement
 440 (SSC) had a strong latitudinal dependence in mid-latitude regions with stations
 441 at higher latitude having relatively lower values and those at lower latitudes hav-

- 442 ing relatively higher values while the event with gradual storm commencement showed
 443 no such dependence.
- 444 2. It is found that the positive storm started a day before the events and remained
 445 so throughout the main phase, then decreased during the recovery phase.
 - 446 3. The cross-correlation analysis of TEC and foF2 with solar storm indices shows two
 447 stationary points at these two time lags with almost equal magnitude of correla-
 448 tion coefficient. This hints strongly to the occurrence of pre-storm phenomenon
 449 at least few hours prior to the main phase of the geomagnetic storm.
 - 450 4. The Maximum Ionization Height of F2 layer (hmF2), showed no pre-storm effect
 451 as highest correlation between hmF2 and solar storm indices occurred mostly at
 452 zero time lag.
 - 453 5. It is observed that there is a strong correlation of Symmetric-H and Auroral Elec-
 454 trojet Indices with other ionospheric parameters. This is attributed to the fact that
 455 the coupling mechanism between ionosphere and magnetosphere produces extreme
 456 electric field disturbances in the middle low latitude regions.
 - 457 6. The highest correlation between ionospheric parameters is mostly observed for Event
 458 1 a day prior to main phase of geomagnetic storm before. This might be due to
 459 the Event 1 being caused by the most intense solar flare (X1.9 flare) among the
 460 events selected which resulted in the strongest pre-storm effects.
 - 461 7. It is observed that despite Events 1 and 3 having the same seasonal condition, the
 462 pre-storm phenomenon is completely different. This difference stems from the na-
 463 ture of the two events i.e. Event 1 occurring with sudden storm commencement
 464 and Event 3 without SSC. Also, Moscow, which lies at the highest latitude, gets
 465 affected by pre-storm phenomenon much more significantly in Event 1 when com-
 466 pared to other events.

467 Acknowledgments

468 In this work, we have used the Omni Web (<http://omni-web.gsfc.nasa.gov/>) for in-
 469 terplanetary magnetic fields, solar wind parameters and geomagnetic indices. Global Iono-
 470 sphere Radio Observatory (GIRO) <https://giro.uml.edu/> provided the ionospheric
 471 parameters. The stations list was obtained from <https://lgdc.uml.edu/common/DIDBFastStationList>.
 472 The Authors would like to thank the support provided.

473 Authors' contributions

474 All the authors contributed equally to this work.

475 References

- 476 Adekoya, B., Chukwuma, V., Bakare, N., & David, T. (2012). On the effects of
 477 geomagnetic storms and pre storm phenomena on low and middle latitude
 478 ionospheric f2. *Astrophysics and Space Science*, *340*(2), 217–235.
- 479 Adhikari, B., Dahal, S., Sapkota, N., Baruwal, P., Bhattarai, B., Khanal, K., &
 480 Chapagain, N. P. (2018). Field-aligned current and polar cap potential and
 481 geomagnetic disturbances: A review of cross-correlation analysis. *Earth and*
 482 *Space Science*, *5*(9), 440–455.
- 483 Baker, D., Jaynes, A., Li, X., Henderson, M., Kanekal, S., Reeves, G., . . . others
 484 (2014). Gradual diffusion and punctuated phase space density enhancements
 485 of highly relativistic electrons: Van allen probes observations. *Geophysical*
 486 *Research Letters*, *41*(5), 1351–1358.
- 487 Bothmer, V., & Schwenn, R. (1994). Eruptive prominences as sources of mag-
 488 netic clouds in the solar wind. *Mass Supply and Flows in the Solar Corona*,
 489 215–220.

- 490 Buonsanto, M. J. (1999). Ionospheric storms—a review. *Space Science Reviews*,
491 88(3), 563–601.
- 492 Chukwuma, V. U. (2010). On ionospheric phenomena during pre-storm and main
493 phase of a very intense geomagnetic storm. *Acta Geophysica*, 58(6), 1164–
494 1192.
- 495 Crooker, N., & McAllister, A. (1997). Transients associated with recurrent storms.
496 *Journal of Geophysical Research: Space Physics*, 102(A7), 14041–14047.
- 497 Danilov, A. (2001). F2-region response to geomagnetic disturbances. *Journal of At-*
498 *mospheric and Solar-Terrestrial Physics*, 63(5), 441–449.
- 499 Du, A., Tsurutani, B., & Sun, W. (2011). Solar wind energy input during prolonged,
500 intense northward interplanetary magnetic fields: A new coupling function.
501 *Journal of Geophysical Research: Space Physics*, 116(A12).
- 502 Fagundes, P. R., Cardoso, F., Fejer, B., Venkatesh, K., Ribeiro, B., & Pillat, V.
503 (2016). Positive and negative gps-tec ionospheric storm effects during the ex-
504 treme space weather event of march 2015 over the brazilian sector. *Journal of*
505 *Geophysical Research: Space Physics*, 121(6), 5613–5625.
- 506 Foster, J., Fairfield, D., Ogilvie, K., & Rosenberg, T. (1971). *Relationship of in-*
507 *terplanetary parameters and occurrence of magnetospheric substorms*. (Tech.
508 Rep.). Univ. of Maryland, College Park.
- 509 Fuller-Rowell, T., Codrescu, M., Moffett, R., & Quegan, S. (1994). Response of the
510 thermosphere and ionosphere to geomagnetic storms. *Journal of Geophysical*
511 *Research: Space Physics*, 99(A3), 3893–3914.
- 512 GAO, Q., LIU, L.-B., ZHAO, B.-Q., WAN, W.-X., ZHANG, M.-L., & NING, B.-
513 Q. (2008). Statistical study of the storm effects in middle and low latitude
514 ionosphere in the east-asian sector. *Chinese Journal of geophysics*, 51(3),
515 435–443.
- 516 Gonzalez, W., Joselyn, J.-A., Kamide, Y., Kroehl, H. W., Rostoker, G., Tsurutani,
517 B., & Vasyliunas, V. (1994). What is a geomagnetic storm? *Journal of*
518 *Geophysical Research: Space Physics*, 99(A4), 5771–5792.
- 519 Gonzalez, W. D., & Tsurutani, B. T. (1987). Criteria of interplanetary parameters
520 causing intense magnetic storms (dst \geq 100 nt). *Planetary and Space Science*,
521 35(9), 1101–1109.
- 522 Gosling, J. (1993a). Coronal mass ejections: The link between solar and geomagnetic
523 activity. *Physics of Fluids B: Plasma Physics*, 5(7), 2638–2645.
- 524 Gosling, J. (1993b). *The solar flare myth in solar-terrestrial physics* (Tech. Rep.).
525 Los Alamos National Lab., NM (United States).
- 526 Hargreaves, J. K. (1992). *The solar-terrestrial environment: an introduction to*
527 *geospace—the science of the terrestrial upper atmosphere, ionosphere, and mag-*
528 *netosphere*. Cambridge university press.
- 529 Kawamura, S., Balan, N., Otsuka, Y., & Fukao, S. (2002). Annual and semian-
530 nual variations of the midlatitude ionosphere under low solar activity. *Journal*
531 *of Geophysical Research: Space Physics*, 107(A8), SIA–8.
- 532 Klimenko, M. V., Klimenko, V. V., Zakharenkova, I. E., Ratovsky, K. G., Ko-
533 renkova, N. A., Yasyukevich, Y. V., . . . Cherniak, I. V. (2017). Similarity
534 and differences in morphology and mechanisms of the fof2 and tec disturbances
535 during the geomagnetic storms on 26–30 september 2011. In *Annales geophysi-*
536 *cae* (Vol. 35, pp. 923–938).
- 537 Kolawole, M. (2003). *Radar systems, peak detection and tracking*. Elsevier.
- 538 Lei, J., Liu, L., Wan, W., & Zhang, S.-R. (2005). Variations of electron density
539 based on long-term incoherent scatter radar and ionosonde measurements over
540 millstone hill. *Radio science*, 40(2), 1–10.
- 541 Liu, J., Chen, Y., & Lin, J. (2003). Statistical investigation of the saturation ef-
542 fect in the ionospheric fof2 versus sunspot, solar radio noise, and solar eu-
543 v radiation. *Journal of Geophysical Research: Space Physics*, 108(A2).
- 544 Liu, L., Wan, W., Ning, B., Pirog, O., & Kurkin, V. (2006). Solar activity varia-

- 545 tions of the ionospheric peak electron density. *Journal of Geophysical Research:*
546 *Space Physics*, 111(A8).
- 547 Liu, W., Xu, L., Xiong, C., & Xu, J. (2017). The ionospheric storms in the american
548 sector and their longitudinal dependence at the northern middle latitudes. *Ad-*
549 *vances in Space Research*, 59(2), 603–613.
- 550 Lugaz, N., Farrugia, C. J., Smith, C. W., & Paulson, K. (2015). Shocks inside cmes:
551 A survey of properties from 1997 to 2006. *Journal of Geophysical Research:*
552 *Space Physics*, 120(4), 2409–2427.
- 553 Luhmann, J. (1997). What do we really know about solar wind coupling? *Advances*
554 *in Space Research*, 20(4-5), 907–911.
- 555 Marques de Souza, A., Echer, E., Bolzan, M. J. A., & Hajra, R. (2018). Cross-
556 correlation and cross-wavelet analyses of the solar wind imf b z and auroral
557 electrojet index ae coupling during hildcaas. In *Annales geophysicae* (Vol. 36,
558 pp. 205–211).
- 559 Mendillo, M. (2006). Storms in the ionosphere: Patterns and processes for total elec-
560 tron content. *Reviews of Geophysics*, 44(4).
- 561 Moen, J., Qiu, X., Carlson, H., Fujii, R., & McCrea, I. (2008). On the diurnal vari-
562 ability in f2-region plasma density above the eiscat svalbard radar. In *Annales*
563 *geophysicae* (Vol. 26, pp. 2427–2433).
- 564 Pandit, D., Chapagain, N. P., Adhikari, B., Nemirovskaya, I. A., Gordeev, V. V.,
565 Kovalenko, D., . . . others (2021). Analysis of the solar wind imf b z and auro-
566 ral electrojet index during supersubstorms. *Russian Journal of Earth Sciences*,
567 21(5), 1–10.
- 568 Prölss, G. (1995). *Ionospheric f-region storms, handbook of atmospheric electrody-*
569 *namics, vol. 2*. CRC Press/Boca Raton.
- 570 Prölss, G., & Očko, M. (2000). Propagation of upper atmospheric storm effects to-
571 wards lower latitudes. *Advances in Space Research*, 26(1), 131–135.
- 572 Rangarajan, G. (1989). Indices of geomagnetic activity. *Geomatik*, 3, 323–384.
- 573 Richards, P. (2001). Seasonal and solar cycle variations of the ionospheric peak elec-
574 tron density: Comparison of measurement and models (paper 2000ja000365).
575 *JOURNAL OF GEOPHYSICAL RESEARCH-ALL SERIES-*, 106(7; SECT
576 1), 12–803.
- 577 Sethi, N., & Pandey, V. (2001). Comparative study of electron density from in-
578 coherent scatter measurements at arecibo with the iri-95 model during solar
579 maximum. In *Annales geophysicae* (Vol. 18, pp. 1630–1634).
- 580 Souza, J., Brum, C., Abdu, M., Batista, I., Asevedo Jr, W., Bailey, G., & Bitten-
581 court, J. (2010). Parameterized regional ionospheric model and a comparison
582 of its results with experimental data and iri representations. *Advances in Space*
583 *Research*, 46(8), 1032–1038.
- 584 Sugiura, M., Kertz, W., Price, A., & Stone, D. (1964). *P. 1. hourly values of equato-*
585 *rial dst for the igy*. Pergamon Press.
- 586 Verkhoglyadova, O., Tsurutani, B., Mannucci, A., Mlynczak, M., Hunt, L., Paxton,
587 L., & Komjathy, A. (2016). Solar wind driving of ionosphere-thermosphere re-
588 sponses in three storms near st. patrick’s day in 2012, 2013, and 2015. *Journal*
589 *of Geophysical Research: Space Physics*, 121(9), 8900–8923.
- 590 Volland, H. (1995). *Handbook of atmospheric electrodynamic*s (Vol. 2). CRC Press.
- 591 Wanliss, J. A., & Showalter, K. M. (2006). High-resolution global storm index: Dst
592 versus sym-h. *Journal of Geophysical Research: Space Physics*, 111(A2).
- 593 Xiong, C., Lühr, H., Wang, H., & Johnsen, M. G. (2014). Determining the bound-
594 aries of the auroral oval from champ field-aligned current signatures–part 1. In
595 *Annales geophysicae* (Vol. 32, pp. 609–622).
- 596 Youssef, M., Mahrous, A., Mawad, R., Ghamry, E., Shaltout, M., El-Nawawy, M.,
597 & Fahim, A. (2012). The effects of the solar magnetic polarity and the solar
598 wind velocity on bz-component of the interplanetary magnetic field. *Advances*
599 *in space research*, 49(7), 1198–1202.

- 600 Zhang, M.-L., Liu, C., Wan, W., Liu, L., & Ning, B. (2009). A global model of
601 the ionospheric f2 peak height based on eof analysis. In *Annales geophysicae*
602 (Vol. 27, pp. 3203–3212).
- 603 Zhang, S.-R., & Holt, J. (2008). Ionospheric climatology and variability from
604 long-term and multiple incoherent scatter radar observations: Variability. In
605 *Annales geophysicae* (Vol. 26, pp. 1525–1537).